Investigation of Melting and Re-Crystallisation Behavior of Polyethylene Nanocrystals

Inaugural-Dissertation zur Erlangung des Doktorgrades der

Fakultät für Mathematik und Physik der

Albert-Ludwigs-Universität Freiburg

Vorgelegt von

Nandita BASU

August 2012

Dekan: Prof. Dr. Kay Königsmann

Leiter der Arbeit: Prof. Dr. Günter Reiter

Referent: Prof. Dr. Günter Reiter

Koreferent: Prof. Dr.

Prüfer (Theorie): Prof. Dr. Alexander Blumen

Prüfer (Experiment): Prof. Dr. Elizabeth von Hauff

Datum der mündlichen Prüfung : 30.08.2012

To my family

Abstract

Polymer crystals are metastable and exhibit morphological changes when being annealed. To observe morphological changes on molecular scales we started from small nanometer-sized crystals of highly folded long-chain polymers. Micronsized stripes consisting of monolayers or stacks of several layers of flat-on oriented polyethylene nanocrystals were generated via evaporative dewetting from an aqueous dispersion. We followed the morphological changes in time and at progressively higher annealing temperatures by determining the topography and viscoelastic properties of such assemblies of nanocrystals using atomic force microscopy. Due to smallness and high surface-to-volume ratio of the nanocrystals, already at 75 °C, *i.e.* about 60 degrees below the nominal melting point, the lateral size of the crystal coarsened. Intriguingly, this occurred without a noticeable reduction in the number of folds per polymer chain. Starting at around 110 °C, chain folds were progressively removed leading to crystal thickening. At higher temperatures, but still below the melting point, prolonged annealing allowed for surface diffusion of molten polymers on the initially bare substrate, leading eventually to the disappearance of crystals. We compared these results to the behavior of the same nanocrystals annealed in an aqueous dispersion and to bulk samples.

We also explained how scanning the AFM probe over a viscous melt led to a deformation of the molten surface as a shear force was acting on the melt surface induced by the moving AFM cantilever tip. The molecular chains within the melt were stretched by the AFM cantilever-tip during scanning. Typically, a large shear rate as well as significant mechanical work was applied on the undercooled melt and this enhanced the possibility of the stretched molecular chains to be aligned along the direction of scan. The aggregation of the stretched and aligned chains along the scan direction resulted in small crystalline domains. The mechanism of tip-induced nucleation has been described in detail. Factors

such as number of scans or more specifically, the shearing time and tapping force affecting the nucleation rate or the nucleation probability have been discussed in detail. How nucleation induction time and contact time between the molten sample surface and the AFM probe influenced the nucleation rate were included in our discussion. It has been shown that the temperature of the undercooled melt is an important parameter in describing the tip-induced nucleation phenomenon. Even in regions consisting of few droplets of different sizes at a temperature close to the melting temperature, it was shown that well aligned edge-on crystalline domains along the scan direction can be found. A mechanism for the formation of stacks of edge-on crystalline lamellae has been proposed.

Contents

Chapter 1

Introduction

1.1 Motivation of the research

Nanoparticles having crystalline order (and thus distinct molecular order and orientation) have been used as functional units and building blocks for larger scale, mesostructured two- and three-dimensional objects (like stripes, films of discrete thickness, stacks of layers and many more) [1–3]. However, mainly inorganic particles have been studied because it has been difficult to synthesize polymeric crystals of such small size which also can be further processed. The mechanism of crystallisation of high molecular weight polymers are distinctly different from crystallisation of a fluid of small molecules, mainly in terms of entanglements. As linear chains contain one dimensionally chemically connected monomers these chains cannot cut through each other. That is the reason why entanglements occur. As the entanglements impose constraints on the motion of the polymer chains, the crystallisation process is strongly affected. Polymer crystallisation leads to two phase structures, the crystallites seperated by amorphous regions. In the crystallite the polymer chains are well alligned in a parallel fashion while the amorphous region is containing the entanglements. Within these crystallites the polymer chains are folded several times if the total length of the polymer chain is long. Different views of polymer crystallisation have been presented. Some consider polymer crystallisation as a thermodynamically controlled process while others described it as a kinetically controlled process. Several studies [4–7] showed that equilibium polymer crystals can be obtained when few polymer chains are involved. Polymer nanocrystals with a small fraction of amorphous regions are nearly perfect and may reach thermodynamic equilibrium based on a high mo-

bility of the polymer repeat units. Mostly crystallisation of polyethylene from bulk have been studied where, entanglements played an important role for high molecular weight samples. Single crystals of polyethylene have been studied first in 1957 [8–10]. These crystals were crystallised from a very dilute solution [11]. Growth of single crystals of polyethylene from a melt were studied as early as in the 90s, starting with the work by Keller and Toda [12].Their research specifically aimed for the general understanding of the molecular mechanisms of polymer crystallization. However, under such conditions, the amount of crystalline material was typically extremely low. Complementary studies were done on crystallization of polyethylne from a highly dilute solution [13, 14]. The morphological changes of such crystals upon annealing were also investigated through atomic force microscopy [14, 15]. Recently, by using water-soluble Ni(II)-complexes as catalysts, aqueous dispersions containing well-defined and melt-characterized polyethylene nano-crsystals have been obtained [16]. These nanocrystals of polyethylene contained a limited number of chains. Such well-separated and easily processable nanocrystals open up new routes for functional structure formation at various lengthsacles. Moreover, synthetic modification of the crystal (via endgroups or via the integration of functional groups at regular position along the polymer chain using acyclic diene metathesis polymerization (ADMET)) [17, 18] allowed generating functional structures having molecular order. Implementation of such crystals into functional devices needs a detailed understanding of their stability and morphological evolution at various temperatures.

Given that we have sufficient control over metastability of polymer nanocrystals, the use of pre-fabricated building blocks with molecular order provides the possibility for advanced molecular ordering on length-scales much larger than the size of the particle [19, 20]. Following appropriate ways of assembly, nanocrystals can be arranged in regular patterns [21–23]. Moreover, using anisotropic nanoparticles, these patterns may also exhibit specific, direction-dependent properties given that a unique orientation of the building blocks was achieved [24, 25]. To reach such goal, structure formation guided through solvent evaporation has been studied previously [26, 27]. Special attention of theoretical and experimental studies has been focused on the behavior in the vicinity of a three phase contact line [26–28], There, hydrodynamic transport of nonvolatile solutes towards the contact line is combined with solvent evaporation. Often the resulting patterns are periodic [19, 20, 26, 27]. Evaporation from a drop containing solid particles typically results in the formation of ring like patterns of precipitate. This phenomenon is related to the so-called coffee stain effect [29–32]. As maximum evaporative loss takes place at the perimeter of the drop [31], all the solutes are

transported to the edge by an outward hydrodynamic flow. Jamming of the solutes [33] at the perimeter caused a local but transient pinning of the contact line.

In general, we performed detailed measurements at the nanoscale level in order to improve our understanding of the morphological changes upon thermal annealing of the polyethylene nanocrystals. Our work utilizes the advantages of tapping-mode Atomic Force Microscopy (AFM) which is extensively applied to polymer materials. This technique is simple to apply and it has the high capability of monitoring in-situ the assembly of materials under controlled atmospheric conditions and temperature. In addition, we used AFM as an essentially surface characterization technique. For probing the interior structure of materials X-ray scattering techniques was applied to probe the bulk structure of the nanocrystals. For the here used PE nanocrystals it was found that the nanocrystals essentially consisted of individual single crystals having single crystalline lamellae of thickness ~ 6 nm covered by two amorphous regions from both sides of thickness $\sim$ 1 nm, confirmed both by small angle X-ray scattering measurements but also cryogenic transmission electron microscope [16].

This work focused on the morphological evolution of polyethylene nanocrystals deposited within self-organized regular patterns upon thermal annealing and recrystallisation of the undercooled melt of these nanocrystals. The motivation of the project is divided into two parts. Firstly, we developed way to organize the polyethylene nanocrystals from an aqueous dispersion into ordered patterns on a solid surface, providing a well defined initial organization of the nanocrystals which enables us to observe the thermally induced morphological changes quite easily. Secondly, we were interested in reorganizing the nanocrystals by applying thermal energy below the melting temperature of the nanocrystals and to follow the changes (especially of the lamellar thickness) which occurred within the deposited nanocrystals as a function of temperature and in time. Finally, we were interested in inducing crystallization within the undercooled melt of these polyethylene nanocrystals as a function of temperature and time.

By monitoring the semi-crystalline morphology in static conditions (*i.e.* at a given constant temperature) but also in the course of heating, we attempted to reveal the thermal behavior of these crystals. In this work, optical microscopy in reflection mode, room temperature AFM and in-situ hot stage AFM techniques were mainly used. These microscopy techniques provided fruitful structural information of the crystals which improved our understanding of melting

and crystallization of such nanoscopic systems.

1.2 Outline of the thesis

The **second chapter** is devoted to a general introduction of concepts of polymer crystallization. It focuses on the role of the surface free energy in the formation of crystalline lamellar structures and in defining their thermal stability. The system selected for the study is an aqueous dispersion of polyethylene nanocrystals; we studied the thermal behavior of well-organized structures of lamellar crystals of nanometer length. Starting from the very early investigations on polymer crystallization, we will focus on the advancement of the crystallization studies by explaining several proposed models and how they succeeded and failed in explaining the underlying basic mechanism. We believe that the main originality of this study concerns the morphological characterization of the system on a molecular scale during stepwise increase in temperature and also during slowly cooling the sample from an undercooled melt.

In the **third chapter**, the synthesis and the crystalline structure of the polyethylene nanocrystals will be explained elaborately. The crystalline lamella represents the basic structural entity of the semicrystalline polymer structure. Detailed information about the crystalline structures of our nanocrystals will be presented. Different strategies of deposition of the crystals are explained in detail *e.g.* coffee stain phenomena and different techniques to confine drops of colloidal solution under restricted geometry will be introduced. The approach we followed for our system *i.e.*, deposition inside a PTFE ring or meniscus driven evaporation technique will be discussed in detail. The floating behavior of the nanocrystals at the air-water interface on a Langmuir-trough will be described. Optical microscopy (OM) and atomic force microscopy (AFM) studies were used to explain regular patterns formation on the substrate, sheding light on the physics involved in the stick-slip regime. Working principle of OM and AFM will be described. Their usefulness along with the importance of phase imaging AFM will be explained.

In the **fourth chapter**, we will be interested in the details of the morphological evolution of the deposited polyethylene nanocrystals during temperature annealing. The different structural changes of the deposited nanocrystals at different temperatures observed in situ by AFM for a monolayer of crystals and also for stacks of several layers will be discussed in this context in detail. The path-

ways which were followed during the reorganization processes upon annealing will be presented. Time evolution of morphologies at different temperatures will also be discussed.

In the **fifth chapter**, we will discuss the recrystallisation from a melt of polyethylene nanocrystals cooled slowly. Well-aligned edge-on crystals were found to crystallize perpendicular to the scan direction of the AFM tip. The mechanism of tip-induced nucleation will be described in detail. How nucleation probability is affected by various tapping forces and number of scans will be described. It will be shown that time of contact between molten sample surface and the AFM tip was found to have no significant influence on the nucleation probability. It will be shown that even in regions consisting of few molten droplets of different sizes at a temperature close to the melting temperature, well aligned edge-on crystalline domains along the scan direction can form. The formation of stacks of edge-on crystalline lamellae will be explained.

In the **sixth chapter**, the overall conclusions of the thesis will be summarized.

Seventh chapter will contain appedix to give some information about the tip-induced crystallisation studies.

Chapter 2

General aspects of polymer crystallization

2.1 Introduction

In the context of the main focus of this study, *i.e.* the polyethylene nanocrystals, we highlight mainly the influence of small lamellar thickness ($\sim$ 8-10 nm) with respect to their differences to the other systems. The Gibbs-Thomson equation of melting-recrystallization of polymer crystals is discussed in detail, sheding light on the very high surface to volume ratio of the small nano-sized crystals. Strobl´s model of polymer crystallization (multi-step process) will be explained along with a discussion of the crystallization and melting line. Consequences of Strobl´s model will be presented on the basis of some proposed kinetic approaches for the basic understanding of the mechanism of polymer crystallization. The mechanisms of chain unfolding in the course of thermal annealing in our case will be illustrated.

2.2 Polymer and Crystallisation

A polymer is a large molecule (macromolecule) composed of repeating structural units. These subunits are typically connected by covalent chemical bonds and known as monomers. The number of subunits is called degree of polymerization N. Most real systems are polydisperse [34,35], *i.e.* they have due to the production process (synthesis) a more or less broad distribution of N. In the year 1920, polymer crystallization was first confirmed when the X-ray diffraction studies were performed on synthetic and natural polymers [36]. The Bragg reflections were broader in comparison with low molecular mass compounds and inorganic materials. In the melt synthetic polymers consist of long chains with variation of the chain length, with a high degree of chain interpenetration and entanglement. So, it was not easy to understand the mechanisms of crystallization in such systems during cooling. Crystallization changes the physical and mechanical properties of polymer systems remarkably. It is important to note that crystallization is not limited to linear polymer chains such as polyethylene (PE) and polyethylene oxide (PEO), but also occurs for more complicated polymer architectures such as brushes. In order to answer the most important question about the polymer crystallites, *i.e.*, how can long polymer chain be incorporated in small crystallites, the chain-folded model was introduced and widely used.

2.3 Chain-folded lamellae

In the year 1938, Storks made electron diffraction measurements on gutta percha films of 27 nm thickness (prepared by evaporation from solution). He found that, the total chain length was much larger compared to the film thickness. He observed that, the films were composed of large crystallites with the chain axis normal to the plane of the film. So, the only possibility was that, the chains folded back and forth upon themselves so that neighboring segments were oriented parallel to each other [37]. This observation led him to first propose a chain-folded structure to explain the crystallization in such kind of systems.

In the 1950s, after the generation of small single crystals from dilute solution, it was found that these crystals are regularly shaped and their lateral

dimension was found to be up to 0.3 mm. But their thickness was found to be only 12 nm. In polarizing microscope, when they were rotated between crossed polarisers they produced uniform darkness at a certain angle confirming that they are really single crystals.

Crystallization from highly concentrated solution or from polymer melt can give rise to several structural evolutions ranging *e.g.* from a multilayer aggregate of lamellar crystals spreading out from a common edge, dendrites to spherulites. The chain folding was first evidenced by works of Keller [38]. In the year 1957 based on electron-diffraction patterns, Keller [38] commented that the direction of the polymer chains runs perpendicular to the basal plane of the crystals and since the length of the polymer molecules exceed by many times the crystal thickness, the polymer chains must be folded many times. The phenomenon of folded-chain crystallization in polymer molecules is a subject of interest within polymer scientists.

Compared with literature studies of bulk PE, the lamellar thickness L_c (for a given polymer of known length, a measure for the degree of folding is the thickness of the crystalline lamellae: the thinner these lamellae are the more folded are the polymer chains) is very small for our nanocrystals which is due to the low temperature of synthesis (15 °C). The crystallization has thus occurred more than 100 °C below the melting point of polyethylene. This extreme supercooling is not accessible by any other method used so far for the crystallization of polyethylene. It results in a higher degree of chain folding into thinner lamellae (the nanocrystals consist of eight chains with several hundred folds per molecule). Consequently, these nanocrystals are highly metastable and therefore will exhibit a strong tendency to change their morphology. Number of folds in the polyethylene nanocrystals was measured using the numerical values of the molecular weight of the polymers of the nanocrystals ($\sim$ 2 x 10^5 g/mole) and a molecular weight distribution or polydispersity index ($\sim$ 2 (M_w/M_n)) in the following way. The maximum length of the molecule in the fully extended form can be calculated by the following formula, $L = \ell_m.N$ where, ℓ_m is the length of a repeat unit. For polyethylene, it is $\sim$ 2.6 $\mathring{A}$ or (2.6×10^{-10} m). N is the degree of polymerization which is the ratio of the total molecular weight of polymer and molecular weight of the monomer unit *i.e.*,=200000 /28 =7143. So, the fully extended chain length for the polyethylene forming the nanocrystals is 7143 x 0.26 = 1857 nm.

The initial lamellar thickness is $\sim$ 8 nm for our nanocrystals. The number

of folds was found to be equal to 1857nm/8nm= 230 to 240, meaning the polymers forming the crystalline lamellae are folded several hundred times.

2.4 The melting temperature

The equilibrium melting temperature T_m^o is defined as the melting temperature of an infinite stack of extended chain crystals, large in directions perpendicular to the chain axis and where the chain ends have established an equilibrium state of pairing. This quantity is one of the most important thermodynamic properties of crystallizable chain polymers, as it is the reference temperature from which the driving force for crystallization is defined. The change in Gibbs free energy ΔG per unit mass at T_m^o is zero. This is the general condition that determines the melting point of any substance. The thermodynamic driving force for crystallization from a liquid or melt to the folded chain conformation of a crystal at a particular crystallization temperature T_c can be expressed as,

$$\Delta G = \Delta H - T\Delta S \tag{2.1}$$

$$\Delta G = \Delta H[1 - T(\Delta S/\Delta H)] \tag{2.2}$$

Where, ΔH is the increase in enthalpy per unit mass and ΔS is the increase in entropy per unit mass.

At the equilibrium melting temperature, T_m^o, $\triangle G = 0$ and

$$T_m^o = \Delta H/\Delta S \tag{2.3}$$

From equation (2.2) and (2.3) we can write,

$$\Delta G = \Delta H(1 - T/T_m^o) \tag{2.4}$$

At a fixed crystallization temperature T_c, the change in Gibbs free energy which initiates the crystallization can be written as,

$$\Delta G = \Delta H(\Delta T)/T_m^o \tag{2.5}$$

Where, ΔT represents the super cooling, $\Delta T = (T_m^o - T_c)$

Polymers with high ΔH and low ΔS have a higher melting point than those having high ΔS and low ΔH. For any crystallite, the total Gibbs free energy can be given by the combined value of the part which is proportional to its volume and parts for which extra energy is involved due to the formation of its surface. For large crystallites, volume to surface area ratio is large and so the contribution due to the surfaces becomes negligible compared with that due to the volume. But for small crystallites the volume to surface area ratio is small and so the surface energy contributes significantly to the enthalpy. So, the effective enthalpy per unit mass is higher. This implies that the increase in enthalpy required to melt the crystallite is lower and if we assume that ΔS is independent of temperature, then we will have, T_m (small crystals) $< T_m$(large crystals).

2.5 Gibbs-Thomson equation: Melting of polymer crystals

The Gibbs- Thomson equation can be represented as,

$$T_m = T_m^o - \frac{2\sigma_e T_m^o}{\rho \Delta H_f l_c} \tag{2.6}$$

σ_e is the surface energy of basal plane per unit area, ρ is the density of the crystallites and ΔH_f increase in enthalpy per unit mass on melting for a thick crystal. This equation helps us to measure the value of equilibrium melting point (T_m^o) and surface energy (σ_e).
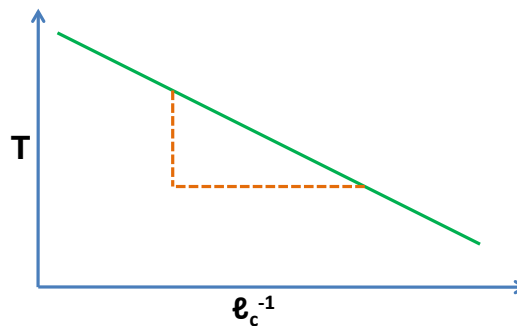
Figure 2.1 – Showing the scheme of the Gibbs-Thomson equation *i.e.*, the temperature is plotted as a function of inverse lamellar thickness.

These quantities can be determined from the plot of melting points as a function of inverse lamellar thickness *i.e.* T_m Vs. $1/\ell_c$. From the slope of the plot, the surface energy (σ_e) can be determined and the equilibrium melting temperature (T_m^o) can be computed from the intercept of the plot. The lamellar thickness can be measured *e.g.* by SAXS measurements or TEM measurements and the DSC measurements normally give the value of T_m.

After the discovery of the folded chain model, scientists tried to explain the consequence of the regularity of chain folding. Two important theories were proposed which were in good agreement with the experimental results. The first theory was proposed by Fischer saying that the fold period is determined thermodynamically corresponding to a minimum in the Gibbs free energy density of the crystal at crystallization temperature. The second theory proposed by Lauritzen [39, 40] and Hoffman [40] is based on a kinetic approach. They considered that the lamellar thickness corresponds to the crystals which have fastest growth rate and it could be that this is not the most stable conformation of the crystals. The extended chain conformation would be the most stable conformation of a crystal but still the question arises, why do polymer chains fold upon crystallization instead of choosing the extended chain conformation. This simple question can be answered by making the argument that the kinetic energy barrier towards the folded chain conformation is lower and therefore this process occurs faster in comparison to the case of extended chain crystals. As a result, the Gibbs free energy for a folded chain is higher than that of equilibrium extended chain crystals and so the melting temperature of the folded chains crystals is lower. So, we can say that crystallization is a kinetically controlled process. For long chains, the equilibrium state, represented by a lamellar crystal consisting of fully extended chains, [41] is never reached.

From the thermodynamic point of view, we can say that the Gibbs free energy of any type of polymer crystal below their melting temperature is always lower compared to that of a liquid.
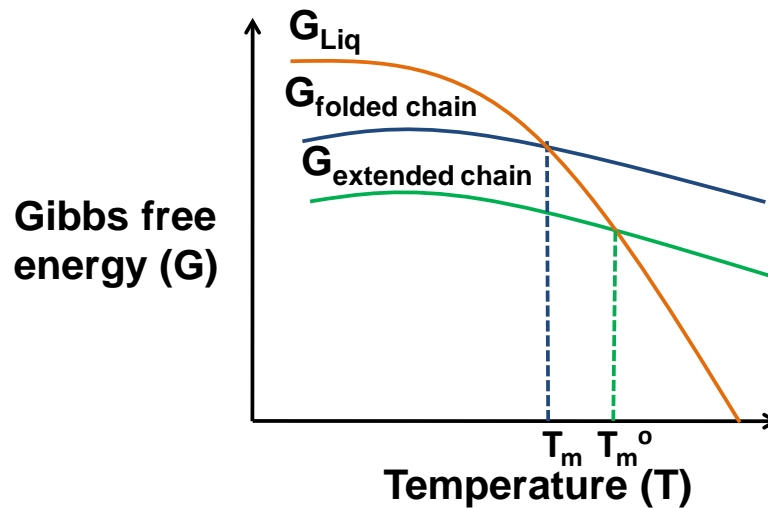
Figure 2.2 – Schematic showing the variation of Gibbs free energy of a liquid, a folded chain crystal and an extended chain crystal with temperature.

At constant temperature and pressure, the required condition for a spontaneous phase transition is that the change in Gibbs free energy ΔG of the process has a negative value. For polymer lamellar crystals, we have to specify the difference between the equilibrium melting temperature T_m^o and the nominal melting temperature T_m as it is dependent on the fold length and consequently the lamellar crystal thickness. So, the fold surfaces contribute the larger part to the surface energy, both because they are much larger in area than the other surfaces and because the surface energy per unit area is much higher owing to the high energy required in order to form these folds.

2.6 Theories of chain folding and lamellar thickness

The way polymers crystallize is often quite different from the pathway followed by small molecules. When a metastable liquid of small molecules undergoes a phase transition into a crystal, the mechanism of this ordering process is considered to be nucleation and growth. One can thermodynamically understand a first-order transition as a relaxation of a metastable melt towards the equilibrium state which requires overcoming a free energy barrier. The height of this barrier depends on the depth of penetration into the metastable state or undercooling (ΔT). In order to introduce a new phase into the metastable melt interfaces must be introduced. This is a nucleation process where the density fluctuations are localized with large amplitude. If the resulting nuclei are larger than a critical size, they continuously

grow towards a stable crystalline phase. According to the nucleation theory, for a single component system, the nucleation barrier from melt to crystal transition does not vanish with temperature. So, the liquid phase is metastable [**42, 43**].

In this small molecule case, the characteristic size of the molecule is much smaller than that of the crystal nucleus. The situation is more complicated if the small molecules are connected together to form polymer chains. Clearly, the ability of different portions of a long polymer chain to take part in different initial nuclei makes the situation difficult (due to the connectivity of the monomeric units in a polymer chain) as this process is associated with entropic frustration (polymer crystallization is frustrated by relatively large free energy barriers, which arise from the necessity to reorganize polymer conformation into ordered states) and leads to incomplete crystallization where polymer chains fold back and forth to form crystalline lamellae. The chain folding problem requires the understanding of entropic frustration associated with chain connectivity. All the kinetic mechanisms involve clear phase boundaries between ordered crystals and disordered liquid phase.

In describing crystallization of polymer chains from melt or in order to understand the process of lamellar growth two approaches have been used. They are the well known Lauritzen-Hoffman secondary nucleation theory [39, 40] and the Sadler´s [44] rough surface or entropic theory introducing the idea that the free-energy barrier might actually be entropic rather than enthalpic in nature. Further developments along these lines by Sadler and Gilmer led to this type of theory being called the Sadler–Gilmer theory [45]. The concept of both models is dealing with the free energy barrier but the nature of the barrier distinguishes these two kinetic theories. L-H theory [39, 40] considered the free energy barrier to be enthalpic while S-G theory [45] explained it to be entropic.

In L-H theory [39, 40], the most important contributions to the free energy barrier are the surface energies of the crystallites, including the high surface energies associated with the folds in the lamellar surfaces. So, the energy barrier is thus mainly enthalpic. In L-H theory it was assumed that once a chain segment has laid down on growing surface parallel to the chains already forming the crystals growth face, the next units of the chain continue to be laid down to form a straight stem. At the lamellar surface, the chain folds and the following units are laid down adjacent to the section previously laid down until the other face of the lamellae is reached when chain folding takes place again. The whole process requires the orderly laying down of segments of length ℓ one after another to form

smooth flat growth faces, no new layer is started until the previous layer is complete. So, regular chain folded lamellae are formed. In the LH theory [39, 40], this first step is considered as the rate determining step as it is associated with the highest energy barrier. The magnitude of this barrier increases with the lamellar thickness (ℓ). In the second step, the segments become crystallographically registered. In the next steps, subsequent stems fold back and again sediment adjacent to the attached stems which again lower the overall free energy. This process continues to happen until reaching a negative free energy change. Certain free energy change associated with this sequential folding process. LH theory [39, 40] treats the attachment of the stems onto the substrate as a one-step process and ignores the entropic behavior of the nucleation process and subsequent spreading of the stems in the early version of this theory. Later, the segmental nature and entropic origin of the initial surface nucleation process have been considered by Hoffman [39]. In the LH model [39, 40], since there is no new lateral surface generated during completion of the rows, the only free energy barrier during this process is associated with folding (*i.e.*, creation of the fold surface). In addition, this free energy contribution is not related to the lamellar thickness, therefore, the substrate completion process weakly depends on the undercooling, as compared to the surface nucleation process which has an exponential dependence on undercooling. The main fact of the LH theory [39, 40] is that it describes the kinetics of crystallization in molecular terms, for linear flexible macromolecules which are crystallized from the melt into chain folded lamellae. In this theory the structures which evolves is one which develops with the highest rate. This maximum is reached for a crystal thickness just above the stability limit of the crystallites as determined by the Gibbs-Thomson equation.
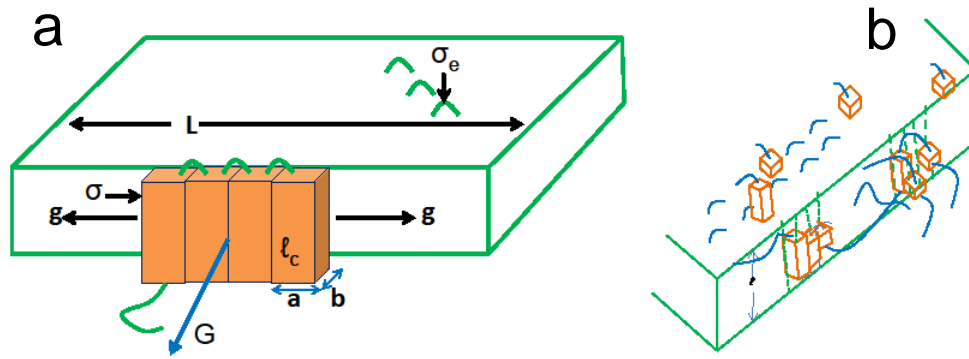
Figure 2.3 – (a) Model of surface nucleation and growth of chain folded crystal. The surface nucleus composed of n stems of length ℓ_c, thickness b and width a, forms on a substrate and proceeds towards the lateral direction with a growth rate g. The surface nucleus then completes a layer of thickness b by covering to crystal width L. This caused the crystal to grow in the G direction. (σ) and (σ_e) are the lateral and fold free energies respectively. Inspired from ref. [39, 40] (b) The Sadler–Gilmer model without any perfectly regular fold surfaces, inspired from ref. [46].

The S-G theory [**45**] was introduced in recognition of the fact that curved growth faces are sometimes observed. This curvature implies steps on the growth surface and is inconsistent with the basic L-H theory [39, 40]. In this theory, units consisting of straight segments of chain containing only a few monomers are imagined to be laid down on the growing crystal face parallel to the pre-existing chains. These units can be added to the places according to a rule which is taking into account the fact that the unit belongs to polymer chains and may thus be connected to the other units, otherwise they are chosen randomly. Several islands of partially crystallized units can exist simultaneously on the growing face and units can even add to incomplete layers. The energy of the interaction of each unit with the surface is only of order kT, so that units not overlaid by others can detach again. Groups therefore attach and detach randomly, but subject to the rules, they take up the required straight conformations that permit the close fitting of groups and the lowering of the energy of the interaction between them. There is thus an entropic barrier, a barrier due to disorder that must be surmounted before the free energy can be lowered. It is clear that the longer the straight segments are the higher this barrier will be [46].

In spite of the large differences in many aspects, atomically smooth or rough growth faces, nucleation or reversible attachment-detachment processes, short-chain sequences or whole stems as elements, the two approaches have one basic feature in common: It is assumed that the lamellar crystallites grow directly into the entangled melt. The growth face sets the border between the crystal and

the melt, and crystallization proceeds by a movement of the face. In a general view the assumed mechanisms agree with those found for single crystals of low molar mass compounds. When crystallized from the melt one there can also find layer-for-layer growth if the growth face is atomically smooth, beginning for each new layer with a nucleation step, or "normal growth", if the growth face is rough, being determined by the balance between the rates of attachment and detachment of single molecules.

Depending on many experimental evidences [47–50] it was proposed that the formation and growth of the crystallites is not a one step process proceeding directly into the melt but follows a route over intermediate states. Thus, considering the experimental basis as reliable and broad enough, a novel model of polymer crystallization was proposed.

2.7 Strobl´s model: a multi-step process

Strobl´s model suggested that crystallization from the entangled melt is a multi stage process but not a one step process [51]. It explains that in the first step there a mesomorphic layer is formed by density fluctuations, where the chains have a preferred orientation but also have liquid like mobility. The thickness of this mesomorphic layer increases until a critical thickness is reached. At this stage the chains within the mesomorphic layer cooperatively transform into a granular crystal layer. Finally these granular crystalline blocks joined together to form a continuous lamellar crystal. Pre-ordering phenomena within the melt are assumed to play an important role in this process.
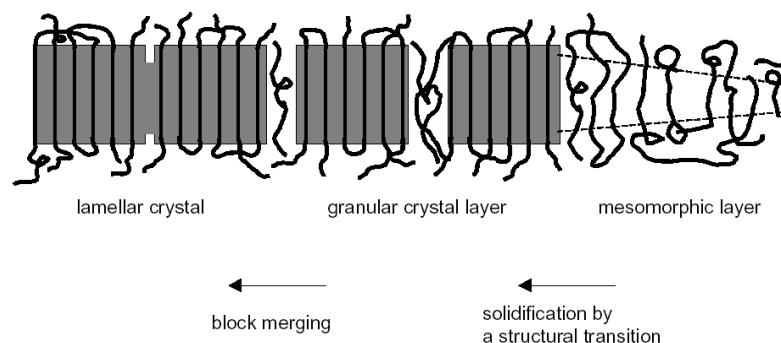
Figure 2.4 – Schematic of the two step model proposed for the formation of polymer crystallites [inspired from Strobl´s model in ref. [51].

2.7.1 Crystallization and melting lines

Considerations about mechanisms of crystallization and melting in polymers require as basic knowledge of the variation of the crystal thickness ℓ_c with the crystallization temperature T_c and the variation of the final melting temperature T_m with crystal thickness.

Time and temperature-dependent SAXS experiments make it possible to determine these relationships and have been carried out for several polymer systems. Investigations were facilitated by the invariance of the crystal thickness during the crystallization process.

The Gibbs–Thomson equation described in **equation (2.6)** suggests plotting the melting points as a function of the inverse crystal thickness ℓ_c^{-1}, and the same representation was then also used for the relation between T_c and ℓ_c. The appearance of the plots is typical of all the samples investigated: two straight lines that cross. The 'melting line' that gives the relation between T_m and ℓ_c^{-1}, confirms the Gibbs–Thomson equation. This allows a determination of the equilibrium melting point T_m^∞ by a linear extrapolation to $\ell_c^{-1} = 0$. The novel feature in the results is the 'crystallization line' which gives the relation between T_c and ℓ_c^{-1}. It has a greater slope than the melting line, intersects the latter at a finite value of ℓ_c^{-1}, and approaches a limiting temperature as $\ell_c^{-1}, \rightarrow 0$, denoted T_c^∞ which differs from T_m^∞. The crossing implies that, the T_c^∞ is always greater than T_m^∞.

Few results derived from temperature dependent measurements during heating [49, 52] led Strobl to an important conclusion concerning the popular Hoffman–Weeks plot. Many authors derived equilibrium melting points of crystallizing polymers from DSC studies, plotting the temperature difference $T_m - T_c$ against T_c and identifying the equilibrium melting point with that crystallization temperature where the temperature difference would vanish. Strobl´s results demonstrate that this procedure is wrong. It yields the temperature of the intersection point between the melting and the crystallization line rather than T_m^∞.
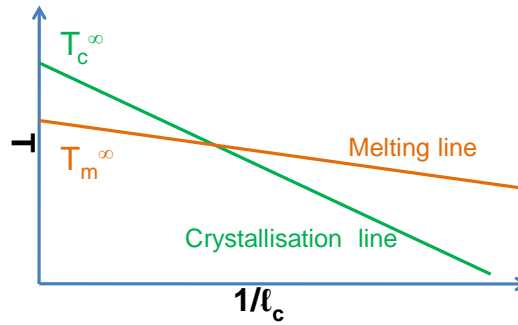
Figure 2.5 – Crystallization (green) and melting line (orange) versus the inverse lamella thickness.

What is the meaning of this state diagram then? The melting line describes the thickness dependence of a phase transition that leads from the crystalline to the isotropic amorphous state. Obviously the crystallization line has to be interpreted in an analogous way: It also represents the ℓ_c dependence of a structural transition, but since $T_c^\infty \neq T_m^\infty$, certainly not one between the crystalline and the amorphous state. Those parts of the structure which melt immediately above T_c experience exactly this transition. The state diagram **Figure 2.5** is therefore an indication for a crystal development in two steps: Crystallites first appear in an initial form which then transforms into the final lamellar crystallites. The latter process provides the stabilization expressed by the temperature differance $(T_m - T_c)$ and it occurs without a change in ℓ_c.

Lamellar crystallites principally exist only at temperatures below the melting line. Therefore, crystals with thicknesses given by the crystallization line can no longer be formed when the temperature of the intersection point is approached. This has indeed been confirmed by experiments [51, 53].

2.7.2 Consequences of the multiphase model

Polymer crystallization is a thermodynamically first order transition. Generally, during crystallization, a favorable enthalpic change leads to the attraction of the molecules to overcome the phase boundary and their subsequent incorporation into the crystals. This is opposed by the loss of entropy which results from the above mentioned steps. This view leads to think about multiple steps in polymer crystallization. Among these steps the rate determining step is the one necessary for overcoming of the nucleation barrier and thus growth is nucleation controlled. Crystallization of many molecules involves at least a partial disentanglement of

these chains.

Independent of the condition for crystallization, *i.e.*, whether one crystallizes from solution or melt; the polymer chains fold back and forth in the crystalline lamellae. The free energy of a folded state results from attraction among non-bonded monomers and loss of bending along the chain backbone. Different folded states of the crystalline polymer have different free energies and must be separated by barriers.

In Strobl´s model the validity of L-H [39, 40] model and S-G models [**45**] is questioned.

A specific pathway of one polymer chain among many others during crystallization in the melt may include several major steps, as indicated by Strobl [51].

It was demonstrated that the kinetics in the very early stage of crystallization is controlled by nucleation and growth directed and not by spinodal dynamics. According to the nucleation and growth mechanism, one starts with the birth of a baby nucleus in the early stages of homogeneous crystallization. Free energy barriers indicate the initial lamellar thickness. Once this baby nucleus has formed, chains diffuse to the growth front where they adsorb and crystallographically attach. This step is not hindered by a barrier, in contrast with the underlying assumptions of the LH theory [39, 40].

If several molecules take part to this adsorption process, a thin layer of molecules in front of the crystal can be formed, but these molecules do not form a mesophase. During or shortly after the adsorption, multiple selection processes take place, which determine whether the adsorbed part of a particular polymer chain is accepted or rejected by the growth front on different length scales. These selection processes must be sequential and cooperative.

The detailed scheme of multiple-steps in polymer crystallization proposed by Strobl [51] gives rise to several questions which needed to be further discussed. Actually, in front of a growing crystal face, there should be a thin adsorption layer rather than an independent mesomorphic phase as the latter can give rise to two difficulties. Firstly, in the case of PE, when the hexagonal mesophase grown at an elevated pressure transforms to the orthorhombic crystal. This can give rise to twinned symmetries having three equivalent orientations 120 º apart from each other. PE spherulites, however, always grow with the b-axis in the radial direc-

tion, as pointed out by Lotz [54], and no twin symmetry can be found. Another difficulty is how to account for thermodynamic function changes, such as enthalpy and density changes, in these two separated phase transitions proposed by Strobl [51] (from the melt to the mesomorphic phase and from the mesomorphic phase to the crystal) to elaborate one crystallization process. In Strobl's contribution, the proposed granular crystal to lamella growth deals with length scales of a few tens of nanometers. It is viewed as a construction mechanism of polymer crystal lamellae [51]. The granular structure, which has been reported for several semicrystalline polymers, is obtained in almost all the cases under specific crystallization conditions. Generalization of this structure depends critically on providing explanations consistent with the necessary regular arrangement of chiral conformational handedness in lamellar crystals [54] and the periodic banded spherulitic formation without the existence of a lamellar continuity. Experimental evidences shows that facetted or nearly facetted single crystals and aggregates of various polymers can be grown in bulk, thick and thin film melts, and blends in broad ΔT regions, yet no granular structures have been reported [**12, 55–60**]. Regarding the granular structure, another question can be raised regarding the extrapolation of the Gibbs-Thomson equation used in Strobl's contribution [51]. This extrapolation used in polymer lamellar crystals was based on the assumption that the metastability of the polymer lamellae is only associated with one-dimensional thickness (an extrapolation of the crystal volume must be used in the original Thomson-Gibbs extrapolation). If the T_c line represents the granular crystals with the same crystal structure as the final lamellar crystals, the assumption using one-dimensional lamellar thickness as the marker of the crystal metastability is not valid. Both the thickness (ℓ) and lateral size (a) of the granular crystals need to be considered when extrapolation is carried out. This requires a two-dimensional extrapolation in a $T_m - 1/\ell - 1/a$ three-dimensional space.

It is necessary to understand the nature of the free energy barrier between various folded states. We need to explain the finite number of chain folds in solution-grown lamellae, the temperature dependence of lamellar thickness and the kinetics of lamellar thickening. How do backbone stiffness (as measured by the characteristic ratio c_∞) and liquid-crystalline nature of stiff backbone segments influence the free-energy landscape? Do these liquid-crystalline tendencies promote a mesomorphic state prior to the formation of lamellae or within the lamellae? Is there a critical chain length below which extended chain crystals form, and above which chain folded lamellae form with or without a mesomorphic precursor? These open questions can be answered perhaps by computer simulations which may give some helpful insight into the nature of these barri-

ers.

In any effort to relate theory and experiments on polymer crystalliza-
tion, it is essential to know the quench depth and consequently T_m. T_m is usually
obtained by various extrapolation schemes [61] based on thermodynamic argu-
ments, but applied to a non-equilibrium system. In particular, there is no reliable
procedure to obtain T_m for copolymers. Marand [61] criticized Strobl´s model
by evoking the risk involved in extrapolating a temperature range above T_m for
the presence of a stable mesomorphic phase.

We did not find the answers of the questions mentioned above using
Strobl´s model. Strobl explained the phenomena of polymer crystallization into
only a few specific steps: the creation of mesomorphic layer as a precursor in all
systems, spontaneous thickening up to a critical thickness, and structural tran-
sition into granular blocks, followed by merging of granular blocks into lamellar
crystals. Lotz [54] mentions the danger in simplifying the crystallization process
in terms of a finite number of discrete steps. Nonetheless, Strobl´s model can be
very useful for making quantitative predictions for each of the four fundamental
steps and to compare them with experimental results for a variety of polymers.
Examples include chemical approaches for stabilization of the mesomorphic phase,
blocking the transition from the mesomorphic phase to the crystalline phase and
avoiding coalescence of granular blocks. It is essential to integrate the answers to
various questions mentioned above into such theoretical developments.

2.7.3 Theoretical studies on explaining mechanism of polymer crystallization

Muthukumar and his group have attempted to evaluate the underlying assump-
tions and ideas of the current growth theories mentioned above under different
conditions. They have approached various issues by a combination of tools. They
have performed Langevin dynamic simulations of many chains in dilute solutions
crystallizing into lamellae. These simulations [4, 62] were based on the united
atom model, and folded-chain-lamellae form due to a competition, mediated by
chain connectivity, between chain stiffness (arising from tensional energy) and at-
traction between non-bonded segments. Using the input from Langevin dynamics
simulations, they have performed coarse-grained simulations to follow the growth
of lamellae of thousands of chains, by using the Monte Carlo method. Further,
they [5] have derived thermodynamic results by using statistical mechanics of

polymer chains. The main results are summarized below.

The major result arising from their theoretical considerations is that chain entropy is the most dominant control parameter that distinguishes polymer crystallization from ordering of small molecules. The substantial reduction of conformational entropy of the chains during the ordering process dictates how the ordering proceeds. In addition, energy considerations used in the crystallization of small molecules must naturally be accounted for. It is the free energy of the system $E-TS$ (E and S being the energy and entropy, respectively) that determines the course of polymer crystallization and the nature of the ultimate crystalline states. The LH theory and its modifications focus on energy considerations. In contrast, Muthukumar's work has included the entropic contributions as well.

The manifestations of chain entropy were present at all temperatures, except at $T = 0$. Two major conclusions that emerge from considerations of free energy by including chain entropy are the following:

(1) The free energy landscape for a single lamella exhibits a set of barriers, many metastable states (separated by free energy barriers), and a globally stable state. Each of these metastable states has a thickness that is much smaller than the extended chain length. Among the metastable states, even the first reasonable state with its free energy just below that of the melt is long-lived, due to the barrier for thickening. The thickness of this long-lived metastable state increases with temperature, in a qualitatively similar manner to the Gibbs-Thompson law. However, if enough time is granted for this metastable state to evolve, then the equilibrium thickness would be reached for each temperature is approached. The equilibrium thickness decreases as the equilibrium melting temperature. The equilibrium melting temperature does not correspond to that of extended chain dimensions.

(2) The lateral growth faces a free energy barrier, due to temporal crowding of entangled chains at the growth front. The linear growth rate G assumes the form,

$$G \sim \left(\frac{D_{in}}{D_{bulk}} \right) exp \left(-\frac{1}{T \triangle T} \right) \left[1 - exp \left(\frac{\triangle H \triangle T}{k T_m T} \right) \right] \qquad (2.7)$$

Where ΔT is the quench depth, T_m is the melting temperature, ΔH is the latent heat of fusion, T is the temperature, D_{in} is the diffusion coefficient inside the growth zone with the barrier, and D_{bulk} is the diffusion coefficient away from

the zone. The first two terms on the right hand side become unimportant for small molecules and for dilute solutions of the polymer. These results are qualitatively different from the classical views on polymer crystallization. Although the new entropic model seems to capture the general trends of phenomenology, much more work is required to make quantitative comparisons with experimental facts. However, there is a promise of unification of ideas on crystallization from small molecules and from polymer chains.

2.8 Mechanism of chain unfolding upon annealing

Annealing of polymer crystals can lead to structural modifications taking place at different spatial scales. This evolution can be particularly complex because, as was shown before, the nanometer-thick crystalline lamellae form essentially metastable phases for which the melting point depends strongly on the lamellar thickness [63]. Therefore it is clear that annealing of semicrystalline materials below the melting point of the constitutive crystals could dramatically change their morphology.

The increase of the fold length by chain unfolding on annealing is undoubtedly one of the most extraordinary properties of chain folded polymer crystals. The process itself can be studied as a function of the two principal variables, annealing time and annealing temperature. The effect of temperature for two fixed annealing times was already demonstrated by Keller [64]. Fischer and Schmidt [65] made the first combined study of the two variables by examining the increase of the long-spacing (the average separation between stacked lamellar crystals, usually measured by small-angle X-ray or neutron diffraction) of polyethylene single crystals as a function of time for different temperatures. It was found that the long spacing increased logarithmically with time as described by the **equation: 2.8**

$$LB = LB_0 + B(T)log\left(\frac{t}{t_0} + 1\right) \qquad (2.8)$$

Where LB_0, is the long spacing at time t_0 and $B(T)$ is a constant corresponding to temperature T. This well known equation has been widely used to account for crystal thickening in the bulk many times in many cases.

Generally, the increase in fold-length directs the system towards the lowest Gibbs free energy, which is achieved for fully-extended chain crystals. However, the mechanisms of chain unfolding can strongly differ for various systems and annealing conditions. In our study, in the case of annealing of the deposited polyethylene nanocrystal, we will show the increase of the stem-length occurred via successive diffusion and aggregation of chain segments, leading to fewer crystals of different sizes. The bigger crystals are getting bigger at the expense of the smaller crystals. For the dry state of the crystals the recrystallization mechanism was first proposed by Kawai [66]. He observed from diffraction patterns that during unfolding the initial crystal orientation, including directions perpendicular to the chain axis, is preserved. This means that at no instant the memory of the original structure is lost during unfolding. Consequently, there could have been no full melting in any portion of the crystal. From many experiments it was evidenced that the overall thickness of melt-crystallized lamellae increases with increasing the annealing temperature. This behavior can be associated with additional crystallization of amorphous portions at the lamellar surfaces, mass transport within the crystal (point defects), or partial intra-chain rearrangement (perfection) of the chain without coordinated displacement of a molecule as a whole along its molecular chain. This can be described as 'fold dislocation' [67] and is accompanied by a discrete increase in lamellar thickness (see **Fig. 2.6**).
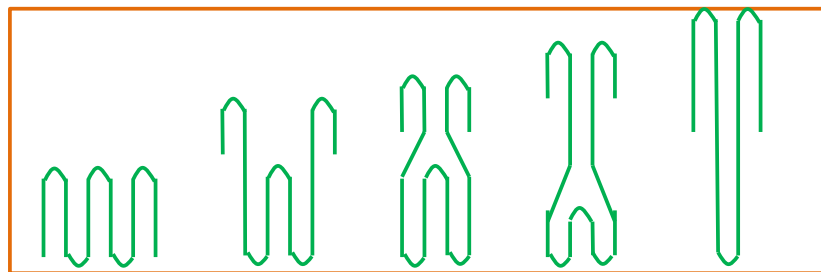
Figure 2.6 – Schematic of successive stages of the increase of stem-length in single crystals on annealing. Inspired from ref. [67].

As it has been said before that due to low temperature of synthesis, polyethylene nanocrystals, in our case, contain extremely folded polymer chains which thus are far from their thermodynamic equilibrium state [16]. Consequently, these nanocrystals will unavoidably change their morphology even when kept at temperatures far below their nominal melting point. The metastable folded chain crystals led to melt formation at a temperature which is well below the equilibrium melting temperature. A key reason for metastability derives from the small dimension of the crystals along the chain direction. In our case, the surface to volume ratio is extremely high for the nanocrystals as our nanocrys-

tals contain most likely single crystalline lamellae of ~ 8 nm thickness having a lateral dimension of ~ 20 nm. The melting temperature decreases as the surface-to-volume ratio of the crystal increases. However, polymer crystals consisting of folded molecules are able to increase their crystallinity by a reduction of the degree of chain folding with temperature or time. In most cases, molecular re-organization into less folded states improves the thermal stability of the crystal and shifts its melting temperature to higher values. In the presence of neigh-boring small nano-crystals, molecules may be exchanged between these crystals. Such exchange may lead to coarsening. Due to their lower surface-to-volume ratio, bigger crystals typically have a higher melting temperature than smaller ones. Consequently, instead of melting, crystals may coarsen and thicken and so increase their melting temperature.

In chapter four we will explain the morphological evolution in terms of lamellar thickness of such highly folded polyethylene nanocrystals as a function of annealing temperature and in time.

Chapter 3

Materials and instruments used, experimental techniques followed, and pattern formation on surface

The earlier chapter intended to give some basic ideas about polymer crystallization. We also have explained different theories of how polymer chains are crystallized from solution or melt. This chapter will contain some detailed information regarding the synthesis of the dispersion containing polyethylene nanocrystal and their crystalline structure. Some deposition techniques in order to form patterns with high regularity will be explained. The experimental set up we used in order to deposit the nanocrystals in an orderly manner is also included in this chapter. Along with the technique we discuss the process of regular pattern formation on a solid substrate as used in our studies. We will also briefly present the experimental instruments used to follow pattern formation in our system such as optical microscope and tapping-mode atomic force microscope.

3.1 Synthesis of aqueous dispersion of polyethylene nanocrystals

Because of interesting mechanical properties and low cost polyethylene has found many applications worldwide. It can be produced either by free radical polymerization, using high temperature and pressure or by metal-organic catalysts which are working in a water free environment. But now ethylene can also be polymerized in water with water soluble Ni(II) complexes [68–70]. Aqueous dispersions of polyethylene nanocrystals were prepared by catalytic polymerization of ethylene.

The aqueous dispersion of polyethylene nanocrystals was synthesized by the group of Prof. Stefan Mecking in the Chemistry Department of the University of Konstanz.

The purpose of using the synthetic procedure for generating nanocrystals had two advantages. Firstly, catalytic polymerization of ethylene in an aqueous medium led to well-defined colloidal particles. Secondly, these particles are suitable for fundamental studies of chain folding in polymer crystallization [71, 72]. This synthetic procedure represents a new way to prepare semi-crystalline PE under mild conditions of pressure and temperature. During this process, crystalline nanoparticles exclusively made of polyethylene are formed. Crystallization probably started while the chains are still growing at 15 ºC. However, it can not be excluded that the fast polymerization process and the slow nucleation in confined nanoparticles [73] might have prevented crystallization from starting before the polymerization was completed. Then polyethylene nanocrystals were formed in a melt at 15 ºC at 40 atm. Crystallization at such a high degree of super cooling has not been reported previously.

By a combination of cryogenic transmission electron microscopy (cryo-TEM [74, 75]) and small-angle X-ray scattering (SAXS [76, 77]) the structure and shape of the nanocrystals were determined. While cryo-TEM allowed studying the shape of the particles in a shock frozen solution, the analysis by SAXS allowed the in situ determination of the internal structure of the particles. By this complementary combination of methods, it was shown unambiguously that the produced polyethylene particles were single faceted nanocrystals and consisted of a lamella covered by an amorphous phase in which the PE chains fold back.

This novel way of generating polyethylene nanocrystals allowed the prepa-

ration of long chains of polyethylene in a well-controlled environment and at ambient temperature.

The system was prepared by catalytic polymerization as characterized previously [78]. The starting dispersion only contained PE (3.5 wt %) and just enough of the surfactant sodium dodecyl sulfate (SDS) to stabilize the particles against coagulation. Unlike typical free radical emulsion polymerization [78, 79] the particles appeared as a result of the polymerization in a non-solvent for the polymer. The surface tension of 65 mN/m of the dispersion (*i.e.* close to pure water: 72 mN/m) demonstrated that virtually all the surfactant was adsorbed onto the particles; no micelles were present in the system. The molecular weight of the resulting polymer was $2 * 10^5$ g/mol and the polydispersity as given by the ratio of the weight-average to the number average molecular weight of the polymer was ~ 2. These dispersions contained essentially separated, nano-sized crystals (lateral size $\sim$ 17-20 nm) consisting of a single crystalline lamella (thickness $\sim$ 6 nm) covered by thin amorphous layers (thickness $\sim$ 1 nm). Specimens for cryo-TEM were prepared by vitrification of a thin liquid film of the diluted dispersion supported by a copper grid in liquid ethane. Examinations were carried out at temperatures around 90 K. Hence, the particles were analyzed in situ, *i.e.*, in the dispersion. Moreover, no staining agent was used to enhance the contrast between the objects and the surrounding medium (for details of the general procedure of sample preparation cf. ref [75]).
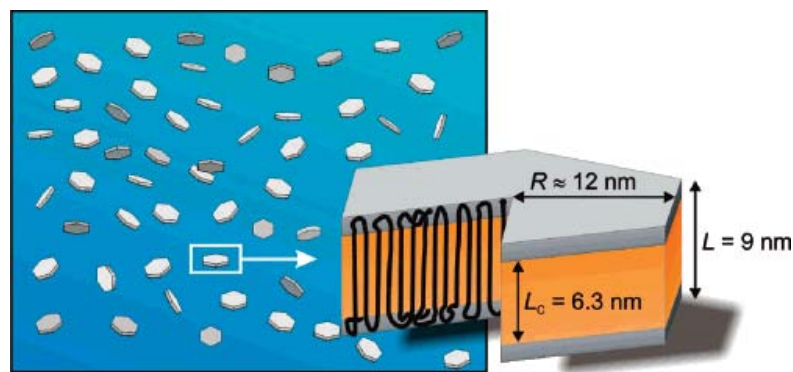
Figure 3.1 – Schematic of polyethylene nanoparticles in water. These particles consist of a single lamella with a thickness L_c of ca. 6 nm sandwiched between two amorphous layers resulting in an overall thickness of 8-9 nm (including the amorphous layers). Adapted from ref. [16].

As suggested by **Fig. 3.1**, many of these nanocrystals exhibited a truncated lozenge habit with a lateral dimension R. Colloidal stability of the particles is brought about by adsorbed molecules of the charged surfactant sodium dode-

cyl sulfate (SDS). For the sake of clarity, the adsorbed SDS-molecules are not shown.

3.2 Crystalline Structure of the polyethylene nanocrystals
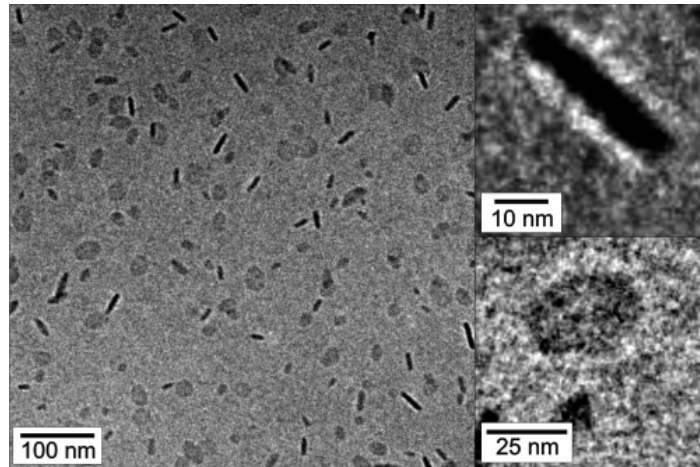
Figure 3.2 – Micrograph showing particles in dilute aqueous solution obtained from cryo-TEM measurements. Adapted from ref. [16].

Polyethylene nanocrystals are the main focus of our study. The aqueous dispersion consisted of flat platelets with a rather narrow size distribution. The different gray scales for different particles seen in **Fig. 3.2** resulted from different viewing angles. If the platelets are nearly parallel to the electron beam, the length of the optical path through the particles is much longer than for nearly perpendicular arrangement. From the cryo-TEM images a lateral dimension or the diameter of (25.4 ± 4.3) nm and a corresponding thickness of the platelets of (6.3 ± 0.8) nm have been determined [16]. These numbers were derived from the image analysis of 67 particles with approximately perpendicular orientation to the electron beam [16].

The nanoplatelets were interpreted as single lamellae of polyethylene with a lamellar thickness L_c of 6.3 nm. This thickness and the lateral dimension of the nanocrystals were confirmed by wide-angle X-ray scattering (WAXS) measurements performed on the dispersion at room temperature.

Due to the unknown tilt of each particle relative to the electron beam and a certain variation of shapes as shown by **Fig. 3.2** it was difficult to characterize the nanocrystals precisely. Nevertheless, most particles were found to contain

straight edges (faceted lamellae), and many of these appear hexagonal as shown in the figure inset (**Fig. 3.2**).

Polyethylene is a semicrystalline polymer [78,79], crystalline lamellae are covered by an amorphous layer. The amorphous layer in which the chains fold back exists on both sides of lamellae. This thin amorphous layer on both sides of the crystalline particles must be taken into account. Cryo-TEM was not able to detect this fact as the electron density of amorphous PE is virtually the same as that of the low density amorphous ice. Hence, there was not sufficient contrast between a possible amorphous layer and the surrounding medium. By applying contrast variation SAXS as an analytical tool this problem was solved. One can also see from **Fig. 3.2** that, the particles are well-dispersed in the aqueous medium and no aggregates were found. This was a prerequisite for a meaningful investigation by scattering methods in solution. The analysis technique of the particles by SAXS was elaborately described by Weber *et al.* [16]. From the measurements as shown by Weber *et al.* [16] it turns out that the thickness of the crystalline lamellae was 6.3 nm and the volume fraction of the crystalline part was determined to be $\phi_{cryst} = 0.70$. From the particle volume, the polyethylene density [79] and the chain molecular weight, it was estimated that each particle was made up of ca. 8 chains. The experimentally determined electron density value for the amorphous parts matches perfectly with the electron density value of low density amorphous ice (314 electrons/nm^3, cryo-TEM background; cf. the discussion of **Figure 3.2** taken from ref. [80]). Thus, it was concluded that the amorphous parts were virtually matched in the cryo-TEM. Scattering measurements also confirmed that colloidal stability of the particles was achieved by electrostatic repulsion between the particles brought about by the adsorbed surfactant SDS. So, a full structural analysis was achieved by the combined study of cryo-TEM and SAXS.

As discussed above, most of the observed nanocrystals were faceted. The shape of a macroscopic polymer crystal resulted from an anisotropic growth rate. Usually the edges correspond to the slowest growing crystallographic planes while the fastest growing planes will disappear during the crystal growth [75]. The basic habit of a PE crystal has the form a lozenge, defined by the slowest {110} planes. At extreme undercooling realized here, many nanocrystals have a truncated lozenge habit while no full lozenge shape has been found. The truncated lozenge habit may result from the very small size of these nanocrystals. The surface/volume ratio is indeed very high for such a small crystal and could result in the unusual equilibrium shape of a truncated lozenge.

Besides SAXS, which has been employed to study the crystalline structures, differential scanning calorimerty (DSC) also allowed to determine polymer crystallinity. DSC was also used for measuring the melting point of the nanocrystals.

3.3 Deposition procedures onto a solid substrate

The aim was to find a technique allowing to deposit the nanocrystals in an organized fashion from the aqueous dispersion onto a cleaned, solid substrate. With the here presented approach we succeeded to self-organize the nano-crystals in form of stripes after the complete evaporation of the solvent. In this part, we will discuss about several possibilities by which solutes of various sizes can be deposited on a solid substrate.

At the beginning spin coating was employed to deposit our nanocrystals onto Si-substrate but only unorganized structures of the nanocrystals or broad range of different patterns of the nanocrystals were left on the substrate, probably due to fast evaporation of the solvent. Spin-coated samples are regarded as being far from equilibrium systems [81, 82].

3.3.1 Coffee stain phenomena

The simple technique of drop deposition consists of placing a drop on a solid substrate followed by evaporation to the open air. Although evaporation in the vicinity of a three phase contact line may seem very simple, this problem is complex as there is a combined effect of hydrodynamics within the dispersion and evaporative mass transfer to the gas phase. The resulting dissipative structures are typically organized randomly without any regularity. An evaporative drop which contains nonvolatile solute forms a ring like precipitate on a solid surface. This phenomenon was termed as coffee stain effect [30–32]. As maximum evaporative loss takes place at the perimeter of the drop, all the solutes are transported to the edge by an outward hydrodynamic flow. Jamming of the solutes at the perimeter causes a local roughness which pins the contact line. Thus, a ring of diposits is formed. The requirement for a coffee stain effect to occur is that there must be a coupling of hydrodynamic flow inside the droplet and the possibility of the drop to be pinned at the contact line.
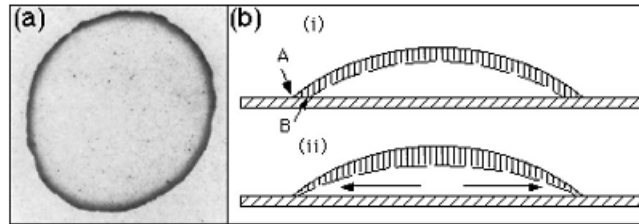
Figure 3.3 – (a) A picture of a dried coffee drop. The dark perimeter is produced by a dense accumulation of coffee particles. The radius is approximately 5 cm. (b) Schematic illustration of the origin of the advective current. (i) If the contact line were not pinned, uniform evaporation would remove the hashed layer, the interface would move from the solid line to the dashed line, and the contact line would move from A to B. However, if the contact line is pinned then the retreat from A to B is not possible, and there must be a flow that replenishes the lost fluid. (ii) shows the actual motion of the interface and the compensating current. Adapted from ref. [30].

A thorough study has been performed by Deegan *et al.* on the dynamics of drying drops [30–32] in particular on the self-pinning of the contact line on the substrate, from which coffee-stain-like drying lines originate (**Fig. 3.3**).

These coffee stains leave large and multilayered, often disordered aggregates and so it is not really of interest for our studies. Thus, drop-deposition method must be used in a controlled way in order to obtain homogeneous and ordered layers of self organized particles over an adequately large area.

3.3.2 Confinement of a drop, a restricting geometry

In recent years, scientists were interested in the consequences of confining the geometry of an evaporating drop. In order to confine a drop, several experimental set ups were used with the intention to form ordered patterns. Confining a liquid drop between two parallel plates and controlling the speed of the upper plate while keeping the lower plate fixed resulted in patterns of high regularity as the meniscus receded [19]. Highly regular patterns also have been produced by confining a drop of polymer (or nanocrystals) solution in a restricted geometry made of a spherical lens on a flat substrate named sphere-on-flat geometry [26, 27, 83–85]. Pattern formation during the drying of a colloidal suspension using capillary rise method has also been reported [86]. Moriarty *et. al.* proposed a meniscus-mediated evaporation technique [23] also to restrict the drop and to guide self assembly of gold nanoparticles.

(a) Meniscus driven evaporation process

We followed the same technique as Moriarty *et. al.* and deposited our nanocrystal dispersion in an ordered manner. The major aim of our work was to find a systematic way to control the evaporation of the solvent with good reproducibility. A novel technique for nanocrystals deposition was inspired by previous work on polystyrene spheres [87, 88]. For a solvent with appropriate wetting properties, such as water, a Teflon ring can be used for creating a meniscus of solution rather than a drop (see **Fig. 3.4**). Indeed, the wetting properties of the [solvent-Teflon ring-substrate] system are such that the affinity of the solvent with Teflon is lower than that with silicon oxide (the samples onto which the dispersion was deposited in this study were cleaned silicon substrates with a native oxide layer), hence the formation of a meniscus. Consequently, during evaporation, the solvent retracted from the centre of the sample towards the edge of the ring. It is important to note that although the ring could be clamped to the substrate like in [87, 88], in our experiments the ring was held in place by the capillary forces caused by the liquid. When the contact line reached a region close to the ring, evaporation encountered the competition of capillary forces, due to the presence of the Teflon ring, which traps the liquid. Consequently, evaporation was considerably slowed down in the region close to the ring, hence giving more time for the crystals to organize. The rate of evaporation in this configuration was mainly dictated by the capillary forces related to the presence of the Teflon ring. Noticeably, for a solution containing excess surfactant molecules, the onset of dewetting in the centre of the sample did not occur as rapidly as for a solution free of surfactants. But this, surprisingly, did not modify significantly the overall evaporation time. The duration of the evaporation in the meniscus technique is much larger compared to that in the spin-coating process (several minutes or more compared to a few seconds). Thus, samples prepared by this approach can be considered as being closer to equilibrium.
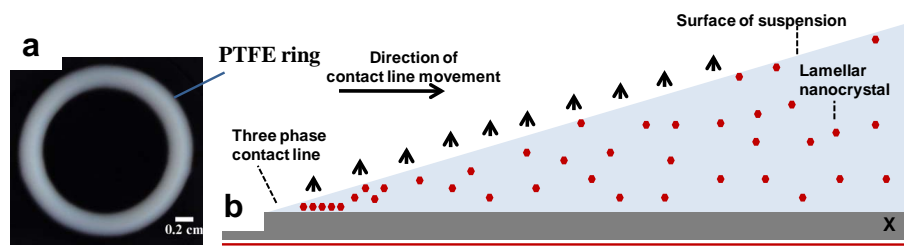
Figure 3.4 – (a) Experimental set up consists of a 1 cm inner-diameter Teflon ring on top of a silicon substrate filled with an aqueous dispersion of polyethylene nanocrystals. (b) Schematic representation of the retracting three phase contact line in the course of evaporative dewetting of a dispersion. The x-axis indicates the direction of evaporation from the center towards the bounding Teflon ring.

(b) Experimental requirements

As a starting point, an aqueous dispersion of polyethylene nanocrystals with a polymer content of 3.5 wt% was chosen for our study. The concentration of the dispersion was changed by adding deionized water to the stock solution. Mostly two different concentrations were used for our experiments. One is of 35 ppm (35 mg/L) and another one is of 70 ppm (70 mg/L). Sodium dodecyl sulphate (SDS) was present in our system as surfactant in order to avoid the coagulation of the nanoparticles. Imposing a circular geometry by means of a Teflon ring (inner diameter of 1 cm), we have deposited a small volume (ca. 0.2 ml) of the aqueous nanocrystal dispersion onto a clean silicon substrate ($\sim$ 1.5 x 1.5 cm^2). The whole set up has been kept at room temperature and left open to air for evaporation of water. Typically, the evaporation processes was completed within 30 – 60 minutes. Due to low-wettibility of water Teflon was chosen as a material for the ring used in our experiments.

(c) Reason for choosing the deposition technique

After deposition the capillary force acting at the inner edge of the Teflon ring created a long range liquid like meniscus rather than a drop. The meniscus mediated evaporation technique led to the formation of a thickness gradient which decreased gradually from the edge to the centre of the ring as shown in **Fig. 3.4b.** Evaporation started from the centre where the solvent-nanoparticle film thickness was thinnest and the contact line gradually moved towards the edge until all the solvent evaporated. To make sure that no solvent was left we kept every sample in room temperature and in a clean environment for at least one day. A high degree of reproducibility of the patterns formed was achieved by this technique

demonstrating that the meniscus driven control of the evaporation process and the associated capillary flow represented a useful process for creating ordered patterns.

In a single experiment, it was possible to span a large number of parameters.

Firstly, the evaporation was not steady or homogeneous across the whole surface and the speed of the contact line was not fixed. That is why near the centre the contact line pinned very irregularly. The contact line spent different times and moving a certain distance depending on the number density of the nanocrystals per unit volume in that region during the course of evaporation. Thus, stripes with various widths and heights were formed.

Secondly, the presence of nanocrystals led to repeated transient pinning and thus to a non-monotonic displacement of the retracting contact line. This stick-slip process resulted in the formation of micrometer-wide concentric annuluses. On a scale smaller than the diameter, these annuluses appear as parallel stripes. The formation of stripe patterns has been discussed in theoretical models [28, 89].

Thirdly, as the solvent evaporated and the liquid front moved towards the edge, the concentration of the nanocrystals in the dispersion increased. Thus in addition to a variation of the contact line velocity a concentration gradient was formed. At centre the concentration was lowest and at the edge it was found to be highest.

Finally, as evaporation was slow, in situ observation under an optical microscope was possible. For a given concentration of the dispersion and depositing the same amount of dispersion inside the ring, the evaporation time and the patterns formed were highly reproducible. That is the main advantage of this deposition procedure.

3.3.3 Floating of nanocrystals in air-water interface

When a monolayer is fabricated at the gas-liquid or liquid-liquid interface, the film is named Langmuir film. A Langmuir film can be deposited on a solid surface and is thereafter called Langmuir-Blodgett film (in the case of vertical deposition) or Langmuir-Schaefer film (in the case of horizontal deposition).

Using Langmuir-Schaefer technique we formed a homogeneous monolayer of the nanocrystals on hydrophobic/hydrophilic Si-surface. In a first set of experiments, a huge amount of the stock (3.5 wt %) dispersion ($\sim$ 500 µL) was spreaded and consequently, after transferring and characterizing by AFM more than one layer of crystals have been formed on the hydrophilic Si-surface. The patterns were similar to depositing the dispersion within Teflon ring *i.e.*, stacks of several layers over the whole Si-surface. But, these stacks of layers, were not well organized as we obtained in the meniscus-driven evaporation technique. This may be due to faster water evaporation rate in this case.

3.4 Characterization techniques

3.4.1 Optical Microscopy

The optical microscope, also known as the "light microscope", is a type of microscope which uses visible light and a system of lenses to magnify images of small samples. There are many complex designs of optical microscopes which aim to improve resolution and sample contrast. The microscope used for our study was a digital microscope which has a CCD camera and allows to store the images directly on a computer.

3.4.2 The imaging principle of an optical microscope

The principal of light microscopy is to shine light or reflect light from a sample through a specimen and examine it under magnification. The major optical parts of a microscope are the objective lens, the eyepiece, the condenser and the light source. The objective lens magnifies the object. The high degree of magnification of the objective lens results in a small focal length and the magnified image actually appears directly behind the objective. The eyepiece delivers this image to the eye or a charged coupled device (CCD) camera. The eyepiece enlarges the image but does not increase the ability to see fine details (*i.e.*, the resolution). The condenser focuses the light source on the specimen. The condenser also eliminates stray light and provides a uniform illumination. An iris diaphragm controls the amount of light reaching the specimen. In addition, the light intensity can also be controlled by adjusting the voltage applied to the lamp on some microscopes.

3.4.3 Applications of optical microscopy in our study

In our case, optical microscope was successfully employed to investigate samples in open air. This certainly makes it advantageous for our studies. We deposited a drop of aqueous dispersion of polyethylene nanocrystals inside a PTFE ring in order to confine the drop onto a cleaned Si surface. With the help of optical microscopy we followed the real time behavior of the evaporative dewetting of the confined drops containing nanocrystals. Applying interference of light reflected from the substrate and from the surface of the deposited structures, a series of parallel stripes representing segments of the concentric rings were found. We were also able to determine the spacing between stripes in different regions and the width of the resulting patterns on the Si-surface through OM studies (as will be discussed later elaborately). The quality of the images was highly dependent on the illumination. The amount of illumination was important for controlling resolution vs. contrast. Resolution and contrast are antagonistic in nature. Resolution was increased by increasing the amount of light. However, the brighter light led to a loss in contrast. We decided upon the optimal mix of contrast and resolution by adjusting the voltage (*i.e.*, intensity or brightness) of the lamp. We were also able to enhance the contrast of the images simply by increasing the exposure time. Even the difference between non-annealed and annealed samples was easily detected using optical microscope. From the above discussion it is very clear that studies through optical microscope were highly important in our case.

3.4.4 Atomic Force Microscopy

Atomic force microscopy (AFM) is a high-resolution type of scanning probe microscopy, with demonstrated resolution on the order of fractions of a nanometer, more than 1000 times better than the optical diffraction limit. G. Binnig and C. F. Quate [90] developed the atomic force microscope to measure the ultra small forces (even less than 1 μN) which are present between the AFM tip surface and the sample surface [90,91]. Tapping-mode atomic force microscopy was employed as the main analysis technique for our studies.

3.4.5 Working principle of atomic force microscopy

The AFM is one of the foremost tools for imaging, measuring and manipulating matter at the nanoscale [92–94]. Different material properties like topography, adhesion, stiffness, friction can be measured by AFM. The information is gathered by "feeling" the surface with a mechanical probe.

An AFM, in general, consists of a cantilever (see **Fig. 3.5 a**) with a sharp tip (probe) (see **Fig. 3.5 b**) at its end that is used to scan the sample surface. The cantilever is typically silicon or silicon nitride with a tip radius of curvature on the order of nanometers. The cantilever is fixed to a glass block, which is locked into the AFM during scanning.
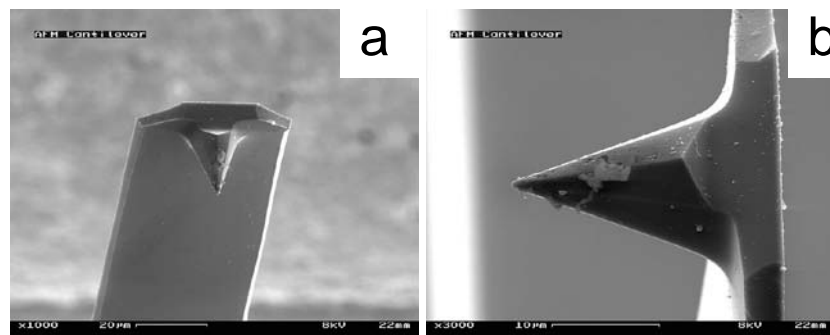
Figure 3.5 – Electron micrographs showing (a) an AFM cantilever and (b) a tip lying on the top of the cantilever. Taken from wikipedia.

The important thing about a tip is the material by which it is made of and the spring constant or the resonance frequency of the cantilevet the tip is attached to. For our measurement we used soft AFM tips made of silicon (type: PPP-NCL-W) obtained from NANOSENSORS. The silicon resistivity was about 0.01-0.02 Ω cm. The cantilever properties were given by its thickness (7 ± 1 μm), length (225 ± 10 μm), width (38 ± 7.5 μm), height ($10 - 15$ μm), resonance frequency ($146 - 236$ kHz) and force constant ($21 - 98$ N/m). The tips were not coated. The downward forces on the sample can be lowered by increasing the flexibility of the cantilever, resulting in less distortion and damage during scanning.

When the tip is brought into proximity of a sample surface, forces between the tip and the sample lead to a deflection of the cantilever according to Hooke's law. As the tip of the cantilever is scanned across the sample its motion is detected by a laser beam that must be focused onto the cantilever. The angle of

the reflected beam from the cantilever is detected by a four-segment photodiode. The reflected laser spot must be at the centre of the detector to give maximum sensitivity for imaging and force control (see **Fig. 3.6**).
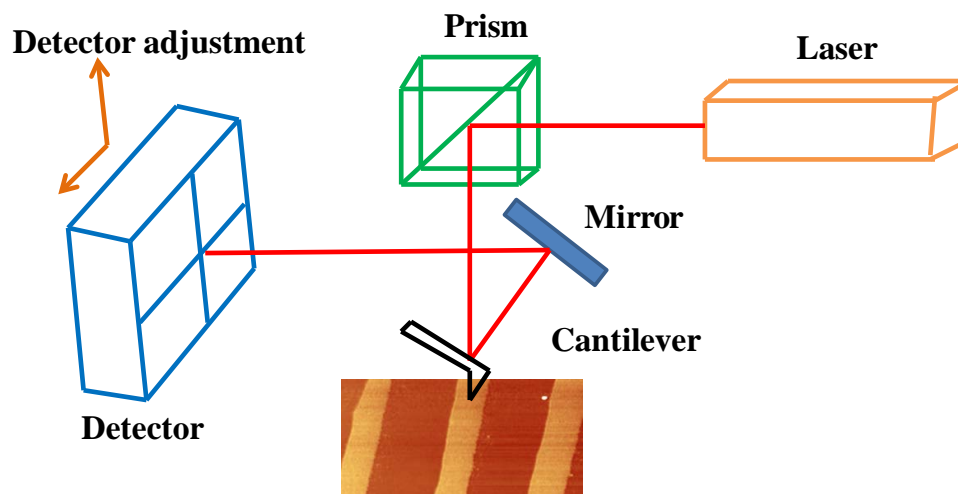
Figure 3.6 – The basic optical path the laser follows in a JPK NanoWizard®II Bioscience AFM has been schematically illustrated in this figure.

3.4.6 Tapping-mode atomic force microscopy

AFM can be performed in two different imaging modes: contact and non-contact modes. All of our studies have been performed in tapping-mode.

Tapping mode is an imaging technique which represents a controlled oscillation of the cantilever. The oscillation is imposed to the cantilever close to its resonance frequency. When there is a difference in force, it is detected by the tip, and then the oscillation amplitude is changed. By detecting and adjusting the change in the oscillation amplitude (via the feedback loop), the AFM can then detect very small variations in forces. Tapping mode is a combined mode of contact and non-contact AFM. It has the advantages of both of the contact mode and non-contact mode. The oscillating cantilever is placed closer to the surface than in non-contact imaging mode which helps the tip to actually come into contact with the surface at every oscillation. Due to the very short period of effective contact between the tip and the surface, destructive lateral friction is removed, preserving the advantages of non-contact mode imaging.

3.4.7 AFM hot stage

(a) Accessories and Calibration

In-situ AFM investigations of the morphology evolution were performed using a TM-AFM with the help of a special accessory designed for measurements in a controlled environment and temperature. The hot stage is based on a Peltier element connected to a suitable DC power supply. The heating device is attached to a Teflon spacer, which is glued with to an AFM sample disk. The temperature controller was connected with sample heater. The sample heater is equipped with a magnetic sample holder for standard AFM sample holder.

The temperature observed or shown by the activated temperature-controller is actually measured by the thermosensor built in the sample heater. The sample heater is inserted into a stage of the Nanowizard TM AFM. The peltier controller and the stage radiator were not covered during measurements.

After proper connection of all the accessories temperature of the sample lying on the heating stage can be well controlled with resolution of 0.1 ºC and temperature can be raised up to 300 °C. Since the sample possesses increased specimen height, the lateral calibration of the scanner must be adjusted by performing a calibration using a standard with the same height. This is normally done by the manufacturer company (JPK). The surface temperature of the Peltier element is monitored by a small thermocouple. The calibration of the device was done, using materials with known melting points (PEO, melting point 69 °C).

(b) Melting and re-crystallisation with AFM hot stage

Real-time studies of polymer melting and crystallization with nanometer resolution have become possible using suitable hot stages and intermittent contact AFM modes [95–98]. If a polymer melt is scanned in TM-AFM, the free amplitude of the resonating lever must be higher (sometime three to four times higher) than for conventional experiments in air in order to overcome the adhesive interactions. In addition, intermediate tapping conditions provide stable imaging conditions. It is necessary to retune the cantilever periodically as the resonance frequency may shift as the cantilever heats up or cooled down.

The temperature was raised slowly while images were continuously captured. The melting process could be monitored in situ, as will be shown in **chapter 4**. It should be taken into account that AFM scanning is relatively

slow compared to the melting process. Upon lowering the temperature of the hot stage, crystallization may set in as will be shown in **chapter 5**. Again, the resulting crystalline domains were observed. In such crystallization experiments, it has been revealed that the AFM tip has significant influence on inducing nucleation.

3.4.8 Applications of AFM in our studies

Just like any other tool, an AFM's usefulness has limitations. When determining whether or not analyzing a sample with an AFM is appropriate, there are various advantages and disadvantages that must be considered.

AFM has several advantages. In our case, AFM was successfully employed to get real time behavior of the deposited polyethylene nanocrystals upon annealing; AFM was very useful in order to get a three-dimensional surface profile for the deposited and afterwards for the annealed crystals. Additionally, samples imaged by AFM in our studies did not require any special treatments (such as metal/carbon coatings). In our study, the tapping-mode AFM worked perfectly well in ambient air. These advantages of using AFM make it possible to study biological macromolecules and even living organisms.

As with any other imaging technique, there is the possibility of image artifacts, which could be induced by vibrations, deformation of the surface by the applied force, thermal drifts, contamination of the tip by the particles or molecules from the sample surface. These image artifacts are often unavoidable. However, their occurrence and effect on results can be reduced through various methods. In order to avoid deformation of the sample surface, one can tap the surface very gently with a relatively weak force. In our case, while performing in-situ AFM hot stage measurements, change in temperature of the sample caused most of the crystals to melt and the sample surface was covered with a very thin liquid layer of the melt. So, it was not possible to see the morphology of the solid objects using very weak force. Thus, we had to increase this force (tapping harder) to go through the thin liquid layer of melt covering the nanocrystal morphology. Using TM-AFM one can approximately estimate the tapping force (F) applied onto the sample surface during intermittent contact [99, 100].

To avoid adhesive tip-sample interactions, large drive amplitudes of the oscillating probe were used. The amplitude ratio ($r_{SP} = A_{SP}/A_o$) is related to the applied force, where A_{SP} is the set point amplitude used for imaging a particular

sample and A_o is the free amplitude of oscillation of the AFM tip. The higher the value of r_{SP}, the weaker is the force the tip applies onto the sample surface at constant drive amplitude.

The tip was often contaminated with polymers which got attached to the tip during scanning resulting in bad quality images containing artifacts. In order to avoid such tip contamination, high oscillation amplitudes were used. Another way of getting rid of contamination is to wash the contaminated tip with some solvents (methanol, chloroform etc.).

During the in-situ hot stage measurements, we often experienced thermal drift caused by the change in temperature along with slow rate of scanning. A temperature change results in a contraction or expansion of the various parts of the microscope. Since these parts are manufactured from different materials, their thermal expansion coefficients will be different. This causes the probe tip to be displaced both laterally and vertically from the old position with respect to the sample. Under hot condition, this problem was sometimes overcome by re-imaging the similar region another time. Another way to solve the problem was to retract the cantilever, retune the resonance frequency of the cantilever one more time and image again the similar region. Thermal drift are more relevant at slow rates of scanning. However, in order to observe fine details and to obtain quality images, a slow rate of scanning was employed in our studies.

3.4.9 Determination of viscoelastic properties through phase imaging

Phase Imaging is a powerful extension of tapping-mode atomic force microscopy that provides nanometer-scale information about surface properties. By mapping the phase of the cantilever oscillation during the tapping-mode scan, phase imaging goes beyond simple topographical mapping and allows to detect variations in composition, adhesion, friction, viscoelasticity [99, 101], and perhaps other properties. Phase imaging results when there is a difference in phase between the imposed oscillation signal and the detected oscillation of the cantilever. This phase shift results from the dissipation of energy occurring during the tapping of the tip on the surface. Different materials will induce different energy dissipation, allowing their differentiation in an image, even on a topographically flat surface. Although it is not a quantitative mode of imaging, like topography measurement, when it comes to self-organization on a flat sample for example, it can provide very useful information on the presence of regions with different

mechanical properties at the surface.

When polyethylene nanocrystals deposited within a monolayer stripe were annealed at 133 ℃ for 1 hour and cooled down to room temperature a reduced number of new aggregated crystals was observed. The height image showed the topography of the surface where individual bigger aggregates of crystals were visible (although not shown here). The phase image of the same area shows exactly the same morphological features but every individual aggregate with a very sharp edge was clearly visible that did not clearly appear in the height trace.

In **Fig. 3.7** the phase images clearly show the differences in properties (or material) over the surface. The crystalline domains are of different nature than that of the melt. While by the height images one can have information about the change in thickness, phase images can clearly differentiate regions of high and low surface adhesion or hardness *e.g.* crystalline and molten regions in our case. When the oscillating AFM probe is scanned along the surface the molten material was detected as softer than the harder crystalline material. This results in a phase difference between molten and crystalline regions, thus providing a distinct contrast between the two. As can be seen from **Fig. 3.7 a**), the as-prepared sample was crystalline (or hard) everywhere within the monolayer stripe with a phase-value comparable with the hard background. As discussed above, the tapping force can easily be varied and we have demonstrated its influence on imaging. We have increased the temperature to 75 ℃ and the sample was kept at that temperature for 10 minutes (see **Fig. 3.7 b**). One can see that compared to the as-prepared sample the phase contrast image shows dark domains in the monolayer region which indicates that few polymer molecules were molten. In this particular case the set point ratio was 0.84 which means that the AFM tip tapped in a soft manner. But applying even softer forces where the set point ratios were 0.9 and 0.97 for **Fig. 3.7 c**) and **Fig. 3.7 d**) respectively one can clearly see that the darkness of the phase contrast images increased. This indicates that, when softer force was applied the AFM tip cannot penetrate through the molten polymer layer but stays on the top of the monolayer stripe and hence cannot detect the crystalline structures underneath the molten layer. Tapping with much higher force (see **Fig. 3.7 e**), the set point ratio for this imaging was 0.67) clearly shows some crystalline domain within the monolayer stripe. Due to higher tapping force, the AFM tip penetrates through the molten polymer layer on top of the stripe and one can image the crystalline structures. **Fig. 3.7 f** shows the similar region after cooling back the sample to room tem-

perature. One can see that almost all the molten polymers became recrystallized and a the similar morphology like the as prepared sample was obtained. Thus, phase imaging helped us to detect the different material properties (crystalline or melt, in our case) by applying various tapping forces. During measurements of crystallisation from the undercooled melt of polyethylene nanocrystals phase imaging was advantageous to detect the tip-induced nucleation of edge-on crystalline domains (will be described and shown in detail in **chapter 5**). The height image alone would not be able to give detailed information about the behavior of the nanocrystals upon annealing; hence the information provided by the phase image is essential in order to understand the crystallization-melting process of our system.
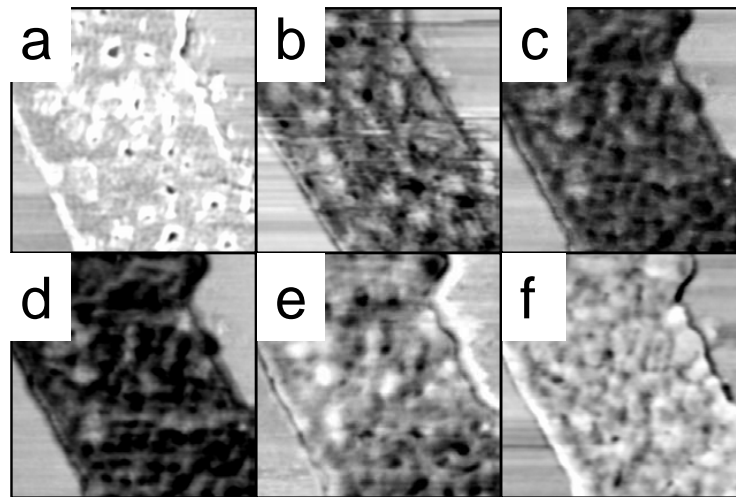
Figure 3.7 – (a-f) AFM phase images showing as prepared, annealed at 75 °C for 10 minutes ($r_{SP} = 0.84$), annealed at 75 °C for 20 minutes ($r_{SP} = 0.9$), annealed at 75 °C for 30 minutes ($r_{SP} = 0.97$), annealed at 75 °C for 45 minutes ($r_{SP} = 0.67$), after cooling back the sample to room temperature respectively. Size of all the images is 1.5 x 1.5 µm^2.

3.5 Regular pattern formation on substrate

Within the aqueous dispersion, polyethylene nanocrystals were transported by convective flow towards the contact line where they got stuck, locally jammed and formed a clog. The so localized nanocrystals exerted a frictional or pinning force which slowed down dramatically or even stopped the motion of the contact line. During pinning the contact area between dispersion and substrate remained constant. As a consequence, the loss of volume due to evaporation caused a steady decrease of the contact angle. In turn, the uncompensated Young force [102]

increased persistently until it overcame the pinning or frictional force. This led to depinning of the contact line, which jumped to a new position where it got arrested once more. The deposited polyethylene nanocrystals were rather strongly adsorbed on the silicon substrate as can be demonstrated by their resistance to desorption even when the whole sample was put in large volumes of pure water. The stripes remained almost unchanged after such a washing procedure. In our study, we observed at a distance of ca. 2 mm from the center of the ring a small slice (ca. 200 x 700 µm^2) with an optical microscope. Exploiting the interference of light reflected from the substrate and from the surface of the deposited structures, a series of parallel stripes representing segments of the annuluses were found (see **Fig. 3.8a**). As confirmed by atomic force microscopy (AFM), the various gray-levels seen in the micrograph (**Fig. 3.8a**) can be directly related to the thickness of the stripe: The darker the gray the thicker the stripe. Close to the center of the Teflon ring *i.e.* where the dewetting process started, stripes were spaced at rather irregular distances (see **Fig. 3.8b**). In the course of the dewetting process, the spacing of the stripes became more regular (see **Fig. 3.8c +d**). This change in regularity may be related to the initially low number density of PE nanocrystals per unit volume which did not allow for frequent pinning of the contact line at the beginning of evaporative dewetting. However, towards the end of water evaporation, the contact line was frequently pinned. This process resulted in regularly spaced stripes. Thus, we expect a gradual change in number density of PE nanocrystals in the dispersion in the course of evaporative dewetting.
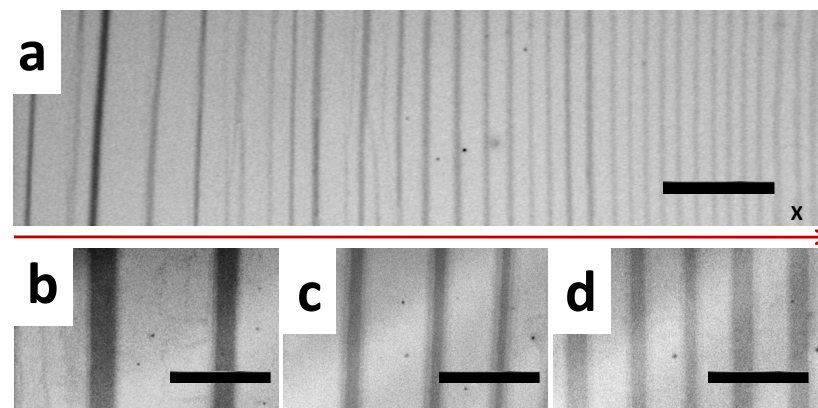
Figure 3.8 – (a) Optical micrograph of a small slice (ca. 200 µm x 700 µm) at a distance of ca. 2 mm from the center, taken after complete evaporation of water. (b-d) Higher resolution optical micrographs showing the typical changes as the dewetting processes move from a position about 2 mm from the center (c) toward the Teflon ring (d +e). The scale bar in images (b) and (c-e) represents 100 µm and 20 µm, respectively.

Using AFM, it could be shown that the deposited stripes had a well-defined thickness. Especially towards the end of the evaporation process, where closely spaced stripes were observed (**Fig. 3.8d**), they all had a uniform thickness of about 8±1 nm (**Fig. 3.9a, b + c**). This thickness is practically identical with the lamellar thickness of the polyethylene nanocrystals, as determined by X-ray scattering and electron microcopy [16, 103]. This uniform thickness suggests that the stripes were formed by a single layer of flat-on oriented nanocrystals, *i.e.* crystals having their lamellar normal in the direction of the surface normal. As shown previously [104], flat-on PE lamellae most likely contain polyethylene chains with the c-axis of the unit cell (*i.e.* the PE-stem) oriented at an angle of ca. 35° to the direction of the surface normal.

The formation of stacks of several layers (**Fig. 3.9 (d + e)**) was observed at early stages of the evaporation process, or when more concentrated dispersions were used. Interestingly, step heights were similar for monolayers and each step of multiple layers (**Fig. 3.9**). From characteristic height profiles (**Fig. 3.9 (c + e)**) we deduced a regular step height of 8±1 nm for these steps. Thus, we concluded that all nanocrystals were oriented flat-on, *i.e.* as lamellae parallel to the substrate surface.

Complementary experiments showed that the width of stripes and their spacing can be influenced by the initial concentration of the dispersion, the rate of evaporation of water and the solvent-substrate interaction. For the purpose of studying the influence of annealing on morphological changes of the nanocrystals, we mainly focused on regular monolayer and multilayer stripes of up to some micrometers in width.
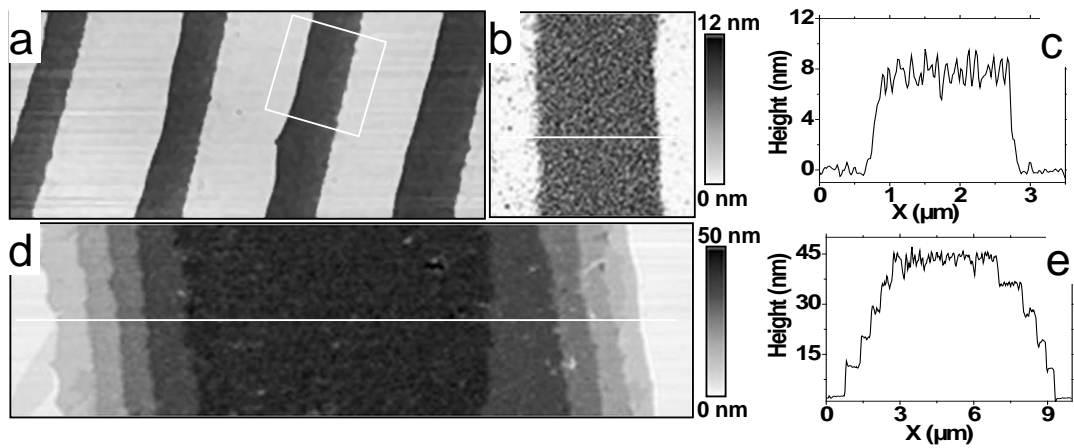
Figure 3.9 – (a) AFM topography image (28 x 13 µm²) of regularly spaced stripes obtained towards the end of the evaporative dewetting process (similar to **Fig. 3.8d**). It should be noted that all stripes exhibited a unique mean thickness as can be deduced from the color code. b) Higher resolution image (3 x 3 µm²) and c) a cross section through one of these stripes. d) AFM topography image (12 x 3.2 µm²) stack of five layers obtained at an earlier stage of the evaporative dewetting process (similar to **Fig. 3.8b**). e) Cross section through this stack. Note that the mean height of the monolayer (ca. 8 nm) is equal to the step height in the stack.

Chapter 4

Morphological changes during annealing of polyethylene nanocrystals

In the previous chapter the crystalline structure and the synthesis procedure of the polyethylene nanocrystals, the main focus of our studies, were explained. Different experimental characterization techniques *e.g.*, optical microscopy, in situ atomic force microscopy equipped with a hot stage were discussed elaborately. Different deposition techniques were described along with that we have employed in order to deposit the nanocrystals in an ordered fashion on solid substrate.

The current chapter will mainly be focused on the reorganizational behavior of the deposited polyethylene nanocrystals within a monolayer and stacks of layers upon annealing below the equilibrium melting temperature of the nanocrystals as a function of annealing temperature and annealing time.

Polymer crystals are metastable and exhibit morphological changes when being annealed. To observe morphological changes on molecular scales we started from small nanometer-sized crystals of highly folded long-chain polymers. Micron-sized stripes consisting of monolayers or stacks of several layers of flat-on oriented polyethylene nanocrystals were generated via evaporative dewetting from an aqueous dispersion. We followed the morphological changes in time and at progressively higher annealing temperatures by determining the topography and viscoelastic properties of such assemblies of nanocrystals using atomic force microscopy. Due to smallness and high surface-to-volume ratio of the nanocrystals, already at 75 °C, *i.e.* about 60 degrees below the nominal melting point, the lateral size of the crystal coarsened. Intriguingly, this occurred without a noticeable reduction in the number of folds per polymer chain. Starting at around 110 °C, chain folds were progressively removed leading to crystal thickening. At higher temperatures, but still below the melting point, prolonged annealing allowed for surface diffusion of molten polymers on the initially bare substrate, leading eventually to the disappearance of crystals. We compared these results to the behavior of the same nanocrystals annealed in an aqueous dispersion and to bulk samples.

4.1 Introduction

Because of its mechanical properties and low cost of production polyethylene (PE) is extensively studied and widely used in many applications. Due to its simple chemical structure, PE also represents one of the most investigated polymers in terms of crystallization in solution, bulk systems or thin films [9, 10, 38, 63, 105–107]. In general, in order to proceed from a disordered polymer melt to a perfectly ordered crystal significant changes in conformations are required [108]. However, in particular the length of the polymer imposes severe steric and kinetic restrictions that result in crystalline states having some degree of disorder like chains fold [109]. For a given polymer of known length, a measure for the degree of folding is the thickness of the crystalline lamellae: the thinner these lamellae are the more folded are the polymer chains. The number of chain folds, and thus the thickness of the lamellae, highly depends on crystallization conditions. For long chains, the equilibrium state, represented by a lamellar crystal consisting of fully extended chains, [41] is never reached.

It turns out that due to the synthesis, which has to be performed at low temperatures, the resulting polyethylene nanocrystals contain highly folded

polymer chains which thus are far from their thermodynamic equilibrium state [16, 103]. Consequently, and these nanocrystals will unavoidably change their morphology even when kept at temperatures far below their nominal melting point. For such highly metastable states of small polymer crystals, it is a non-trivial task to define and measure the melting process. Like for small inorganic crystals or clusters, an individual crystal may melt at a lower temperature than the bulk melting temperature [46, 110]: The melting temperature decreases as the surface-to-volume ratio of the crystal increases. In addition, polymer crystals consisting of folded molecules are able to increase their crystallinity by a reduction of the degree of chain folding with temperature or time. In most cases, molecular re-organization into less folded states improves the thermal stability of the crystal and shifts its melting temperature to higher values. In the presence of neighboring small nano-crystals, molecules may be exchanged between these crystals. Such exchange may lead to coarsening, *i.e.* slightly bigger crystals may become larger at the expense of smaller crystals [111]. Due to their lower surface-to-volume ratio, bigger crystals typically have a higher melting temperature than smaller ones. Recently, computer simulation results were compared to experiments on alkane chains and functional olefins validating the inverse thickness dependence of the melting temperature (Gibbs-Thompson behavior) which also was influenced by the crystal environment, *i.e.* interfacial tensions [112]. Consequently, instead of melting, crystals may coarsen and thicken and so increase their melting temperature.

Here, we will explore the consequences of metastability of polymer crystals by detecting changes in morphology as a result of annealing. Using well-defined nanometer-sized polyethylene crystals consisting of highly folded long-chain polymers we followed these changes as a function of temperature and annealing time.

4.2 Morphological evolution of polyethylene nanocrystals

A polymer crystal containing folded chains does not represent the lowest free energy state and thus is only metastable. Such folded states of reduced degree of crystalline order are prone to morphological changes which are accompanied by a reduction of the number of folds per molecule. A process of morphogenesis [113] can be identified, following characteristic paths which lead to a reduction of the total free energy. The process can be modeled by computer simulation [114] considering individual chains as the basic units which have the possibility of internal

reorganization, even behind the growth front, *i.e.* in a crystalline environment. As indicated by these computer simulations, the process of morphogenesis is more pronounced for small crystals of initially highly folded polymer chains. The here investigated nanocrystals consist on the average of eight chains with several hundred folds per molecule. This high degree of folding of the polymers is the consequence of the low temperature (large undercooling) at the stage of polymerization and nanocrystal formation. Consequently, these nanocrystals are highly metastable and therefore will exhibit a strong tendency to change their morphology. In the present study, we followed the pathways taken during morphogenesis through in-situ AFM-studies on monolayer stripes of these nanocrystals.

The limited number of polymer chains per nanocrystal and their well-defined orientation with respect to the substrate facilitate to follow and to relate the observed morphological changes to molecular transport and conformational changes (reduction of chain folds). The high surface-to-volume ratio, *i.e.* the large number of molecules located at the periphery of the crystal with respect to the interior, translates directly into a high detachment probability for polymers from the nanocrystal and thus favors rapid morphological changes.

In the following, we will present our results as a function of increasing annealing temperature which enables progressively faster and more long-ranged morphological changes. We will also compare observations on monolayers with the simultaneously occurring changes in multilayers.

4.2.1 Annealing experiments at T< 110 °C

Monolayer stripes obtained by the here employed evaporative dewetting process are built up from a random assembly of nanocrystals which are neither all uniquely oriented nor perfectly ordered without having empty space in between. Accordingly, due to such boundaries within the monolayer, many polymer molecules (or parts of them) are located at crystal surfaces where they are lacking neighboring polymers. Consequently, as temperature increases, these molecules have a higher probability for detaching from the crystal and becoming part of a molten phase surrounding the nanocrystals. Using tapping mode AFM the amount of molten polymers can be visualized via the phase-signal.

In **Fig. 4.1**, we observed the morphological changes occurring in a monolayer stripe during annealing at a comparatively low temperature where according to DSC the nanocrystals do not melt. We have chosen 75 °C, *i.e.* almost 60 °C

below the nominal melting temperature of 133 °C. Similar observations of morphological changes, though at varying rates, were made at all temperatures in between ca. 60 °C and 110 °C. As can be seen from **Fig. 4.1a'**, the as prepared sample showed already some heterogeneities indicating the random assembly of nanocrystals which did not results in a highly ordered pattern. The corresponding phase image (**Fig. 4.1a''**), indicates that the whole stripe consisted of highly elastic material similar to the surrounding substrate, as represented by the bright color of the phase signal. (**Fig. 4.1a''**). No molten regions were detectable. However, when increasing the temperature to 75 °C the phase signal changed significantly (**Fig. 4.1b''**), indicating that some molecules were molten. Even after prolonged annealing, the phase contrast did not change much (**Fig. 4.1c''**). Alongside with the change in phase contrast, an apparent change in thickness (height) of the stripe was observed (**Fig. 4.1b' + c'**) [115]. When pushing the AFM tip harder into the sample, *i.e.* penetrating through a layer of molten polymers on top of the stripe, the heterogeneous arrangement of fused crystals became visible in topography (**Fig. 4.1d'**). The corresponding phase image (**Fig. 4.1d''**) shows that in between the nanocrystals a significant number of molten polymers existed already at 75 °C. Analogous to an Ostwald ripening process, these more mobile molecules allowed for fusion of nanocrystals. After the sample was cooled back to room temperature (**Fig. 4.1e**), all molten polymers recrystallized. Hence, during annealing for about one hour at 75 °C, the arrangement (morphology) of the crystalline material changed due a melting and re-crystallization process involving the detachment of polymers from one nanocrystal and attachment at another crystal surface. This process led to a coarsening of the morphology: Small crystals transformed into bigger aggregates. Interestingly, during this coarsening stage the thickness of the crystalline domains did not change significantly. Thus, diffusion of molecules between neighboring crystals and subsequent re-attachment/re-crystallization at crystal surfaces was probably so fast that polymers were not able to achieve less folded chain. We conclude that at such comparatively low temperatures with respect to the equilibrium melting temperature of ca. 141 °C [116] the process is driven by the reduction of the number of molecules at crystal boundaries, *i.e.* a reduction in total perimeter of all crystals. This is achieved by making the crystalline domains bigger than the initial nanocrystals (fusion of small crystalline domains into bigger ones).
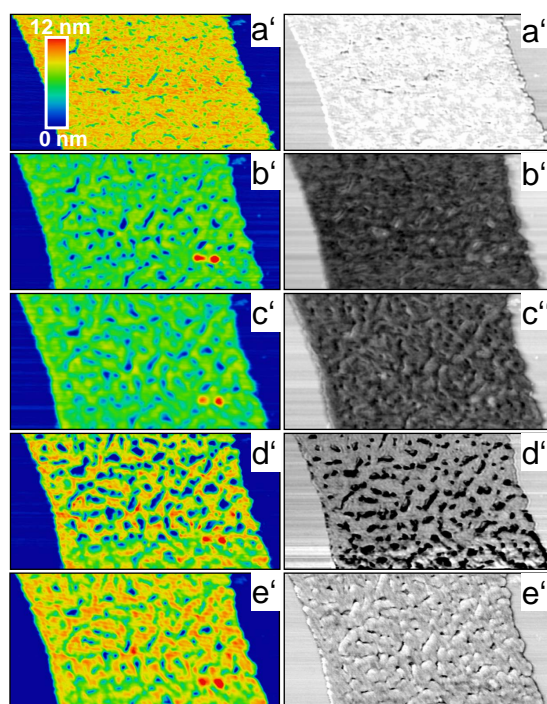
Figure 4.1 – AFM topography (left column, the color code ranges from 0 – 12 nm) and phase (right column) images (3 x 1.5 µm²) showing reorganization within a monolayer of nanocrystals induced by annealing at 75 °C, *i.e.* ca. 60 °C below the temperature where melting is detected by DSC. a) as prepared, b) 15 min, c) 60 min, d) 75 min after reaching the chosen temperature of 75 °C. Images e) show the sample after being quenched back to room temperature. The tapping oscillation amplitude and force were similar for all images except d) where much harder tapping conditions (lower amplitude and lower set point ratio) were applied.

As can be seen in **Fig. 4.2**, the rate of the coarsening process and the degree of coarsening was affected by the number of stacked layers of nanocrystals. At the edge of a multilayer stack one can observe a monolayer, a double layer and a triple layer simultaneously (**Fig. 4.2a**). For the as-prepared sample, the phase contrast in all these regions indicates rather elastic, *i.e.* crystalline material (**Fig. 4.2b**). After raising the temperature to 80 °C (**Fig. 4.2c**), first the monolayer partially melted and started to reorganize. Only about one hour later, also the double layer showed clear indications of partial melting and rearrangements (**Fig. 4.2d**). A few hours later, the monolayer has coarsened to such an extent that the fraction of molten polymers was so small that it was hardly detectable in the phase image while the region of the double layer contained still a significant amount of molten polymers (**Fig. 4.2e**). The triple layer was still comparatively unaffected. These differences in annealing behavior of the various layers might be attributed to the change in interfacial energy between substrate and nanocrystal and between layers of nanocrystals. Zhang *et al.* [117] showed that layered lamellar crystals

of short polyethylene molecules showed a sequential melting behavior: the top lamella melted before the bottom lamella, quantitatively related to stabilization via Van der-Waals interactions. In our experiments on layers of nanocrystals annealed at significantly lower temperatures rearrangement processes driven by detachment of molecules from the nanocrystals occurred first in the monolayer region, probably favored by a reduced areal density of polyethylene molecules.
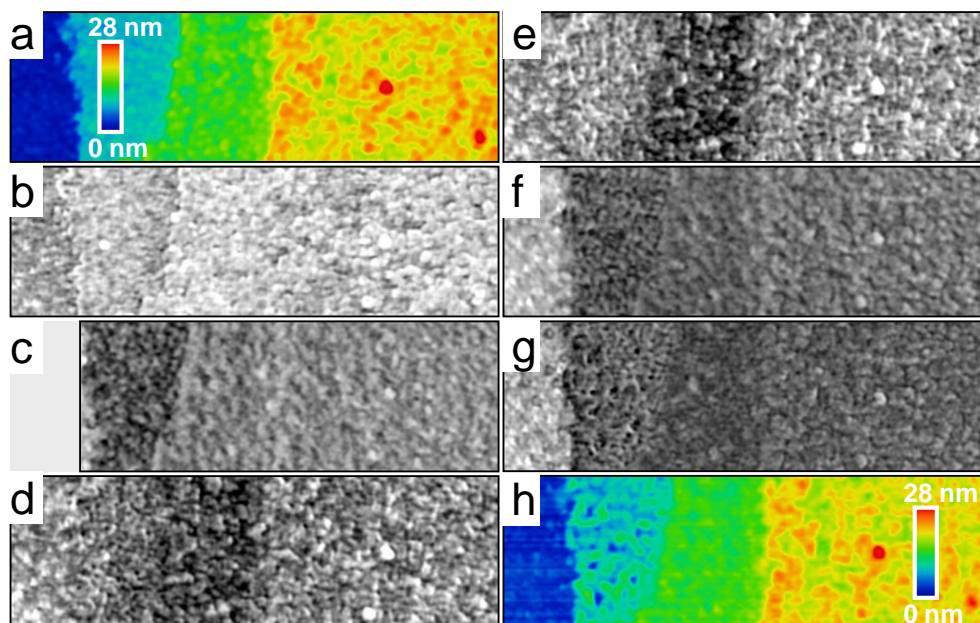
Figure 4.2 – AFM topography (a + h, the color code ranges from 0 – 28 nm) and phase images (b – g) (5 x 1.5 µm²) showing the evolution of a stack of three layers of nanocrystals at 80 °C [c) 15 min, d) 60 min, e) 330 min] followed by annealing at 100 °C [f) 15 min, g)+h) 240 min]. Images a) and b) show the as prepared sample.

At 100 °C, the fraction of molten polymers increased homogeneously for all regions as can be deduced from a homogeneous "darkening" of the phase contrast. The most elastic (hardest) part of the image corresponds to the substrate, seen on the outmost left part of the image of **Fig. 4.2f**. Even during annealing for several hours no significant further changes were detectable on the scale of the image (**Fig. 4.2g**). Comparing the topography after this annealing procedure (**Fig. 4.2h**) with the initial stage (**Fig. 4.2a**) demonstrates that only local coarsening had occurred, crystals fused to larger object without change in the degree of chain folding. As the thickness of these layers has not changed, we suppose that no interdiffusion between layers had occurred.

In summary, we attribute the observation of significant changes at such low temperatures in polyethylene crystals mainly to the enormous number of poly-

mers attached to crystal surfaces (*i.e.*, lateral faces of lamellar crystal). These molecules have a low but still measurable probability to detach from the crystal and diffuse to other crystalline surfaces. Of course, the same process is also present in larger crystals but there the absolute number of molecules detaching/attaching per unit time is less and thus the resulting morphological changes are hardly detectable or would require significantly longer annealing times.

4.2.2 Annealing experiments at T< 120 °C

Annealing behavior of solution grown polyethylene single crystals and investigations of morphological changes during annealing of such crystals have been studied previously by various groups [15, 118–120]. In particular, upon annealing of single crystals placed on a solid substrate the formation of picture frame-like structures was studied in situ using AFM at elevated temperatures which indicated that the reorganization process started at the crystal edges at a temperature above ca. 120 °C. In our case, the thickness of the crystalline regions changed gradually but clearly when annealing at temperatures higher than ca. 100 °C (**Fig. 4.3**). While at the lower temperatures only reorganization without detectable changes in height occurred (**Fig. 4.3a**), thickness started to increase at higher temperatures and isolated crystalline domains formed at around 110 °C (**Fig. 4.3b**). At even higher temperatures (**Fig. 4.3c+d**), the process accelerated. From these images it is quite notable that the boundaries of the monolayer region thickened more rapidly than regions within the monolayer, analogous to what was observed for monolayer crystals of poly (ethylene oxide) [113, 114, 121–123], or polyethylene [15, 118–120]. Based on these results, we conclude that at temperatures higher than ca. 110 °C the reduction of chain fold became possible. The higher thermal energy increased the probability of chain desorption, allowed for faster rearrangements over larger distances. This favored the formation of isolated domains and, in turn, provided sufficient time for thickening before additional polymers reattached to the crystal front. Thickening was more prominent in regions with a lower amount of surrounding polymers, in particular at the boundaries of the initial monolayer stripe.
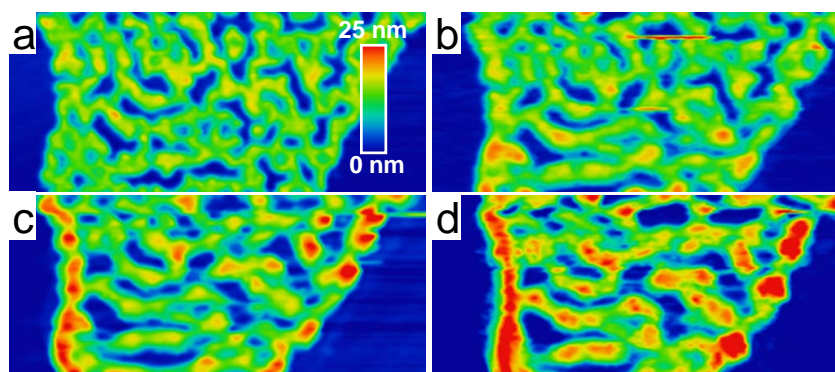
Figure 4.3 – AFM topography images (3.5 x 1.5 µm²) of a monolayer of nanocrystals, measured after short annealing times at progressively higher temperatures: a) after 30 min at 100 °C, b) after 15 min at 110 °C, c) after 15 min at 117 °C, and d) after 20 min at 120 °C.

4.2.3 Annealing experiments at T< 130 °C

When annealing a stack of three layers, additional features were observed (**Fig. 4.4**). Similar to the monolayer of **Fig. 4.3d**, after one hour at 122 °C (**Fig. 4.4b**), the monolayer part had reorganized into an array of almost individual crystalline domains with a thickness up to three times the initial thickness. Taking into account that the volume, *i.e.* the amount of molecules, of this monolayer region has not changed detectably, this implies that the polymers chains became less folded. Secondly and rather surprisingly, the triple layer region became thinner, as thin as the double layer region. This implies that in the triple layer significant interdiffusion occurred between the layers of nanocrystals. After such annealing, the height of the initial triple layer was found to be the same as for the initial double layer. This suggests that the degree of chain folding is the same in both regions. The most prominent thickness was around 16 nm, *i.e.* twice the starting thickness, which can be interpreted as a reduction in the number of chain folds by a factor of two. Taking into account that we have observed significant melting-recrystallization taking place even at lower temperatures, we tentatively conclude that the double layer region has transformed into a monolayer of crystalline domains having more extended chains. Along these arguments, the reduction in thickness of the triple layer can be interpreted also by the formation of a monolayer of thicker crystalline domains. However, as more nanocrystals (roughly 1.5 times the number of nanocrystals deposited in the double layer region) were available at the beginning of annealing, the resulting coarsened crystalline domains were less separated. This conclusion is supported by the formation of comparatively large empty regions within this double layer region, which did not appear

in the triple layer region, when the sample was further annealed at 124 °C for one hour. One of these spots is indicated by an arrow in **Fig. 4.4c**. It is highly intriguing to observe that for a given annealing time thickening was the more significant the fewer molecules were surrounding the crystalline domain. This is the case at the periphery of the initial monolayer (**Fig. 4.3d**) and within the monolayer (**Fig. 4.4**). In regions with a higher amount of molecules per area, the attachment probability is higher, the time between successive attachments is shorter and thus the available time is shorter for molecules at the crystal boundaries to remove chain folds. The lateral faces of the crystals are identified as a key element during annealing and, in particular, in the coarsening process. It is at these faces where molecules attach and detach. Thus, for small nanocrystals the number of molecules at these surfaces is significant with respect to the total number of molecules in the crystal. Following these fundamental arguments which lead to the Gibbs-Thomson relation, we thus expect that the surface to volume ratio of small nanocrystals is not only determined by the thickness of the lamellar crystal (the thinner the lamella the higher is the surface to volume ratio) but also by the lateral size. In addition, the strength of attachment of molecules at the various faces of the crystal may be different (as it is the case for polyethylene crystals) and consequently one has to "weigh" the contributions of the different faces not only according to their area but also as a function of their attachment strength (=surface tension) which is also a function of temperature. As our results are not providing all the necessary details for an in-depth analysis with respect to the contributions of the individual faces we are only able to discuss this point in general terms.
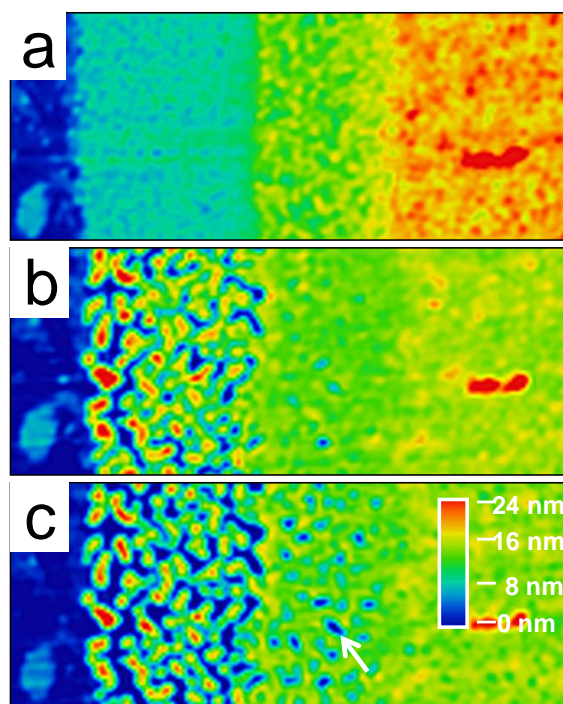
Figure 4.4 – AFM topography images (5 x 2 µm²) of a stack of three layers of nanocrystals, all measured at room temperature. a) as prepared, b) after 1 hour at 122 °C, and c) after 1 hour at 124 °C. The monolayer reorganized faster than the double and triple layer. The three layers merged and resulted in a layer having about the thickness of a double layer. The double layer visible reorganized before the triple layer. In the monolayer region isolated crystalline islands started to form. The height of some of these islands increased even beyond the thickness of the double layer.

At 120 °C, the coarsening process in a monolayer region was followed in time and in situ in **Fig. 4.5**. Already after 15 min, the monolayer had transformed into an array of droplet-like domains of a variety of sizes (**Fig. 4.5a**). Interestingly, the corresponding phase image clearly indicates that most of these droplets exhibited a liquid-like behavior, at least at their surface (The chosen conditions of tapping mode AFM, *i.e.* the set-point ratio [99,115], allowed only for small penetration of a few nanometers). Initially, only very few droplets contained detectable crystals. Interestingly, in the course of annealing over several hours (keeping the conditions of tapping mode AFM constant), more of these liquid-like droplets crystallized and grew in size (**Fig. 4.5c − g**). The thickness of the crystalline domains reached values of up to ca. 60 nm. The layered topography pattern, together with the internal structure of the crystalline domains is visible in the phase image. The data presented in **Fig. 4.5** and results from many other samples consisting of droplet-like regions strongly indicate that the droplets contain stacks of lamellae. From AFM it is not possible to decide definitely if

these lamellae are fully edge-on or somewhat inclined. *E.g.*, we cannot exclude that the lamellae are tilted by ca. 35 – 45°, which would suggest that the stems are parallel to the substrate but lamellae are inclined.

After cooling the sample back to room temperature, the phase image (**Fig. 4.5h**) demonstrates that all the molten polymers crystallized. The corresponding topography image (**Fig. 4.5i**) clearly shows that the thickness of the resulting new crystalline domains was mostly only around 10 nm (see the differences between **Fig. 4.5f and Fig. 4.5i**), *i.e.* a thickness consistent with the lamellar thickness obtained when annealing the sample at temperatures below ca. 110 °C.
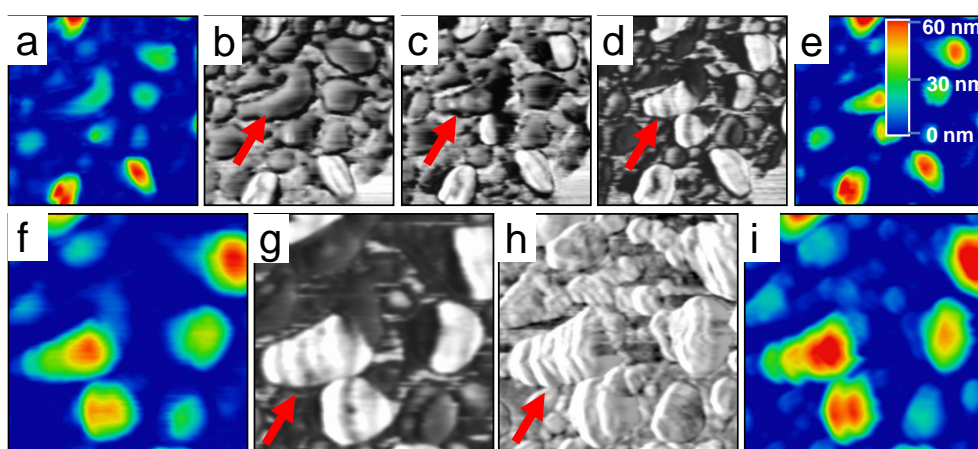
Figure 4.5 – AFM topography [a), e), f), and i), color code ranging from 0 – 60 nm] and phase [b), c), d), g) and h)] images of a monolayer of nanocrystals pre-annealed at 110 °C for 30 min and then measured during annealing at 120 °C [a) and b): 15 min, c): 55 min, d) and e): 120 min, f) and g): 190 min] and after quenching to at room temperature [h) and i)]. The red arrow highlights one droplet-like region which melted as the temperature was raised from 110 °C to 120 °C but then re-crystallized during annealing at 120 °C. In the course of annealing, progressively more of these droplet-like regions re-crystallize. The arrows are used to highlight one of these droplets which clearly underwent crystallization in the course of annealing. The size of images a) – e) is 1.8 x 1.8 µm² and of images f) – i) is 1.2 x 1.2 µm².

4.2.4 Annealing experiments up to T = 133 °C

In order to follow the reorganization process at comparatively high annealing temperatures, we decided to use a small pile of a limited number of nanocrystals which allowed observing simultaneously the evolution of regions of different thickness. The focus was on which part of this pile "survives" the annealing process at a given temperature. We would like to emphasize that such a pile of a lim-

ited number of nanocrystals sitting on a bare substrate has to be considered as an "open system" as polymer chains have the possibility to diffuse away from the pile once they are detached from the nanocrystals. This has to be contrasted to the "closed system" of nanocrystals dispersed in an aqueous medium used by [103]. There, no exchange of polymers between nanocrystals is likely to occur. Thus, equilibration of nanocrystals at various temperatures is feasible.

In the present experiments, we kept the annealing time as short as possible for each temperature chosen. Under such conditions, we did not allow for long-time rearrangement and coarsening processes. The equipment used required a minimum of ca. 15 min to stabilize the temperature and to obtain a suitable AFM image. As shown already for nanocrystals deposited in stripes, annealing at temperatures up to ca. 110 °C allowed only rearrangement processes on small length-scales. It can be seen (**Fig. 4.6c**) that in comparison to thicker parts the thinner parts of the sample exhibited a more liquid-like behavior. Above ca. 110 °C significant coarsening occurred and resulted in very few crystals of different sizes. The biggest crystal evolved from the thickest region of the initial pile. Increasing the annealing temperature step-wise (**Figs. 4.6f − g**) led to fusion of the smaller crystals and to some increase in size of the bigger ones. As indicated by the pronounced contrast in the phase images of **Fig. 4.6**, at elevated temperatures all crystals were surrounded and covered by molten polymers. Thicker crystals were able to attract more of these mobile molecules from the thinner ones and thus got larger in the course of the measurement. On the contrary, smaller (and thinner) crystals became even smaller by losing their molecules to the thicker crystals. This observation is in accordance with a theoretical study by Rabani *et al.* who concluded that thermal coarsening of nanoparticle domains proceeds via diffusion and coalescence of domains [22].
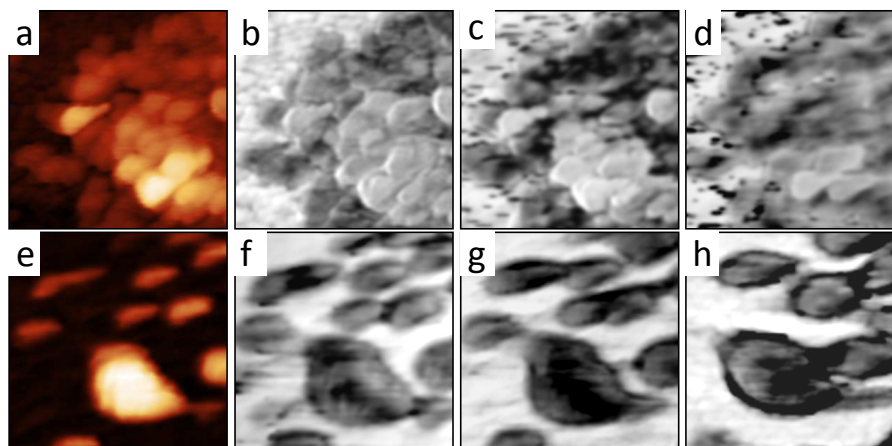
Figure 4.6 – AFM topography [a) and e), color code ranging from 0 – 40 nm] and phase [b) – d), f –h)] of a disordered pile of nanocrystals. a) + b): as prepared, c) after 15 min at 75 °C, and after each time additional 15 min at d) 100 °C, e + f) 120 °C, g) 126 °C, and h) 133 °C. The size of images is 1 x 1 µm².

Besides the number of chain folds per polymer, the thickness of crystalline polyethylene lamellae depends also on the degree of chain tilting within the crystal. However, based on AFM measurements alone, we are not able to determine the tilt angle. Previous works *e.g.* for long alkanes [124] have shown that for lamellae crystallized at temperatures lower than ca. 100 °C chain tilting is less pronounced than upon annealing at temperatures closer to the melting point. For fully extended alkanes of a total length of about 30 nm the tilt angle increased from 0° to about 40° upon heating from ca. 100 °C to ca. 125 °C. By means of electron diffraction Labaig *et al.* [125] observed for crystals grown on a supporting substrate at temperatures as high as $\sim$ 125-131 °C chain tilt of $\sim$ 45° (cited *e.g.* by Keith *et al.* [55]). Thus, we may assume that also in our (mono) lamellar crystals chain tilt will increase as we increase the annealing temperature.

This coarsening process at temperatures between 120 °C and 133 °C is associated with a size-dependent melting temperature: at a comparatively low temperature the smaller crystals started to melt and disappeared eventually while at this temperature bigger crystals still increased in thickness. In order to explore the influence of annealing time we kept the sample of **Fig. 4.6** at a constant annealing temperature of T_A = 133 °C (**Fig. 4.7**). The choice of T_A was inspired by the position of the melting peak observed in DSC. Comparing **Fig. 4.6e** with **Fig. 4.7a** shows that the step-wise increase of T_A from 120 °C to 133 °C did not lead to melting of all crystals. Only some of the small crystals melted and fused.

On the contrary, the biggest crystal slightly increased in size.

Furthermore, from a comparison of the total volume of the all objects, either crystalline or molten, we conclude that after such short annealing times the amount of polymeric material stayed approximately constant. However, keeping the sample at 133 °C for many hours eventually led to the disappearance of all crystals (**Figs. 4.7b and c**). After ca. 1000 min at 133 °C (**Fig. 4.7c**), one hardly can detect any crystalline domain. The AFM phase contrast image suggests that all crystals have been transformed into thin liquid droplets. From the topography image, it is obvious that the volume of the crystalline domains was not conserved. Taking into account that polymers cannot evaporate, a significant number of polymers must have diffused out of the frame of the image. These polymers probably coat the surrounding substrate with a layer too thin to be detectable by AFM (at the measurement parameters chosen). We interpret this disappearance of crystals in the following way: Molecules at the surface of any crystal have a non-zero probability to detach from this crystal, *e.g.* sublimation of ice below the melting point. At temperatures largely below the melting temperature, the detachment probability is low and almost no molecule would detach from a crystal within a given time, say, several hours. However, at temperatures close to the melting point, the detachment probability can be quite significant. As the crystals were deposited on an initially bare substrate they were surrounded by a large surface which does not contain any polymers (no free polymers were adsorbed onto the substrate because only nanocrystals were deposited). Thus, some of the detached molten polymers gained translational entropy by diffusing away from the crystal and so covered the initially bare substrate. This diffusion process away from the crystals progressively lowered the probability for re-attachment as the density of detached molecules close to the crystal decreased. Consequently, crystals progressively lost more and more molecules, got smaller and eventually reached a size where the surface-to-volume ratio was high enough to allow for complete melting of the crystal. Accordingly, small isolated crystals on any bare substrates can never "survive" for long times, they will eventually disappear as can been seen in **Fig. 4.7c**. A related study for alkane monolayers and sub-monolayers showed the dependence of the melting temperature on surface coverage. There, crystals found to be in equilibrium with a thin liquid layer covering the whole substrate [126]. We conclude that isolated crystals deposited on a bare substrate are prone to disappear even at temperatures well below the melting temperature of such crystals surrounded by its melt.
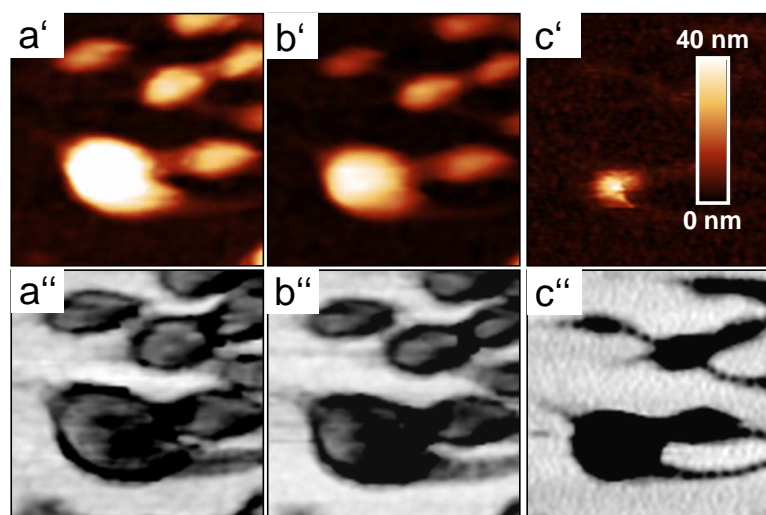
Figure 4.7 – AFM topography (top row, color code ranging from 0 – 40 nm) and phase (bottom row) images showing the disappearance in time of the nanocrystals from **Fig. 4.6h** after a) 15 min, b) 300 min and c) 1000 min at 133 °C. The size of images is 1 x 1 µm^2.

4.3 Three distinct paths for changes in morphology

From the above results we can identify three processes for lowering the free energy of an ensemble of nanocrystals (see **Fig. 4.8**). Annealing nanocrystals at progressively higher temperatures allows accentuating them differently.

Path 1:

Due to their small size and their high surface-to-volume ratio, a large amount of molecules at the periphery of these nanocrystals shows a high tendency for detachment. This favors the formation of bigger lamellar crystals at the expense of smaller ones. Interestingly, this Ostwald ripening process is not necessarily involving a reduction of the number of chain fold. *i.e.*, the thickness of the lamellar crystals remains constant. Thus, we may tentatively conclude that the required energy for removing chain folds is higher than for detaching polymers from a crystal. Alternatively, the kinetics of fold removal may be slower in comparison to the exchange of molecules between individual nanocrystals.

Path 2:

The existence of chain folds in an otherwise crystalline polymer reduces crystallinity and thus represents a cost in crystallization energy. Thus, states of

highly folded crystalline chains are never stable and will evolve into less folded states, *i.e.* lamellar crystals of higher thickness. Such can either be achieved at constant temperature by increasing the annealing time (the increase in lamellar thickness depends on the logarithm of annealing time [127, 128] or for a constant experimental (annealing) time by increasing the annealing temperature. Due to the high mobility of polyethylene along the chain axis lamellar thickening is easily possible even in the crystalline state [129–131]. In accordance with this tendency; our observations show an increase in lamellar thickness at temperatures above ca. 110 °C. We expect that some increase of lamellar thickness would also occur at lower temperatures but at a drastically lower rate.

Path 3:

For our "open system", even below the thermodynamic equilibrium melting temperature crystals can show a melting-like behavior. Similar to sublimation, bordered by empty space or a bare substrate, crystals of small volume (*i.e.*, with a large number of molecules located at the crystal surface) will decrease in size due to the loss of molecules to the surrounding space. We would like to re-emphasize that such a decrease in crystal volume and eventual melting is not possible in a "closed system" like the one studied by Rochette *et al.* [103].
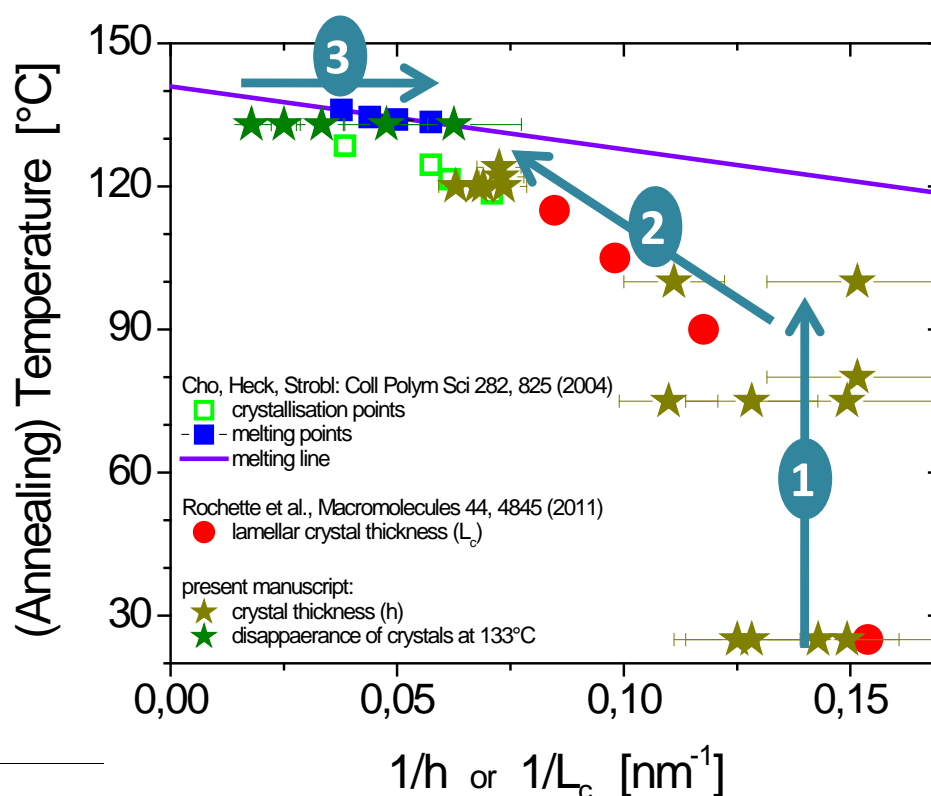
Figure 4.8 – Compilation of the thickness values determined from AFM measurements on monolayers shown in this manuscript, represented in a Gibbs-Thompson plot (temperature vs. reciprocal thickness). Our results are compared with literature data on bulk samples and on nanocrystals in aqueous dispersion analogous to the ones studied here on a solid support. The arrows 1 – 3 indicate pathways followed during annealing. Details are described in the text.

4.4 Concluding remarks

Taking advantage of the well-defined small size of the initial nanocrystals, which were deposited in a controlled way to result in a layered assembly, we investigated the process of molecular reorganization and the corresponding morphological changes as a function of temperature and annealing time. Due to the kinetic features of the various pathways taken, a representation of the reciprocal crystal thickness in a Gibbs-Thompson plot yields a complex pattern. A large spectrum of possible correlations between annealing temperature and crystal thickness is explored, as shown in **Fig. 4.8.** No crystal will be able to resist melting if the temperature is increased above the melting line which reflects the size-dependent melting temperature. We note that the representation as a function of inverse

thickness implies that the crystal size in the other two dimensions is large. Thus, for the initial nanocrystals having a nanometer size in all dimensions, a representation as a function of inverse volume might be more appropriate. Below the melting line, the actual thickness of the crystal depends on the pathway taken, allowing to obtain for a given annealing temperature crystals of different lamellar thickness.

A comparison with literature results on bulk samples [132] and results obtain by annealing the same type of polyethylene nanocrystals in an aqueous dispersion [103] demonstrates that our results are consistent with previous conclusion. As shown in [103] for a "closed system", crystals having a well defined lamellar thickness can be stabilized (equilibrated) at temperatures well below the melting line for large lamellar crystals of a certain lamellar thickness as studied *e.g.* in [132]. Furthermore, by using assemblies of small nanocrystals ("open system"), we were able to display that polymer crystals are thermodynamically not stable below the melting line. While such crystals will always try to reach energetically more favorable states of less folded chains, *i.e.* increased lamellar thickness, they may also loose molecules to the surrounding bare substrate, decrease in volume and eventually melt due to their small size. Consequently, a manifold of crystalline states, differing *e.g.* in lamellar thickness and volume, are possible for a given annealing temperature. In an "open system" these states are only metastable. Thus, morphological changes will occur in the course of time. The molecular architecture of polyethylene allows for comparatively fast reorganization processes and a relatively facile thickening of lamellar crystals which can be easily detected even after rather short time and modest annealing temperatures. We anticipate that also other semicrystalline polymers will follow the same pathways during annealing. However, steric constraints or specific intra- or intermolecular interaction may drastically reduce the rate of these kinetic processes. Thus, on typical experimental timescales no changes in thickness or morphology may be detectable.

[1]

---

[1]All the results shown and explained in this chapter have been published in ref. [133]

Chapter 5

Shear induced crystallization by AFM cantilever tip from an undercooled melt of polyethylene nanocrystals

In the previous chapter, we have performed systematic in situ annealing measurements and have discussed reorganization processes of deposited polyethylene nanocrystals upon annealing as a function of annealing time and annealing temperature for both monolayer and stacks of multiple layers. In this chapter, we will discuss crystallization experiments from the undercooled melt of polyethylene nanocrystals.

Scanning the AFM probe over a viscous melt leads to a deformation of the molten surface as a shear force is acting on the melt surface as a consequence of the moving AFM cantilever tip. The molecular chains within the melt are stretched by the AFM cantilever-tip during scanning. Typically, a large shear rate as well as a huge mechanical work is applied (as will be shown later) on the undercooled melt and this certainly enhanced the possibility of the stretched molecular chains to be aligned along the direction of scan. The aggregation of the stretched and aligned chains along the scan direction may result in small crystalline domains. Different nucleation processes in polymer crystallization will be explained. The mechanism of tip-induced nucleation will be described in detail. Factors such as number of scans or more specifically, the shearing time and tapping force affecting the nucleation rate or the nucleation probability will be discussed in detail. How nucleation induction time and contact time between the molten sample surface and the AFM probe do influence the nucleation rate will also be included in our discussion. It will be shown that the temperature of the

undercooled melt will be an important parameter in describing the tip-induced nucleation phenomenon. Even in regions consisting of few droplets of different sizes at a temperature close to the melting temperature, it could be shown that well aligned edge-on crystalline domains along the scan direction can be found. A mechanism for the formation of stacks of edge-on crystalline lamellae will be proposed.

5.1 Introduction

The crystallization behavior of polymer melts under flow is an important and interesting subject of polymer processing which directly affects the final properties. In most polymer processing operations, such as extrusion, injection molding, fiber spinning, etc., the molten polymer is exposed to varying levels of flow fields (elongation, shear, mixed) [134]. In comparison with quiescent crystallization, crystallization under flow is much faster which results in different morphologies *e.g.* shish kebab morphology. It is well-known that during polymer processing the crystallization kinetics and the final morphology, (spherulitic, cylindrical, or fibrillar) are deeply influenced by molecular orientation induced by flow (in the molten state) and deformation (in the solid state) [42,72,135–137]. Many studies have been carried out to investigate the molecular orientation in the deformed melt and the resultant morphological changes during the crystallization process utilizing various combined characterization techniques. These involve some methods such as optical microscopy, atomic force microscopy (AFM), and transmission electron microscopy (TEM) [138,139].

To map out the surface topography AFM is mainly relying on monitoring the deflection of a tip caused by its interaction with the sample surface during scanning. Typically, imaging is carried out in a condition of low force between the tip and the surface molecules. Several studies have been performed to investigate nucleation induced by AFM tips during the crystallization experiments [140–142]. Pearce and Vansco investigated the possibility of tip-induced nucleation during crystallization of poly(ethylene oxide) (PEO) near the melting point [140]. They concluded that the tip did not induce nucleation. A similar conclusion was made by Godovsky and Magonov during their study of PE crystallization using AFM [141]. However, Beekmans found that tip induced nucleation was possible in the study of crystallization of poly(-caprolactone) (PCL) [142]. The difference in the behavior between PEO and PCL was attributed to the difference in the shear force. High shear forces will cause chain alignment at the surface

of the melt. It is important to point out that in the studies on PCL [**142**] and PEO [**140**] the contact mode, which in general produces high shear forces during scanning, was used at temperatures near the melting points of the polymers. During the experiments, the amorphous areas around the growing crystallites were scanned for a long time without detection of nucleation. Control of molecular orientation within polymer films introduces anisotropy of the physical properties. Control of orientation in a specific localized space is quite helpful in developing ordered nanometer sized structures in polymers. These nano-sized structures could be applied for device preparation. Atomic force microscopy is a powerful tool to introduce such structures in different organic films with nanometer resolution. Several kinds of polymer thin films (*e.g.* polystyrene) were modified by scanning or indenting using AFM cantilever tip, resulting *e.g.* in ripple structures perpendicular to the fast scan direction [143] which were accompanied by an increase in volume. The modification mechanism is considered to be a mechanical deformation [**144**–**149**]. AFM has been used before for mechanical indentation and to scratch the sample surface. Usually, stretching method is one of the most powerful orientation control techniques for thick polymer films but is not suitable for controlling specific localized areas. Orientation control of liquid crystals using AFM has also been studied [**150, 151**] where a thin polymer film was rubbed by an AFM tip for aligning liquid crystals on a surface driven by the grooves or some structural changes on the surface induced by rubbing. This method is very useful for nanolithography and for alignment of liquid crystal molecules. AFM tip has been used in the contact mode to scratch/rub the surface of a glassy polymer thin film of isotactic polystyrene (i-PS) at room temperature. After subsequent isothermal crystallization, an extremely high nucleation density of edge-on crystals within the rubbed region was observed. This study demonstrated that both, soft rubbing or hard scratching, allow for lowering the nucleation barrier for polymer crystallization and to control the orientation of the resulting crystalline lamellae [152].

Recently, people have succeeded [153–155] to align polymer molecules in a desired direction with precise control of film temperature and applied load by scanning an AFM cantilever tip in contact with the sample surface in a way named modification scan. Well aligned edge on lamellae appeared after the scan [153–155]. Film thickness measurements were conducted in situ after removing polymers from a selected region of the sample through a process of tip-sample force adjustments described as nanodozing [145].

5.2 Experimental procedure

Samples were prepared for these experiments in a similar way as discussed in **chapter 3**. Using AFM hot stage, the deposited monolayer and multilayer stripes were annealed at a temperature (mostly at 130 ºC) close to the nominal melting temperature of the crystals (*i.e.* 133 ºC) and kept at that temperature for some time ($\sim$ 30-40 minutes) in order to obtain molten polymers. As the crystals were molten below the equilibrium melting temperature some memory of the crystalline state may have been retained for some time. Subsequently, crystallization experiments were carried out by cooling the sample down slowly to a temperature range from 122 ºC to 118 ºC where nucleation was observed. In this temperature range we also observed the process of lamellae thickening during systematic annealing of the deposited crystals in the previous chapter. There, stretching of the polymer chains by the moving AFM tip followed by aggregation of the stretched chains resulted in the formation of small crystalline domains built up by polymers aligned along the scan direction of the AFM probe. Although in our studies the experiments were done in tapping mode (the tip was not in continuous contact with the sample surface) AFM tip was none the less able to induce such stretching and aligning of polymers.

5.3 Nucleation process in polymer crystallization

Polymer crystallization normally starts with primary nucleation. Nucleation can be defined as the formation of small crystalline domains due to fluctuations in density or order in the super cooled melt [156]. The formation of these initial or primary nuclei is the first step of the crystallization process. The continuation of crystallization by attachment of more and more polymer molecules on the growth surface is normally known as secondary nucleation. If no foreign surface or existing nuclei is present, nuclei formation may take place spontaneously with a probability depending on supercooling. This phenomenon is termed homogenous nucleation. However, if any second phase is required (it may be a foreign particle or the surface of a nuclei/crystal from the same polymer), then nucleation is termed heterogeneous nucleation. Wunderlich *et. al.* [**157**] based on an earlier work [**158**] have further advocated the subdivision of this classification by incorporating a third category called self-nucleation or self-seeding. Polymer crystallization from the melt is often associated with thermal memory effects *i.e.*, the dependence of the crystallization kinetics on thermal history. If a

semi-crystalline polymer is molten and then recrystallized, crystallization kinetics depends on temperature and time in the molten state (*e.g.* Ziabicki) [**159**]. The memory effect causing self-seeding can be explained as an indication that chain segments from former crystalline lamellae retain their conformational crystalline arrangement even when surrounded by melt.

While primary nucleation can be homogenous or heterogeneous, secondary nucleation by its definition is heterogeneous.

In order to form stable nuclei (primary or secondary), the free energy barrier of crystallization needs to be overcome. The size of the required critical nucleus obviously depends on this free energy barrier: larger critical nuclei require longer times to form. In any nucleation process, the free energy barrier $\triangle G$ of the nucleation process (crystallization) is given roughly by,

$$\triangle G = \triangle G_c + \sum \gamma^* A \tag{5.1}$$

where, the first contribution $\triangle G_c$ represents the change of Gibbs free energy per unit volume of the solid or crystalline phase. This leads to an energy reduction of the system which is then counterbalanced by the introduction of surface energy *i.e.* the second contribution of the **equation 5.1**. $\sum \gamma^* A$ results in increase in the surface energy of the system where the specific surface free energy is given by $\gamma*$. Primary nucleation involves the largest specific area A while the area is somewhat reduced for secondary nucleation on the surface. Tertiary nucleation, which can be defined as nucleation in a corner, involves yet lesser specific area.

5.4 Nucleation under shear: induced by AFM cantilever tip

A variety of features can be induced in thin polymer films with an AFM tip through tip-sample force alteration. When relatively low forces are employed, the polymer surface can be imaged non-destructively. Under such conditions images can be obtained even when the sample surface is scanned many times with no visible changes in the images. In addition, enlarging the scan area shows no evidence for irreversible changes in the area previously scanned. Application of high forces results in the removal of polymer material from the substrate surface, *e.g.* via the nanodozing process [**145**], producing holes in the films. Intermediate

forces can cause polymer material to become transported by the tip into ridges which generally lie perpendicular to the AFM fast scan direction. Here, we will show how an AFM tip can induce nucleation even when using the intermittent tapping-mode.

In rheological approaches, there are at least four different geometries which allow shear induced crystallization and orientation studies. These are the cone-plate [160], rectilinear parallel plates (sandwich rheometer or sliding plates) [**161**], slot flow (duct flow) [**162**], and torsional parallel disks (rotating parallel plates) [**163**]. Cone-plate geometry and rectilinear parallel plates produce a uniform shear rate across a sample but both slot flow geometry and torsional parallel disks cause a continuous variation of shear rates across the sample, depending also on the viscoelastic properties of the material [**164**]. When the flow parameters controlling the formation of oriented structures are not known and need to be determined, then geometries with a broad distribution of shear rates could be advantageous as they can be used in a combinatorial approach to detect the conditions necessary for the onset of oriented nuclei. Another advantage of slot flow and torsional parallel disks is that each point in the sample associated with different shear flow rate experiences the same temperature protocol, thus eliminating errors associated with the reproduction of temperature history possible with the repetition of the measurements required by the first group of geometries [165]. Compared to the recent flow induced crystallization studies [**165**–**168**] our study is different in the sense that no large scale flow was induced by external forces. The molten surface was locally deformed by repeated scanning of the AFM probe over the molten surface.

Fig. 5.1a shows an AFM phase image of a triple layer stripe after it has been kept at 127 °C for 30 minutes. During this time both the temperature stabilisation and imaging were carried out. This sample was first annealed at 133 °C. There, all crystals were molten. After $\sim$ 20 minutes when temperature stabilisation and first time imaging was completed, the temperature was slowly reduced to 130 °C and imaged once. The next step was to reduce the temperature to 127 °C. No indication of nucleation was observed even at 127 °C after the same region was scanned first time at that temperature. But, when the sample was cooled down from 125 °C to 122 °C and scanned a significant number of edge-on crystalline domains were found, oriented perpendicular to the scan direction (see **Fig. 5.1.b**). From the topography image (see **Fig. 5.1.c**) one can also deduce an apparent difference in thickness between the formed edge-on aggregated crystals and the still molten region surrounding them. This becomes very obvious from

the height profile taken at the position of the white line in **Fig. 5.1(c)** (see **Fig. 5.1.d**). The temperature-time protocol followed for this particular sample have been schematically shown (see **Fig. 5.1e**).
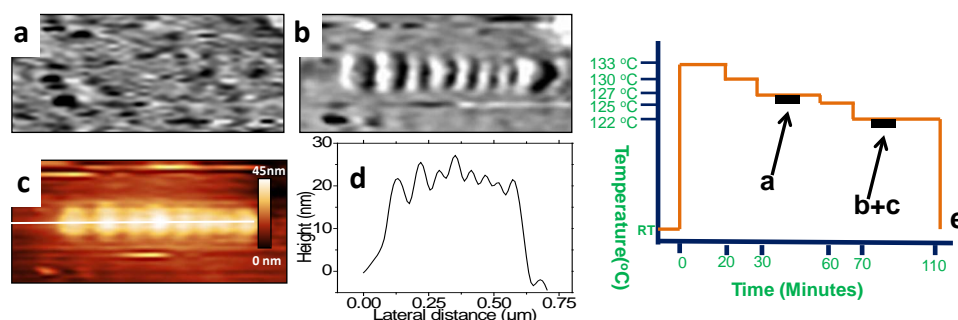
Figure 5.1 – AFM phase images (a–b) showing crystallsation in a molten film resulting from a stack of three layers of nanocrystals. (a) 30 min at 127 °C, (b) 20 min at 122 °C. Some edge-on crystals were found to form, aligned perpendicular to the scan direction. (c) The corresponding height image (the color code ranges from 0 – 45 nm) of (b) showing height difference between the resulted edge-on crystals and the molten surrounding film. Size of each image is 0.7 x 0.3 µm². (d) Corresponding height profile of the line drawn in image (c). (e) Schematic showing thermal history (the temperature-time protocol) of the sample. The black rectangular boxes represent the time of imaging for each image shown in a and b+c.

In published works on flow induced crystallization using different methods similar temperature-shear protocols have been followed [**165**–**168**] in order to observe nucleation. The first step was to heat the polymer above its equilibrium melting point to remove all memory of previous heat treatments and the second step was to cool the polymer down to the temperature where a shear pulse was applied to the undercooled melt followed by isothermal crystallization and/or a further cooling to lower a temperature to complete the polymer crystallization. In our studies we never heated our samples above the equilibrium melting temperature and memory may not have been lost completely.

Due to the temperature-dependent change in the resonance frequency of the oscillating cantilever-tip, the value of amplitude set point has to be set properly in order to image the molten surface with a low tapping force. Due to stickiness of the melt there is a possibility of adhesive interaction between the AFM probe and the molten sample surface. Adhesion becomes more pronounced when the set point amplitude ratio is decreased *i.e.* at increased tapping force. Thus, one may expect that polymer chains are also sheared or deformed more at higher tapping force. While the AFM probe is scanning over the molten surface the polymer chains within the viscous melt may be stretched by the AFM tip.

These chains may become nuclei for the crystals when several of them align and aggregate along the scan direction. In fact, scanning of the AFM tip over the undercooled viscous melt has two consequences on the polymer chains. They can be oriented and stretched at the same time. In our experiments, polymer chains were deformed in the scanning direction. In edge-on lamellae chains are lying flat-on the substrate (parallal to the surface of the film) with the c-axis aligned in the scanning direction (see **Fig. 5.2**).
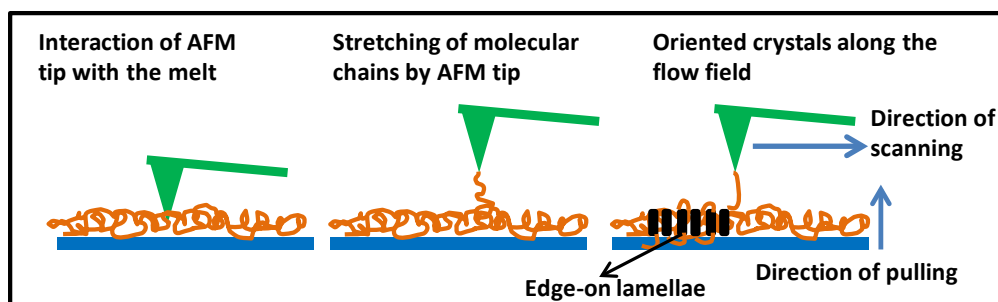
Figure 5.2 – Schematic of the shear induced nucleation by AFM tip in our study.

The applied tapping force may cause deformation of the chains at the surface of the melt in the direction of scanning. Thus, the sample experiences lateral shear forces, the amount of which depends on the amplitude set point value and the scan rate. These shear forces might be sufficient to induce nucleation during scanning by aligning polymers predominantly along the scanning direction. When the shear rate is smaller than the reciprocal Rouse relaxation time the orienting effect is dominant while stretching becomes significant at higher shear rates [169]. Interestingly, experimental results [170–174] show that even small deformation considerably enhance the crystallization rate at high shear rates. In our case, the shear rate was calculated to be approximately $10^3 s^{-1}$ to $10^4 s^{-1}$ (will be shown later). At such high shear rates one even can stretch shorter molecules and, therefore, increase the concentration of stretched molecules which can be potentially involved in the formation of primary nuclei. It should be noted that the scanning direction is horizontal in all AFM images. If, as a result of such stretching, a stable nucleus is formed with a horizontal orientation of the c-axis of the polymers, this nucleus should serve as the starting point for further growth of lamellar crystal structures.

Under shear-flow condition, it has been observed that mechanical work per volume above a certain value must be applied to the polymer melt at a shear rate larger than the reciprocal Rouse relaxation time of the longest polymer chain within the polymer melt in order to observe shear-induced crystallization. Below

this work, nucleation is not possible [165–168, 175]. This mechanical work w was found to be

$$w = \int_0^{t_s} \eta \left(\frac{d\gamma}{dt}(t) \right) \left[\left(\frac{d\gamma}{dt}(t) \right) \right]^2 dt \qquad (5.2)$$

$\frac{d\gamma}{dt}$ is the shear rate (the rate of change of shear strain or particularly deformation in our case), η is the shear rate dependent viscosity and the integration is performed over the entire time of shearing t_s. Time of shearing is important, as it demonstrates that not only the shear rate is important in order to be able to stretch the chains but also the time of stretching needs to be sufficiently long in order to allow aligning and aggregation of polymers. Different experimental methods have been proposed in literature to determine the "critical" value of the mechanical work that needs to be applied to the polymer [165, 167, 176].

The approximate mechanical work performed during shearing on the undercooled melt of the polyethylene nanocrystals necessary to induce crystallization was calculated using **equation 5.2**.

In our case, the lateral tip velocity V_t was ~ 10 µm/s (as given by the software JPK during scanning) and the contact time t_c (defined by the time per oscillation that the tip is interacting repulsively or stays in mechanical contact with the sample) was of the order of µs. The shear rate in our studies was related to the penetration depth of the AFM probe into the melt and it was $\sim 10^{-3}$ to 10^{-2} µm.

The shear rate $(d\gamma/dt)$ = tip velocity/ penetration depth = 10 µm s^{-1}/(10^{-3}- 10^{-2}µm) = 10^4- 10^3 s^{-1}

From **equation 5.2** the mechanical work performed on the melt can be calculated. From literature the viscosity of polyethylene melt at a temperature range 125 ºC to 130 ºC was found to be of order 10^4 Pascal second for low density polyethylene samples ($M_w \sim 120$ kg/mole) [177]. We know that with increasing temperature of the polymer melt the viscosity is reduced. So, at high temperature (~ 150 ºC) the viscosity would be of the order of 10^2 Pascal second. As for most of our studies the deposited crystals were molten $\sim$ at 130 ºC, viscosity of order 10^4 Pascal second will be taken into account.

$$w = \int\limits_{0}^{10^{-6}s} 10^4 Pa.s \left[10^4 s^{-1}\right]^2 dt \tag{5.3}$$

Where, 10^{-6} seconds is the time of shearing. In our experiments, the tip was penetrating through the molten surface, as this was necessary for producing shear force within the melt. The penetration depth was in the range of few nanometers as we have discussed before. During stretching the cantilever was oscillating near its resonance frequency. In most of our experiments the resonance frequency of the used cantilever was $\sim$ 160 KHz. During imaging the oscillation frequency of the cantilever was in the range of $\sim$ 157-159 kHz. Oscillation frequency is number of osillations of the cantilever per unit time. So, the shearing time was taken as a fraction of the reciprocal of the oscillation frequency, *i.e* ca. 1 µs.

$$w = \int\limits_{0}^{10^{-6}s} (10^{12} Pa.s^{-1}) dt \tag{5.4}$$

$$w = \left[10^{12} Pas\right]_{0}^{10^{-6}s} \tag{5.5}$$

$$w = 10^6 Pa \tag{5.6}$$

If the shear rate is used as 10^3 s^{-1}, considering the penetration depth of the AFM tip through the melt surface to be a little higher ($\sim$ 10 nm) then the workdone comes out as $10^4 Pa$.

The mechanical work done on the polymer melt in our case was found to be high ($\sim 10^6 Pa$). This value of the mechanical work performed on the melt was found to be somewhat smaller than the one mentioned in ref. [168] ($\sim 10^8 Pa$). Nonetheless, inducing nucleation under such high shear rate seems possible by the AFM cantilever tip even under low deformation.

5.4.1 Nucleation and growth of the aligned crystals

Polymer crystallization is a two step process which includes nuclei formation and subsequent growth. The shear enhanced crystallization rate is generally associated with a significant increase of the first step *i.e.* the nucleation rate. According to classical nucleation theory, the nucleation rate for quiescent conditions (when there is no shear applied) depends on the free energy difference between the crystalline and amorphous phase. The effect of shearing on the kinetics of nuclei formation is understood by considering that the increase of the degree of order due to shear results in an effective change in the free energy of the melt. In that context, several models have been proposed which directly relate the free energy changes to some measure of flow intensity. Dumbbell-like models have been initially used to calculate the flow-induced change in free energy and the subsequent crystallization rate enhancement [178]. Theoretically, a simple approach is to associate the external work and the Gibbs free energy, which considerably reduces the nucleation barrier and thus enhances the nucleation rate.

The following question arises: What would be a driving force for the formation of stable clusters in polymer crystallization? One possible answer is that stable inert nuclei exist at all temperatures below the equilibrium melting point of the polymer [179]. However, a systematic comparison of results on shear-induced crystallization [180] suggests by direct experimental observations [167] that stretching is a necessary condition for the formation of an oriented morphology. Stretching of polymer chains which is generated by surface crowding leads to an increase in surface free energy of the polymer melt, which consequently reduces the nucleation barrier and increases the thermodynamic driving force $\Delta G = \Delta G_\ell - \Delta G_s$ (ΔG is the free energy difference between the liquid and the crystalline phase. ΔG_ℓ and ΔG_s are the free energy changes of the solid and liquid phase, respectively). Stretch contributes an extra work (ΔG_f) to increase thermodynamic driving force (ΔG). The good correlation between experimental results and ΔG suggests that combining classical nucleation theory with the extra work ΔG_f in the driving force can be generalized to all shear enhanced crystallization conditions. Thus, stretching of polymers should be considered as the first step in the formation of nuclei which are created from the initially quiescent melt. These nuclei have to be made stable and one possible reason for their stability under shear deformation is that stretched segments of the coiled molecule reduce the configurational entropy of the chain allowing the stretched portions to come into closer contact with each other and the aggregates to get bigger. An inert nucleus (*i.e.* a nucleus too small to grow) cannot survive without the shear flow

as it may dissolve in the melt at quiescent conditions. However, while it has been created and stabilized under shearing condition it will collide with other inert nuclei, where the number of collisions, facilitated by the mechanical work performed on the system during shear, transforms low quality inert nuclei into stable aggregate nuclei. If shearing is stopped at this point, the aggregates formed, in contrast to dormant nuclei, will still be stable as their sizes are above the critical size of active nuclei required at these thermodynamic conditions. Aggregates possessing a size smaller than the critical size will dissolve.

Deformation of amorphous chains has two effects on the nucleation kinetics: stretching reduces the entropic penalty for crystallization; and monomer alignment increases the probability of suitable alignment with the nucleus.

We need to consider several parameters which are related to the shear induced crystallization in our studies. In a pure polymer melt, shear force between the melt and the AFM probe orients and aligns the polymer chains in the melt to form stable nuclei consisting of chains having their c-axis oriented along the scan direction. The stability of these structures depends very much on the relaxation behavior of the oriented polymer chains in the melt. The relaxation behavior mainly depends on chain length and temperature. Longer chains take longer time to relax from the deformation than shorter ones and thus have a better chance to be oriented after shear. Short chain molecules relax in a short time after deformation and hence often cannot form nuclei under shear. Under certain shear conditions, longer chains will remain oriented (because of longer relaxation time) whereas the rest of the molecules will relax and become un-stretched.

Both, an increase of temperature and a decrease in molecular weight of the high molecular weight tail would result in a reduction in relaxation time and thus an increase of the minimum shear force parameter. As we have discussed previously that the viscosity of polyethylene melt at a temperature range 125 ºC to 130 ºC was found to be of order of 10^4 Pascal second for low density polyethylene samples ($M_w \sim 120$ kg/mole) [177]. We know that with increasing temperature of the polymer melt the viscosity is reduced. So, at high temperature (~ 150 ºC) the viscosity would be of the order of 10^2 Pascal second. At high temperature, the polymer chains quickly relax and nuclei dissolve within the melt and cannot induce crystallization. That is the reason why at relatively high temperature the system contains only molten polymers but no stable crystals (see **Fig. 5.3a+a´**). A temperature decrease corresponds to an increase in relaxation time. In turn, this increases the degree of orientation of the polymer chains at a

given shear rate, thus leading to higher probability of nucleation as can be seen in **Fig. 5.3 b+b´**. With the decrease in temperature, well aligned crystals were formed, directed along the scan direction. In our study, phase imaging provides sufficient resolution for the visualization of individual crystalline aggregates of varying thickness (for a given polymer of known chain length a measure for the degree of chain folding is the thickness of the crystalline lamellae) in the range of 20 to 50 nm but the width (defined as the linear lateral extent of the resulted crystalline regions from one side to other side) of these regions are large ($\sim$ 150 nm or even more). With time these crystalline domains were growing and new crystalline domains appeared around the previous domains in the course of scanning at a fixed temperature (see **Fig. 5.3c+c´**). From the latter observation we conclude that the nucleation probability increases with number of scan.
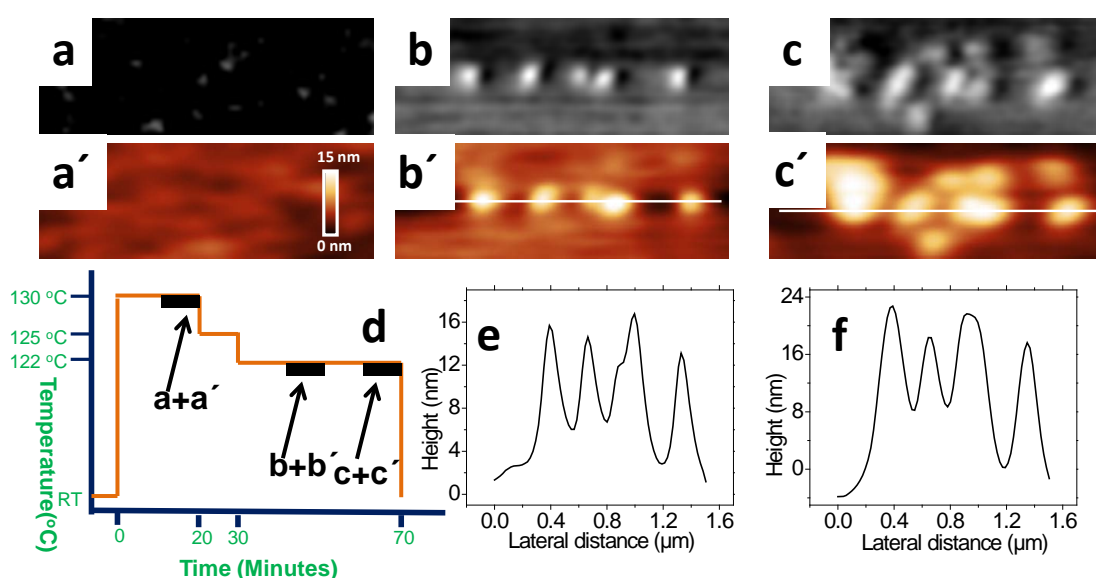
Figure 5.3 – AFM phase (a–c) and corresponding topography images (a´-c´, the color code ranges from $0 - 15$ nm) showing crystallization from an undercooled melt of polyethylene nanocrystals. [a)+a´) 20 min at 130 °C, b)+b´) 20 min at 122 °C, c)+c´) 40 min at 122 °C (considering the time for temperature stabilisation and imaging, after the temperature got stabilized the sample was contineously imaged)]. Well-aligned edge-on lamellae were found to form perpendicular to the scan direction. Size of each image is 1.5 x 0.5 μm^2. (d) Schematic showing thermal history (the temperature-time protocol) of the sample. The black rectangular boxes represent the time of imaging for each image shown in a, b and c. (e) and (f) Corresponding profiles of the white lines drawn in fig b´ and c´ respectively.

5.4.2 Increase in nucleation probability with number of scans

In **Figure 5.4**, the effect of number of scans is shown for a sample that was cooled down from 122 °C to 120 °C and kept at that temperature for 30 minutes considering the temperature stabilisation and imaging time. This sample was scanned at 120 °C only two times. While the temperature stabilisation and first scan took $\sim$ 20 minutes, the second scan took $\sim$ 10 minutes. After finishing of the second scan the sample was kept at 120 °C for 10 more minutes without scanning and then cooled down to room temperature.

In general, in most of our experiments, it was found that a several times scanned region contained a larger number of lamellae per unit area as compared to a region scanned once only. As we are dealing with a melt and the AFM tip is scanned over the same region several times, it is possible that the AFM tip oriented progressively more polymer chains (by stretching of them and subsequently orient them in the shear direction) during each single scan.

In order to scan the whole investigated area by an AFM tip, some 100 scan lines are needed which takes about 10-15 minutes. Thus time of stretching of an individual polymer is short. At such a small time the probability may be not so significant for the tip to induce crystallization, as a result no stable nuclei were observed except one at the top left corner (see **Fig. 5.4 a´+a´´**). During the later scans, *e.g.* here in the second scan (see **Fig. 5.4 b´+b´´**) the time that the tip is scanning over the same region of the viscous melt is progressively increased which subsequently increases the probability of stretching (**Fig. 5.4 b´+b´´**) and consequently, the probability for the AFM tip to induce nucleation increased. Increasing number of scans increases the probability for the AFM tip to stretch the polymer chains by interacting more often with melt and inducing more deformation on the molten surface. That is why we found an increased number of crystalline domains per unit area after finishing of each scan even if we kept the temperature fixed. It is important to note that the sample was imaged continuously *i.e.* the total time that a sample has been kept at a particular temperature is the combined time for temperature stabilisation and imaging.
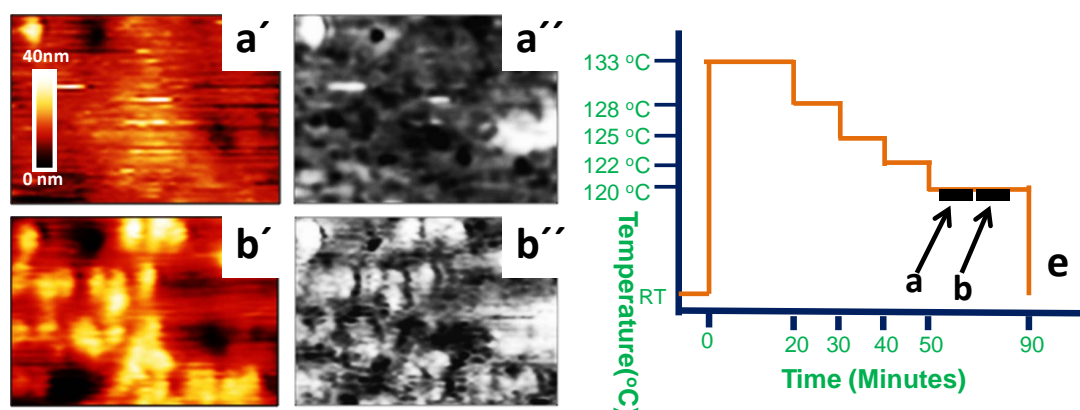
Figure 5.4 – AFM topography (a´ and b´, the color code ranges from 0 – 40 nm) and the corresponding phase images (a´´ and b´´) showing the effect of number of scans on nucleation probability at 120 °C during crystallsation from an undercooled melt of nanocrystals. [a´ and a´´) 20 min at 120 °C scanned for the first time, b´, b´´) 30 min at 120 °C, scanned secend time. Size of each image is 1 x 0.7 µm^2. (e) Schematic showing thermal history (the temperature-time protocol) of the sample. The black rectangular boxes represent the time of imaging for each image shown in a and b.

5.4.3 Increase in nucleation probability with tapping force

Our next aim was to verify the effect of tapping force on the tip-induced nucleation process. It was found that during cooling down from 120 °C to 118 °C nucleation started. At 118 °C the AFM cantilever-tip was scanned over three different regions of the sample for about 40 minutes with various tapping forces. For the first scan all three regions were scanned with a same tapping amplitude ($r_{SP} = 0.53$) for about 10 minutes. The nucleation probability for this first scan was almost similar for all regions (see **Fig. 5.5 a+a´+a´´**). The exactly same three regions were then scanned for the second time with varying tapping forces separately. Scanning of each regions took $\sim$ 10 minutes and so imaging all three regions took $\sim$ 30 minutes (see **Fig. 5.5 b+b´+b´´**).

It is important to note that at 118 °C the sample was continuously scanned. In the first region (see **Fig. 5.5 b**) a relatively small tapping force was applied ($r_{SP} = 0.53$) compared to the other two regions (see **Fig. 5.5 b´+b´´**) where the applied tapping forces were higher ($r_{SP} = 0.37$ and $r_{SP} = 0.23$ for the second and third region, respectively) and it was found that with increasing tapping force the nucleation probability increased (see **Fig. 5.5 b´+b´´**). The set point amplitude was varied right after finishing of the first scan over the regions mentioned in **Fig. 5.5 a+a´+a´´**. After $\sim$ 10 minutes, when the first region

has been scanned for the second time, the set point was varied and at that set point the second region was scanned for the second time for another ~ 10 minutes. The set point then was reduced to an even lower value to image the third region for the second time which took again ~ 10 minutes. At higher tapping force, the shear force between the tip and the polymer melt increased which increased the nucleation rate. Not only the number of scan increases the nucleation probability but also the tapping force contributes to an enhanced nucleation rate in our study. The same three regions were again scanned for a third time with $r_{SP} = 0.5$ for another ~ 10 minutes and so in total the sample was kept at 118 °C for ~ 45-50 minutes with continuous imaging. From the results mentioned above it is clear that crystallization contributed significantly in all the three regions (see **Fig. 5.5 c+c´+c´´**).
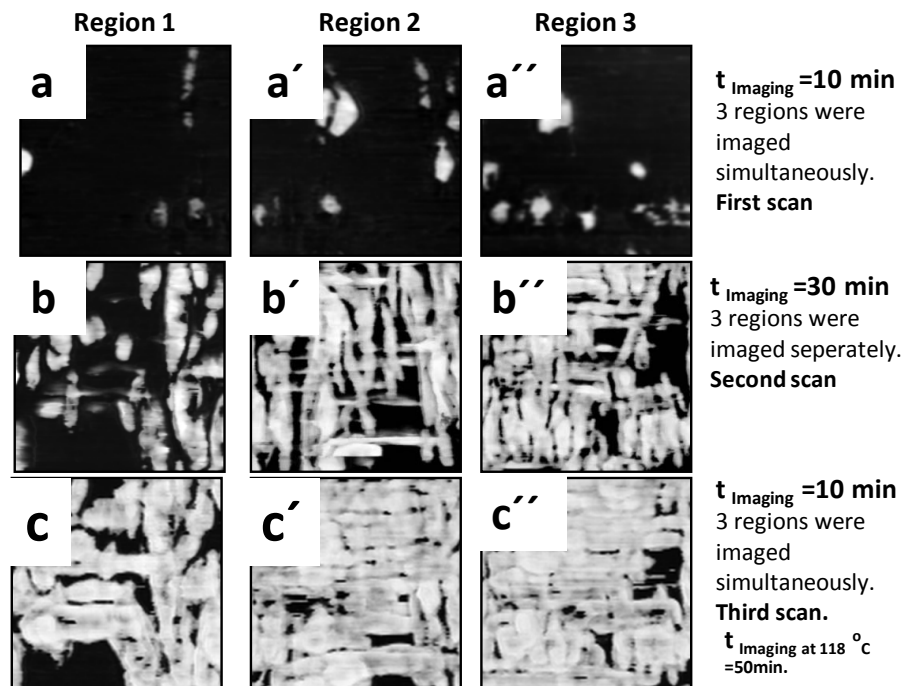
Figure 5.5 – AFM phase images (**a+a´+a´´, b+b´+b´´, c+c´+c´´**) showing the effect of varying tapping forces on the nucleation probability or nucleation rate at 118 °C during crystallsation experiments from an undercooled melt of nanocrystals [a, a´, a´´) three regions scanned simultaneously for $\sim$ 10 min with $r_{SP} = 0.53$, (b, b´, b´´) three regions scanned seperately $\sim$ 10 minutes each with $r_{SP} = 0.5, 0.37, 0.23$ respectively ($\sim$ 30 min for three scans), (c, c´, c´) third time the same regions were scanned simultaneously for another ~ 10 min ($r_{SP} = 0.5$). So, the tip was scanned over the sample ~ 45 minutes in total. Size of the images is 2 x 2 μm^2.

5.4.4 Effect of contact time and nucleation induction time on nucleation rate

Contact time t_c is defined by the time during one period of oscillation that the tip is interacting repulsively or stays in mechanical contact with the sample. The force is averaged over an oscillation period. This time t_c is a useful quantity to understand the behavior of tapping operation as well as for the estimation of the deformation done to the sample surface. The contact time increases with the tip-sample proximity. For a small separation in relation to the free amplitude of oscillation there is a steep increase in contact time. So, in this case there is a contact almost during the whole oscillation cycle.

The contact time depends on the mechanical properties of the sample. The contact time increases with decreasing Young's modulus. Softer samples have larger contact time values as compared to stiff materials. For hard elastic materials the product of contact time and the force is almost constant [181]. In that case forces and contact times are inversely proportional. Experiments performed on samples with very low elastic moduli (*e.g.* polymer melt in our case) could have contact times close to oscillation period of the cantilever tip. The contact time cannot be directly measured but average force measurements are somehow analogous [182].

At elevated temperatures where there is viscous melt everywhere within the system, the contact time between the melt and the AFM tip increased compared to the room temperature measurements where the system contains only hard or crystalline materials with high elastic moduli. This provides more time for shearing and stretching of polymer chains within the melt and subsequent alignment of the resulting nuclei in the direction of scan.

It has been observed that the necessary condition for the formation of oriented nuclei is that the polymer must experience a mechanical work (as we have roughly estimated before) performed in its melt state. This work has to be larger than a threshold value at a shear rate which should be larger than the inverse Rouse time of the polymer chains. In our study, the stretch relaxation time or the Rouse time is much larger than the contact time between the polymer melt and the AFM tip. So, increasing relaxation time increases the time for alignment of polymer chains and favors the formation of oriented crystals.

Variation of time of contact between the AFM tip (by varying the free

amplitude of oscillation and the set point value) and the molten sample surface was found to have no significant influence on the tip induced nucleation probability (see **Fig. 5.6**). The movement of the cantilever is measured by the deflection of the reflected spot position on the photodiode. This vertical deflection value is usually displayed in Volts in the used softwere and this is the differance in voltage between the different section of the photodiode. This value is sufficient as the conversion from Volts to an actual deflection distance is relatively linear across the centre of the photodiode. But for some measurements it is important to know the deflection of the cantilever in units of length. The free amplitude of oscillation is defined by the amplitude of oscillation at which the cantilever is freely oscillating near it´s resonance frequency and no force is applied between the tip and the sample surface. At the biginning of a measurement the resonance frequency of a cantilever is tuned by setting the free amplitude of oscillation value and thereby allow the cantilever to oscillate with a frequency very close to the resonance frequency of the cantilever. During oscillation of the cantilever the amplitude value in Volt can be converted to nanometer value using calibration manager of the JPK softwere. Thus the free amplitude of oscillation values were changed manually before starting of a measurement and the conversion to nm values were done. Even applying large free amplitude of oscillation (see **Fig. 5.6 b, b´** where the heights and phases were recorded with free amplitude of oscillations (A_o) $\approx$ 21 nm and 15 nm respectively but, the amplitude of force at which the cantilever was driven during imaging *i.e* the drive amplitude in this case was $\sim$ 7.9 nm and $\sim$ 5.5 nm respectively) it was still possible to induce nucleation with almost the same probability as in the case of long contact time between molten sample surface and the AFM tip with small free amplitude of oscillation in **Fig. 5.6 b´´** where height and phase were recorded with free amplitude of oscillations (A_o) $\approx$ 6 nm and with a drive amplitude of 2.2 nm. The decrease in cantilever oscillation amplitude values from the free amplitude of oscillation values during imaging was resulted from the close proximity of the cantilever to the sample surface when the tip intermittently contacts or taps the surface.

It is important to note that elongated regions appeared in **Fig. 5.6 b´, b´´** and **Fig. 5.6 c, c´, c´´** are parallel to each other. The reason of such parallel stacks formation will be explained in detail in **section 5.4.6** of this chapter.

Region 1   Region 2   Region 3
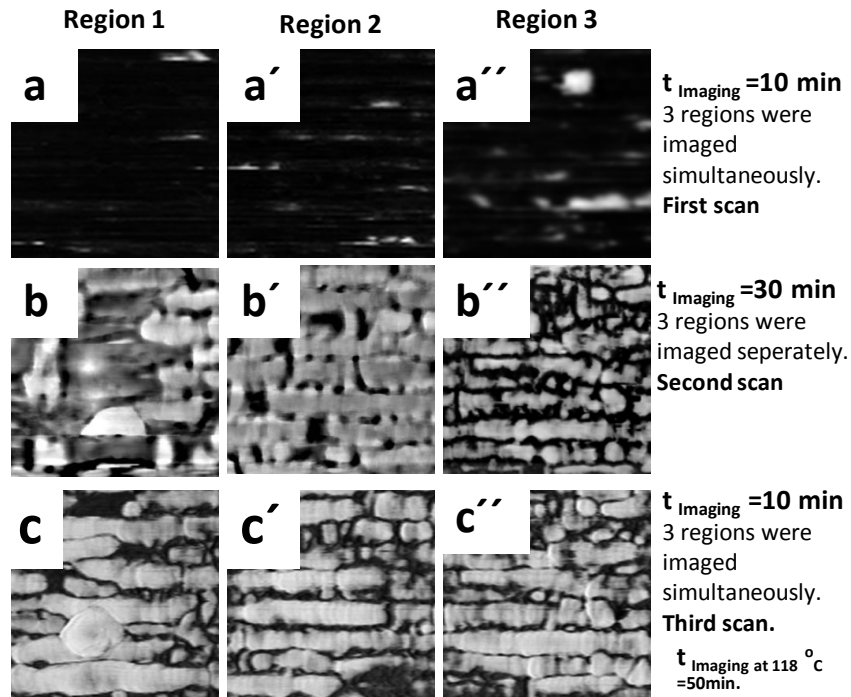
Figure 5.6 – AFM phase images **(a+a´+a´´, b+b´+b´´, c+c´+c´´)** show-ing the effect of varying time of contact between the AFM tip and molten sample surface on nucleation probability at 118 °C during crystallsation from an undercooled melt of polyethylene nanocrystals. **(a, a´, a´´)** first scan for $\sim$ 10 minutes ($r_{SP} = 0.5$). Height and phase were recorded with free amplitude of oscillation (A_0) $\approx$ 9 nm, **(b, b´, b´´)**, each region scanned seperately $\sim$ 30 minutes ($\sim$ 10 minutes for each scan) with $r_{SP} = 0.74$, 0.7, 0.55 respectively. As the free amplitude of oscillation was changed (to vary the time of contact between polymer melt and tip) during the imaging of three different regions, the set point amplitude was also changed in order to maintain proper imaging conditions. Heights and phases were recorded with free amplitude of oscillations (A_0) $\approx$ 21 nm, 15 nm and 6 nm respectively. **(c, c´, c´´)** third scan $\sim$ 10 minutes ($r_{SP} = 0.55$). Height and phase were recorded with free amplitude of oscillation (A_0) $\approx$ 6 nm. Size of the images is 1.5 x 1.5 μm^2.

Both the samples (as shown in **Fig. 5.5** and in **Fig. 5.6**) were ther-mally treated in a similar way. The thermal history for these two samples are schematically shown in **Fig. 5.7**.
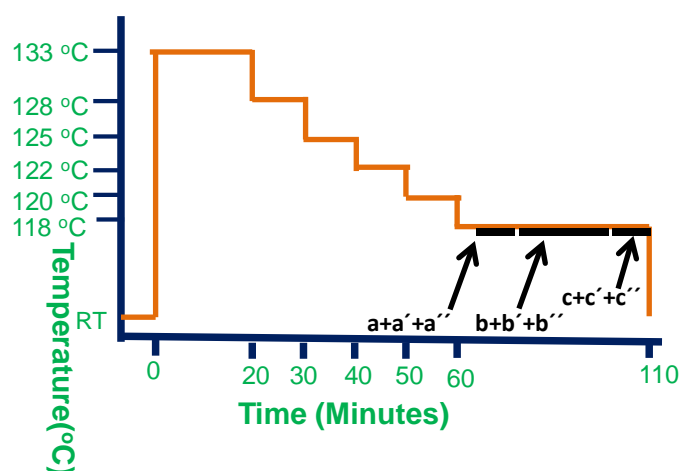
Figure 5.7 – Thermal history followed for the samples to investigate the effect of tapping force and the time of contact between melt and the tip on the nucleation probability. The black rectangular boxes represent the time of imaging for each image shown in a, b and c of **Fig. 5.6** and **Fig. 5.7**.

Typically, in isothermal experiments at imposed shear rate, the time corresponding to a sudden rise in the shear viscosity is taken as indicator for the onset of crystallisation [171]. Such a quantity, usually referred to as "induction time", is roughly proportional to the inverse of the nucleation rate. Characterization of the crystallization kinetics under shear is based on induction time, *i.e.*, the time required for the onset of crystallization.

Polymer viscosity has an influence on the shear rate and hence on the process of shear induced crystallization. Viscosity of the polymer as a measure of resistance of the polymer to the shear is one of the factors controlling both the behavior of the polymer melt and the formation of oriented nuclei. The induction time of crystallization decreases monotonically with the increase of the strain [183]. It means that with the increase in induction time the extent of surface deformation or the applied strain decreases. That is the reason that at a relatively high temperature the extent of surface deformation is less and nucleation is thus more difficult. Larger induction times are observed at higher temperatures, that is, closer to the thermodynamic melting point (T_m of the nanocrystals is 133 °C as determined by DSC).

Detailed simulations of polymer crystallization have provided much useful information on the growth process [184–186], yet simulating primary nucleation has proven difficult, especially at low undercooling, because of the extremely long nucleation times. That is why at a relatively high temperature (*e.g* 126 °C),

where initial scanning revealed only molten polymers (see **Fig. 5.8 a**) homogeneous nucleation was not observed due to low undercooling. However, keeping the sample for a long time at this temperature while scanning many times leads to nucleation (see **Fig. 5.8 b**). This particular sample was not molten at 133 °C as it was found before that at a temperature close to melting temperature (126 °C in this case) significant amount of molten polymer exists in the system (as can be seen from **Fig. 5.8a**). In between **Fig. 5.8 a** and **Fig. 5.8 b** six more scans were performed. Last scan before **Fig. 5.8 b** was done after 90 minutes of continuous scanning at 126 °C without appearance of any nuclei. Then the sample has been kept at 126 °C for ∼ 1 hour without imaging. After one hour when the sample was scanned again nucleation occured (see **Fig. 5.8 b**). The sample was again scanned for another 3 times for ∼ 30 minutes without any significant changes (figures are not shown).
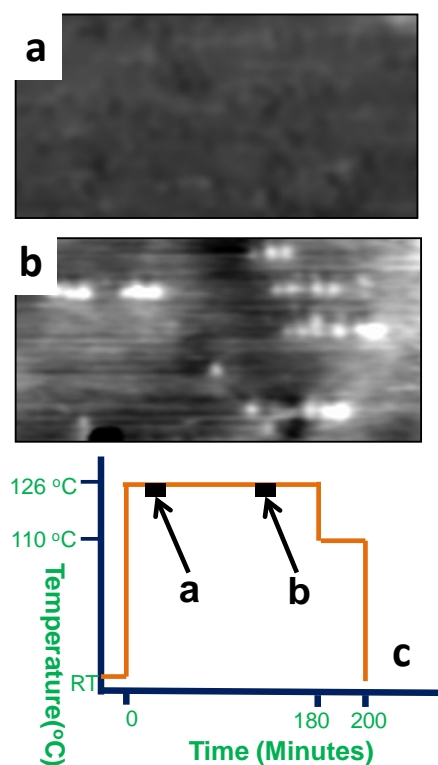
Figure 5.8 – AFM phase images (a-b) showing the effect of crystallization induction time at a temperature very close to the melting temperature (at 126 °C kept for 30 min considering the temperature stabilisation and the first scanning time, 150 min respectively for **a-b**). In between **Fig. 5.8a** and **Fig. 5.8b** several scans were performed. At such a high temperature the crystallization induction time is relatively high. Size of the images is 2 x 1 μm^2. (c) Schematic showing thermal history (the temperature-time protocol) of the sample. The black rectangular boxes represent the time of imaging for each image shown in a and b.

A more pronounced sensitivity of the induction time to shear intensity is found at the higher temperature. In other words, the slower the crystallization in quiescent conditions, the more pronounced is the relative effect of shear. This fact can be interpreted in terms of polymer chain orientation. As the temperature increases, both the orientational effect and the quiescent crystallization kinetics are decreased. The latter, however, is much more sensitive to temperature [187]. Furthermore, while the intrinsic crystallization rate (*i.e.*, in the absence of shear) tends to zero as the temperature approaches the thermodynamic melting point, the shear-induced orientation effect survives at any temperature. Induction time is inversely proportional to the nucleation rate [187, 188].

5.4.5 Shish-kebab structure formation by AFM tip

In our study of shear induced nucleation by AFM cantilever tip, shish-kebab type of structures were found to form (see **Fig. 5.9**). Actually, this is the typical morphology formed by a flow induced crystallization process. The mechanism of formation of shish-kebab under flow is still under debate but some ideas are proposed.

There are several proposals for the primary nucleation process under flow condition in the molten state. But two ideas were accepted mostly. **A)** The chains of longer relaxation time within the polymer melt are stretched by flow and aggregate to form shish nuclei upon which the bulk of materials are crystallized as kebabs. **B)** An accumulation process where aggregation occurs as soon as the number of point nuclei becomes large enough resulting in a row of small nuclei forming a shish [175]. In **Fig. 5.9a** one can see when the sample was cooled down from 125 °C to 122 °C and imaged a well defined shish structure was formed. Cooling down from 122 °C to 120 °C generates kebab structures after first imaging at 120 °C which were crystallized on the shish structure (see **Fig. 5.9b**). With time the kebab structures were growing (see **Fig. 5.9c**). After the same region scanned third time (see **Fig. 5.9d**) the shish sturucture was invisible and the kebabs were stacking together forming stacks of edge-on crystals.
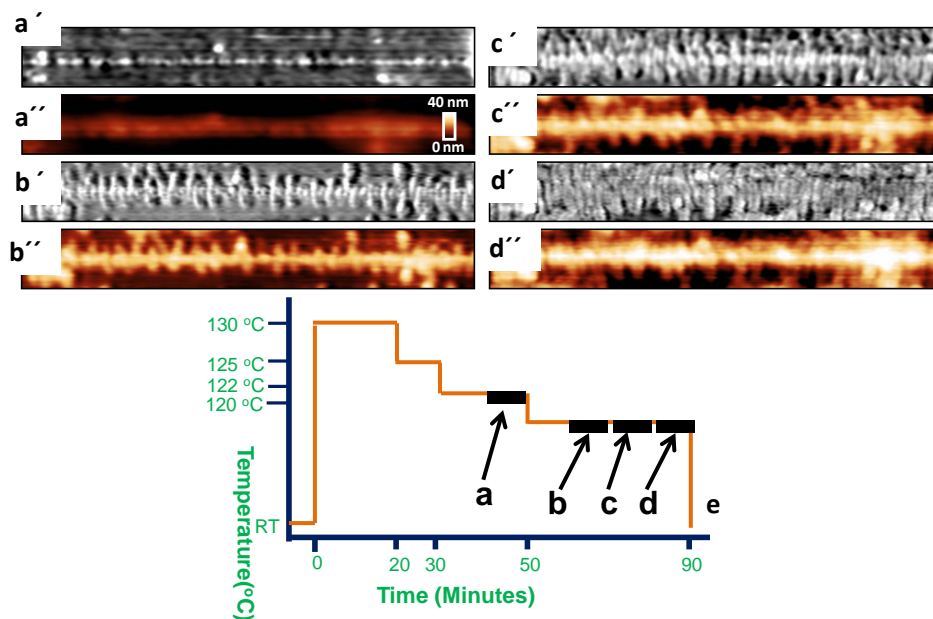
Figure 5.9 – (a´)-(d´) represent the phase contrast and (a´´)-(d´´) the corresponding topography images (the color code ranges from $0 - 40$ nm) showing shish-kebab structure formation by the AFM tip from the undercooled melt of polyethylene nanocrystals during crystallization experiments. When the sample was cooled down from 125 °C to 122 °C the temperature stabilisation and first imaging took ~ 20 minutes. A well defined shish structure was formed. Cooling down from 122 °C to 120 °C generates kebabs structures which were crystallized on the shish structure (temperature stabilisation and first time imaging at 120 °C took ~ 20 minutes). With time the kebab structures were growing. Size of each image is 3.5 x 0.5 µm^2. (e) Schematic showing thermal history (the temperature-time protocol) of the sample. The black rectangular boxes represent the time of imaging for each image shown in a, b, c and d.

5.4.6 Formation of stacks of crystals under shear

Some elongated crystalline regions were found to appear over a long distance across the double or triple layer region (see **Fig. 5.10 a**) where nucleation was induced by the AFM tip and vertical growth of one elongated crystalline region is stopped by the appearance of another two elongated crystalline regions just above and below the mentioned region (see **Fig. 5.10 a**). Nucleation was induced when the sample was cooled down from 125 °C to 120 °C. The only difference of this sample from that explained in **section 5.4.5** is that formation of shish structure was not observed in this case. Due to the limitation in AFM phase contrast resolution at elevated temperatures these regions appeared somewhat diffuse. In many of our experiments we observed these long crystalline regions (see **Fig. 5.5** and **Fig. 5.6** also). No clear height variation and no change in phase contrast

were observed within the stacks across the lines of crystalline regions. But, after quenching the sample to room temperature, these long crystalline regions were found to contain aggregated stacks of crystalline lamellae (see **Fig. 5.10 b**). The most interesting feature is the alignment of the stacks in one direction. The stacks of lamellae were only well visible at room temperature for most of the samples.
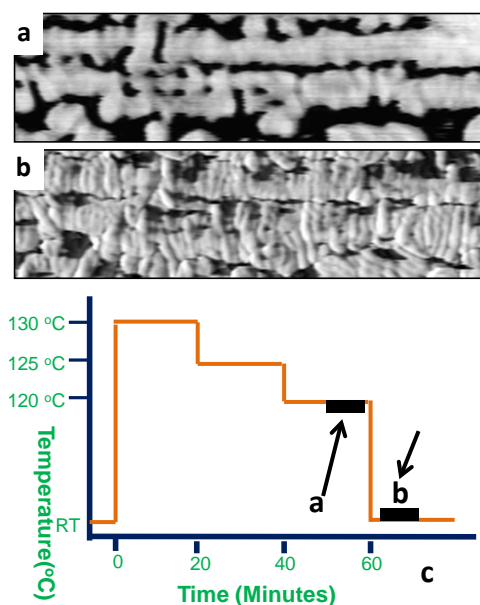
Figure 5.10 – AFM phase contrast images (a) imaged at 120 °C for first time for $\sim$ 20 minutes considering the temperature stabilisation and imaging time. (b) at room temperature. Size of each image is 3 x 0.8 μm^2. Stacks of crystals along a long distance are well visible at room temperature. (c) Schematic showing thermal history of the sample. The black rectangular boxes represent the time of imaging for each image shown in a and b.

The phenomenon of the stacking of crystalline domains during polymer crystallization (preserving the chain direction) is not fully explained. For crystallization from the quiescent melt, it was assumed that the stacking was related to the screw dislocation [41, 189, 190]. However, we have no evidence hinting at the presence of such dislocations in the measured images. We note that we observed the formation of the stacked lamellae of polyethylene at elevated temperatures ($\sim$ 118 °C-122 °C), but well below the equilibrium melting temperature.

May be in our case the stacking of the lamellae is due to the ordering influence of shear at the molten surface. Part of the chains emerging from the growing crystals remain molten, but in an extended rather than folded conformation. If this part of the chain is long enough, it serves as a nucleation site for

the new adjacent crystal. Such a mechanism can lead to the growth of stacked crystals, forming large domains in which the chain direction is the same. One has to consider also the possibility that the thickness of the lamellae in the elongated crystalline layer is large (less folded polymers) because crystallisation took place at low supercooling. For the origin of large lamellar thickness, possible thickening processes should also be taken into account.

5.4.7 Tip-induced nucleation within a molten monolayer of nanocrystals

The tip induced nucleation was found to be similar in nature in an initial monolayer region and within a densely packed bi- or tri-layer regions. From the beginning within the monolayer regions the nanocrystals were not densely packed because of the limited number of nanocrystals per unit area in the monolayer region.

So, when the temperature was raised (here in this paricular case to 130°C) few droplet-like domains with varying sizes were formed in the monolayer region (see **Fig. 5.11a+b**). When the temperature was reduced slowly, edge-on crystalline domains were nucleated by the AFM tip within these droplet-like domains which were found to be aligned along the scan direction (see **Fig. 5.11**). The mechanism responsible for the formation and alignment of edge-on crystals is similar to the one discussed in **section 5.4** of this chapter.
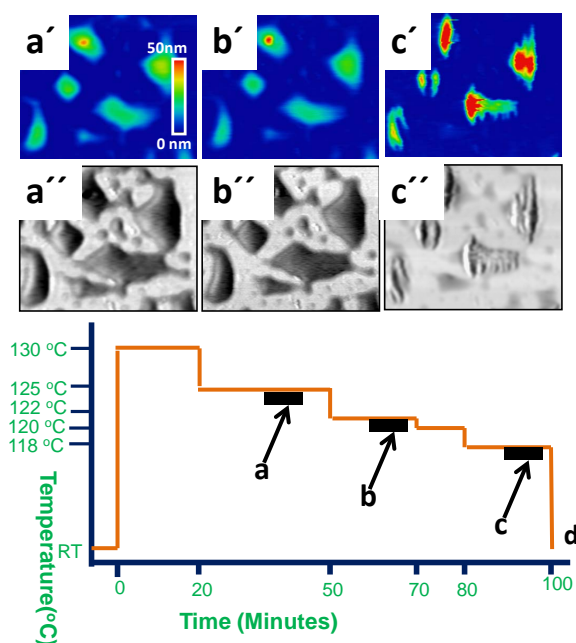
Figure 5.11 – AFM topography (a´-c´, the color code ranges from $0 - 50$ nm and phase images (a´´-c´´) showing the tip induced crystallsation within a molten monolayer region from an undercooled melt of nanocrystals. [a´+a´´) 30 min at 125 °C considering time for temperature stabilisation and first time imaging at 125 °C, b´+b´´) 20 min at 122 °C considering time for temperature stabilisation and first time imaging at 122 °C, c´+c´´) 20 min at 118 °C considering time for temperature stabilisation and first time imaging at 118 °C. Size of each image is 1.6 x 1.3 µm^2. Well aligned edge-on crystals were found within the droplets. (d) Thermal history (the temperature-time protocol) followed for this particular measurement. The black rectangular boxes represent the time of imaging for each image shown in a, b and c.

5.5 Concluding remarks

We have shown that nucleation can be induced by the AFM tip in an undercooled melt of polyethylene nanocrystals using tapping-mode under a high shear rate. The resulted edge-on crystals were aligned and oriented in the direction of scanning. The applied shear rate was found to be significant and the critical mechanical work done on the melt (below which nucleation is not possible) was also found to be high. We have calculated w from the equation of a literature study recently done by D´Haese *et al.* [168]. Although the amount of work performed to deform the melt in our case is 2-3 order of magnitude lower in our case, AFM tip was succesfully employed in our studies to induce nucleation. Scanning the same region several times increased the nucleation probability. For that reason,

several times scanned regions were found to contain a larger number of lamellae per unit area as compared to regions scanned once only. Nucleation probability was found to increase with tapping force. Contact time between sample surface and the AFM tip was found to have no influence on the nucleation process as for soft samples (melt in our system) the contact time is rather long and almost similar to the oscillation period of the cantilever tip. At relatively high temperatures nucleation was induced after a long time of scanning over the molten surface, due to a long nucleation induction time. Shish-kebab like structures were found to form. Thus we are inclined to think about a mechanism of structure formation induced by deformation *i.e.*, stretching of long polymer chains within the polymer melt caused by the AFM cantilever tip and subsequent crystallization of the smaller chains onto it. Elongated crystalline regions containing stacks of crystalline aggregates aligned edge-on were observed. Due to strong influence of the AFM cantilever-tip to induce nucleation, even in the monolayer regions which only contain some molten droplet-like domains, well aligned edge-on crystals were observed.

Chapter 6

Overall conclusion

The motivation of the project was to follow the morphological evolution of deposited polyethylene nanocrystals within self-organized regular patterns upon thermal annealing and recrystallisation of the undercooled melt of these nanocrystals. The primary necessity for that was to organize the polyethylene nanocrystals from an aqueous dispersion into ordered patterns on a solid surface. A well defined organization of the nanocrystals helped us to observe the thermally induced morphological changes throughout the study. Reorganization of the nanocrystals, in particular the changes of the lamellar thickness, occuring within the deposited nanocrystals as a function of temperature and in time were followed. How crystallization was induced within the undercooled melt of these polyethylene nanocrystals was also studied as a function of temperature and time.

We took advantage of the well-defined small size of the initial nanocrystals to follow the process of molecular reorganization and the corresponding morphological changes. A large spectrum of possible correlations between annealing temperature and crystal thickness have been explored. Due to the kinetic features of the various pathways taken, a representation of the reciprocal crystal thickness in a Gibbs-Thompson plot yielded a complex pattern. No crystal will be able to resist melting if the temperature is increased above the melting line, which reflects the size-dependent melting temperature. We note that the representation as a function of inverse thickness implies that the crystal size in the other two dimensions is large. Thus, for the initial nanocrystals having a nanometer size in all dimensions, a representation as a function of inverse volume might be more appropriate. Below the melting line, the actual thickness of the crystal depends on the pathway taken, allowing to obtain for a given annealing temperature crystals

of different lamellar thickness.

We compared our data with literature results on bulk samples [132] and a recent result obtained by annealing the same type of polyethylene nanocrystals in an aqueous dispersion [103]. The comparison demonstrated that our results are in good agreement with previous conclusion. As shown in [103] for a "closed system", crystals having a well defined lamellar thickness can be stabilized (equilibrated) at temperatures well below the melting line for large lamellar crystals of a certain lamellar thickness as studied *e.g.* in [132] Furthermore, by using assemblies of small nanocrystals on a bare substrate ("open system"), we were able to show that polymer crystals are thermodynamically not stable, even below the melting line. While such crystals will always try to reach energetically more favorable states which contain less folded chains, *i.e.* increased lamellar thickness, they may also loose molecules to the surrounding bare substrate when the sample is been kept at a relatively high temperature for several hours. This leads to decrease in volume of the crystalline materials and eventually melting of the crystals due to their small size. Consequently, a manifold of crystalline states, differing *e.g.* in lamellar thickness and volume, are possible for a given annealing temperature. In an "open system" these states are only metastable. Thus, morphological changes will occur in the course of time. The molecular architecture of polyethylene allows for comparatively fast reorganization processes and a relatively facile thickening of lamellar crystals which can be easily detected even after rather short time and modest annealing temperatures. We anticipate that also other semicrystalline polymers will follow the same pathways during annealing. However, steric constraints or specific intra- or intermolecular interaction may drastically reduce the rate of these kinetic processes. Thus, on typical experimental timescales no changes in thickness or morphology may be detectable.

We have shown that nucleation can be induced by an AFM cantilever-tip in an undercooled melt of polyethylene using tapping-mode. The resulting edge-on crystals were aligned and oriented with respect to the direction of scan. The applied shear rate was found to be high and the critical mechanical work done on the melt (below which nucleation is not possible) was also found to be somewhat lower compared to literature values like in the study by D´Haese *et al.* [168]. Scanning the same region several times increased the nucleation probability. For that reason, regions which were scanned several times contained larger number of lamellae per unit area as compared to regions scanned once. Nucleation probability was found to increase with tapping force. Contact time between sample surface and the AFM tip was found to have no detectable influence on the

nucleation process. At relatively high temperatures nucleation was induced only after a long time scanning over the molten surface due to very high nucleation induction time. Shish-kebab like structures were found to form which suggests a mechanism of structure formation like, stretching of polymer chains within the polymer melt by the AFM cantilever tip under high shear rate and subsequent attachment and crystallization of the other chains. Elongated crystalline regions containing stacks of crystalline aggregates aligned edge-on were observed. Well aligned edge-on crystals were observed even in the monolayer regions which only contained some molten droplet-like domains.

Finding reorganization of polymers within crystalline regions at much lower temperatures than expected contributes to understand the non-equilibrium processes of those nanometer-sized polymer crystals.

APPENDICES

Chapter 7

Appendix: Some information for tip-induced crystallisation study

7.1 Alignment of crystals without shear

A complementary approach was made to examine the tip-induced nucleation effect. A sample containing stripes patterns of polyethylene nanocrystals prepared by eveporative dewetting as described in **chapter 3** have been used for this study. One of these samples was kept at 133 °C for 30 minutes in a linkam hot stage and then stepwise cooled down from 133 °C to room temperature at a slow cooling rate of 1°C/min in between temperatures where no AFM measurements were performed. The time at each temperature was $\sim$ 30 minutes. It is important to note that at these high temperatures the sample was only kept within a linkam hot stage not measured by AFM or any other tools. This sample was then measured under AFM using tapping-mode at room temperature for the first time after the above mentioned treatment of the sample. It is very clear that, in this experiment an AFM tip has no influence inducing nucleation and ordering as the sample contains only crystalline materials. Still, well-aligned crystalline domains were found in every multilayer stripe throughout the whole sample, where the crystalline domains were oriented parallel to the stripe edge (see **Fig. 7.1 a) and b**)
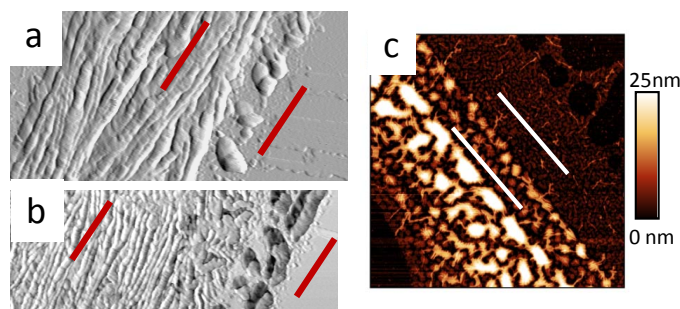
Figure 7.1 – (a-b) phase images measured at room temperature (the sample was cooled down stepwise with a cooling rate of 1°C/min) Size of each images are 4 x 1.5 µm^2 and 3.5 x 1.5 µm^2 respectively. (c) AFM topography image (size of the image is 15 x 15 µm^2, the color code ranges from $0 - 25$ nm)where the sample was cooled down directly from 133 °C to room temperature with a cooling rate of 50 °C/min. In the first case due to slower cooling rate the edge-on crystals found sufficient time to orient but in the later case although an upward direction of the aggregated crystal was observed, due to faster cooling rate resulted crystals found less time to orient.

Experiments on fast cooled samples (cooled from a higher temperature to room temperature with a cooling rate of 50 °C/min), still oriented edge-on lamellae parallel to the oriented stripe edge were observed (see **Fig. 7.1 c**). Obviously, the boundary of the stripe has an orientational effect within the polyethylene melt. However, tip-induced lamellae are oriented perpendicular to the scan direction. At temperatures close to melting temperature of the crystals the crystalline domains are aligned by the AFM tip along the scan direction.

7.2 Number of nuclei per unit area is larger in the many times scanned regions

The two regions (above and below to the white rectangular box in **Fig. 7.2a**) scanned once after keeping the sample at 100 °C for 20 minutes) showing a similar kind of orientation of the lamellae as the region scanned several times (*i.e.*, perpendicular to the scan direction). However within white box the tip induced nucleation rate is higher as the number of crystalline domains (per unit area or unit distance perpendicular to the orientation of the crystals) is higher in this region which was scanned many times.
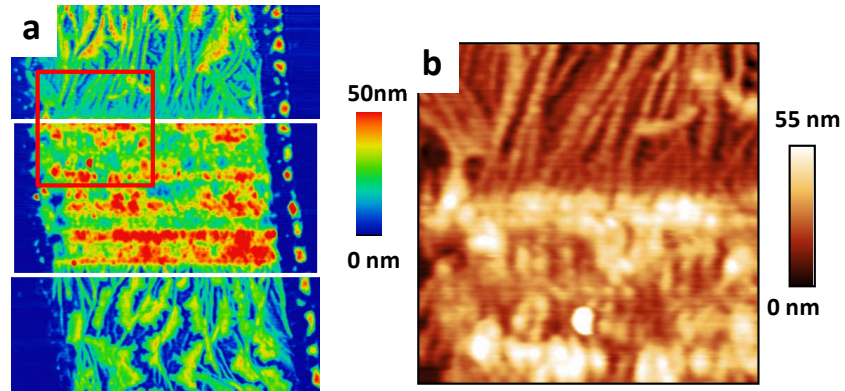
Figure 7.2 – AFM topography (a+b, the color code ranges from 0 – 50 nm and from 0 – 55 nm respectively for a and b) showing that during crystallsation experiments from an undercooled melt of polyethylene nanocrystals the number of nuclei per unit area is higher within an area which is scanned by the AFM tip many times as compared to regions scanned once. [a)+b) 20 min at 100 °C], (b) is zoomed in image from the red square box in the image (a). Size of the images are 8 x 10 µm^2 and 3 x 3 µm^2 respectively.

References

[1] Hanarp, P., Sutherland, D. S., Gold, J., and Kasemo, B. *Colloids and Surfaces A: Physicochemical and Engineering Aspects* **214**, 23–36 (2003).

[2] Schmitt, J., Decher, G., Dressick, W. J., Brandow, S. L., Geer, R. E., Shashidhar, R., and Calvert, J. M. *Advanced Materials* **9**, 61–65 (1997).

[3] Shenhar, R., Jeoung, E., Srivastava, S., Norsten, T., and Rotello, V. *Advanced Materials* **17**, 2206. (2005).

[4] Welch, P. and Muthukumar, M. *Phys. Rev. Lett.* **87**, 218302 Nov (2001).

[5] Muthukumar, M. *Philosophical Transactions: Mathematical, Physical and Engineering Sciences* **361**(1804), pp. 539–556 (2003).

[6] Sommer, J.-U. *The European Physical Journal E: Soft Matter and Biological Physics* **19**, 413–422 (2006). 10.1140/epje/i2005-10055-1.

[7] Larini, L., Barbieri, A., Prevosto, D., Rolla, P. A., and Leporini, D. *Journal of Physics: Condensed matter* **17**, L199–L208 (2005).

[8] Till, P. H. *Journal of Polymer Science* **24**(106), 301–306 (1957).

[9] Fischer, E. W. Z. *Naturforsch, Teil A* **12**, 753 (1957).

[10] Keller, A. and OŽConnor, A. *Nature* **180**, 1289 (1957).

[11] Jacodine, R. *Nature* **176**, 305 (1955).

[12] Toda, A. and Keller, A. *Colloid & Polymer Science* **271**, 328–342 (1993). 10.1007/BF00657415.

[13] Kwan, A. T., Efremov, M. Y., Olson, E. A., Schiettekatte, F., Zhang, M., Geil, P. H., and Allen, L. H. *J. Polym. Sci. Polym. Phys.* **39**(11), 1237–1245 (2001).

[14] Magonov, S. N., Yerina, N. A., Godovsky, Y. K., and Reneker, D. H. *Jornal of Macromolecular Science,Part B. Physics.* **45**, 169–194 (2006).

[15] Tian, M. and Loos, J. *Journal of Polymer Science, Part B, Polymer. Physics.* **39**, 763–770 (2001).

[16] Weber, C. H. M., Chiche, A., Krausch, G., Rosenfeldt, S., Ballauff, M., Harnau, L., Göttker-Schnetmann, I., Tong, Q., and Mecking, S. *Nano Letters* **7**(7), 2024–2029 (2007).

[17] Wagener, K. B., Valenti, D., and Hahn, S. F. *Macromolecules* **30**, 6688–6690 (1997).

[18] OGara, J. E., Portmess, J. D., and B., W. K. *Macromolecules* **26**, 2837 (1993).

[19] Yabu, H. and Shimomura, M. *Advanced Functional Materials* **15**(4), 575–581 (2005).

[20] Ghosh, M., Fan, F., and Stebe, K. J. *Langmuir* **23**, 2180 (2007).

[21] Govor, L. V., Reiter, G., Parisi, J., and Bauer, G. H. *Phys. Rev. E* **69**, 061609 (2004).

[22] Rabani, E., Reichman, D. R., Geissier, P. L., and Brus, L. E. *Nature* **426**, 271–274 (2003).

[23] Pauliac-Vaujour, E. and Moriarty, P. *J. Phys. Chem. C* **111**, 16255 (2007).

[24] Murphy, C. J., Sau, T. K., Gole, A. M., Orendorff, C. J., Gao, J., Gou, L., Hunyadi, S. E., and Li, T. *The Journal of Physical Chemistry B* **109**, 13857 (2005).

[25] Sau, T. K. and Murphy, C. J. *Langmuir* **21**, 2923 (2005).

[26] Hong, S., Xia, J., and Lin, Z. *Advanced Materials* **19**(10), 1413–1417 (2007).

[27] Xu, J., Xia, J., Hong, S. W., Lin, Z., Qiu, F., and Yang, Y. *Phys.Rev.Lett.* **96**, 066104 (2006).

[28] Adachi, E. and Dimitrov, A. S.and Nagayama, K. *Langmuir* **11**, 1057 (1995).

[29] Karthaus, O., Grasjo, L., Maruyama, N., and Shimomura, M. *Chaos* **9**, 308 (1999).

[30] Deegan, R. D. *Phys.Rev.E* **61**, 475 (2000).

[31] Deegan, R. D., Bakajin, O., Dupont, T. F., Huber, G., Nagel, S. R., and Witten, T. A. *Nature* **389**, 827 (1997).

[32] Deegan, R. D., Bakajin, O., Dupont, T. F., Huber, G., Nagel, S. R., and Witten, T. A. *Phys.Rev.E* **62**, 756 (2000).

[33] Hu, H. and Larson, R. G. *J. Phys. Chem. B* **110**, 7090 (2006).

[34] de Gennes, P. G. *Scaling concepts in polymer physics.* Cornell University, (1979).

[35] Rubinstein, M. *Polymer Physics.* Oxford University Press, Oxford, (2003).

[36] Katz, J. R. *Kolloid Z* **37**, 19 (1925).

[37] Storks, K. H. *Journal of the American Chemical Society* **60**(8), 1753–1761 (1938).

[38] Keller, A. *Philos Mag* **2**, 1171 (1957).

[39] Hoffman, J. D. *Polymer Engineering & Science* **4**(4), 315–362 (1964).

[40] Hoffman, J. and Lauritzen, J. I. *Jr. J. Research NBS* **65 A**, 297 (1961).

[41] Hikosaka, M., Amano, K., Rastogi, S., and Keller, A. *J. Mater. Sci.* **35**, 5157 (2000).

[42] Keller, A. and Cheng, S. D. Z. *Polymer* **39**, 4461 (1998).

[43] Debenedetti, P. G. *Metastable Liquids.* Princeton University, New Jersey, (1996).

[44] Sadler, D. M. *Journal of Polymer Science: Polymer Physics Edition* **23**(8), 1533–1554 (1985).

[45] Sadler, D. and Gilmer, G. *PRL* **56**, 2708 (1986).

[46] Bower, D. I. *An Introduction to Polymer Physics.* Cambridge University Press, (2002).

[47] Zahn, K., Lenke, R., and Maret, G. *Phys. Rev. Lett.* **82**, 2721 (1999).

[48] Chi, L., Anders, M., Fuchs, H., Johnston, R., and Ringsdorf, H. *Science* **259**, 213 (1993).

[49] Heck, B., Hugel, T., Iijima, M., Sadiku, E., and Strobl, G. *New J. Phys.* **1**, 17 (1999).

[50] Rastogi, S., Hikosaka, M., Kawabata, H., and Keller, A. *Macromolecules* **24**, 6384 (1991).

[51] Strobl, G. *Eur. Phys. J.E.* **3**, 165–183 (2000).

[52] Hauser, G., Schmidtke, J., and Strobl, G. *Macromolecules* **31**(18), 6250–6258 (1998).

[53] Hugel, T. Master's thesis, Freiburg Institut für Physik Universität Freiburg, (1999).

[54] Lotz, B. *Eur. Phys. J. E* **3**, 185 (2000).

[55] Keith, H., Jr.Padden, F. J., Lotz, B., and Wittmann, J.-C. *Macromolecules* **22**, 2230 (1989).

[56] Toda, A. *Colloid & Polym. Sci.* **270**, 667 (1992).

[57] Lotz, B., Lovinger, A., and Cais, R. *Macromolecules* **21**, 2375 (1988).

[58] Bu, Z. *Macromolecules* **29**, 6575 (1996).

[59] Keith, H. D. and Padden Jr., F. J. *J. Polym . Sci. Polym . Phys.* **25**, 2371 (1987).

[60] Patel, D. and Bassett, D. *Proc. R. Soc. Lond. A* **445**, 577 (1994).

[61] Marand, H., Xu, J., and Srinivas, S. *Macromolecules* **31**, 8219 (1998).

[62] Liu, C. and Muthukumar, M. *J. Chem. Phys.* **109**, 2536 (1998).

[63] Strobl, G. *The Physics Of Polymer*. Springer, Berlin, (1997).

[64] A.Keller. *Rep.Prog.Phys* **31**, 623 (1968).

[65] Fischer, E. W. and Schmidt, G. *Angew. Chem.* **74**, 551 (1962).

[66] Kawai, T. *Kolloid Z u Z Polymere* **201**, 104 (1965).

[67] Dreyfuss, P. and Keller, A. *J. Macromol. Sci.-Phys.* **B4**, 811 (1970).

[68] Bauers, F. M. and Mecking, S. *Angewandte Chemie International Edition* **40**(16), 3020–3022 (2001).

[69] Soula, R., Novat, C., Tomov, A., Spitz, R., Claverie, J., Drujon, X., Malinge, J., and Saudemont, T. *Macromolecules* **34**(7), 2022–2026 (2001).

[70] Bauers, F. M., Thomann, R., and Mecking, S. *Journal of the American Chemical Society* **125**(29), 8838–8840 (2003).

[71] Strobl, G. *Prog.Polym.Sci.* **31**, 398 (2006).

[72] Wunderlich, B. *Macromolecular Physics*. Academic press, new York, (1973).

[73] Loo, Y.-L., Register, R. A., and Ryan, A. J. *Phys. Rev. Lett.* **84**, 4120 (2000).

[74] Li, Z., Kesselmann, E., Talmon, Y., Hillmyer, M. A., and Lodge, T. P. *Science* **306**, 98 (2004).

[75] Wittemann, A., Drechsler, M., Talmon, Y., and Ballauff, M. *Journal of the American Chemical Society* **127**(27), 9688–9689 (2005). PMID: 15998064.

[76] Guinier, A. and Fournet, G. *Small angle scattering of X-rays*. John Wiley, New York, (1955).

[77] Dingenouts, N. and Ballauff, M. *Acta. Polym* **44**, 178 (1993).

[78] Göttker-Schnetmann, I. and Korthals, B., M. S. *J.Am.Chem.Soc.* **128**, 7708 (2006).

[79] Taden, A. and Landfester, K. *Macromolecules* **36**(11), 4037–4041 (2003).

[80] Petrenko, V. F. and Whitworth, R. W. *Physics of Ice.* Oxford University Press: Oxford, (1999).

[81] Ge, G. and Brus, L. *The Journal of Physical Chemistry B* **104**(41), 9573–9575 (2000).

[82] Moriarty, P., Taylor, M. D. R., and Brust, M. *Phys.Rev.Lett.* **89**, 248303 (2002).

[83] Hong, S.-W., Xu, J., Xia, J., Lin, Z., Qiu, F., and Yang, Y. *Chemistry of Materials* **17**(25), 6223–6226 (2005).

[84] Byun, M., Hong, S. W., Zhu, L., and Lin, Z. *Langmuir* **24**(7), 3525–3531 (2008). PMID: 18275235.

[85] Hong, S. W., Jeong, W., Ko, H., Kessler, M. R., and Lin, Z. Q. *Advanced Functional Materials* **18**, 2114 (2008).

[86] Bodiguel, H., Doumenc, F., and Guerrier, B. *The European Physical Journal - Special Topics* **166**, 29–32 (2009). 10.1140/epjst/e2009-00873-3.

[87] Denkov, N., Velev, O., Kralchevski, P., Ivanov, I., Yoshimura, H., and Nagayama, K. *Langmuir* **8**(12), 3183–3190 (1992).

[88] Gigault, C., Dalnoki-Veress, K., and Dutcher, J. R. *Journal of Colloid and Interface Science* **243**(1), 143 – 155 (2001).

[89] Frastia, L., Archer, A. J., and Thiele, U. *Phys. Rev. Lett.* **106**, 077801 (2011).

[90] Binnig, G., Quate, C. F., and Gerber, C. *Phys. Rev. Lett.* **56**, 930–933 Mar (1986).

[91] Binnig, G., Rohrer, H., Gerber, C., and Weibel, E. *Phys. Rev. Lett.* **49**, 57–61 Jul (1982).

[92] Sarid, D. *scanning force microscopy.* Oxford University Press, Oxford, (1991).

[93] Rugar, D. and Hansma, P. *Phys. Today* **43**, 23 (1990).

[94] Magonov, S. N. *Appl. Spectrosc. Rev.* **28**, 1 (1993).

[95] Pearce, R. and Vancso, G. J. *Macromolecules* **30**, 5843 (1997).

[96] Pearce, R. and Vancso, G. J. *Polymer* **39**, 1237 (1998).

[97] Hobbs, J. K., McMaster, T. J., Miles, M. J., and Barham, P. J. *Polymer* **39**, 2437 (1998).

[98] Schultz, J. M. and Miles, M. J. *J Polym Sci B Polym Phys* **36**, 2311 (1998).

[99] Knoll, A., Magerle, R., and Krausch, G. *Macromolecules* **34**(12), 4159–4165 (2001).

[100] Höper, R., Gesang, T., Possart, W., Hennemann, O. D., and Boseck, S. *Ultramicroscopy* **60**(1), 17 – 24 (1995).

[101] García, R. and Pérez, R. *Surface Science Reports* **47**(6-8), 197 – 301 (2002).

[102] Popov, Y. O. and Witten, T. A. *Phys. Rev. E* **68**, 036306 (2003).

[103] Rochette, C. N., Rosenfeldt, S., Henzler, K., Polzer, F., Ballauff, M., Tong, Q., Mecking, S., Drechsler, M., Narayanan, T., and Harnau, L. *Macromolecules* **44**(12), 4845–4851 (2011).

[104] Zhang, F., Liu, J., Huang, H., Du, B., and He, T. *The European Physical Journal E: Soft Matter and Biological Physics* **8**, 289–297 (2002).

[105] Bartczak, Z., Argon, A. S., Cohen, R. E., and Kowalewski, T. *Polymer* **40**, 2367–2380 (1999).

[106] Mellbring, O., Kihlman Oiseth, S., Krozer, A. J., and Hjertberg, T. *Macromolecules* **34**, 7496 (2001).

[107] Wang, Y., Ge, S., Rafailovich, M., Sokolov, J., Zhou, Y., Ade, H., LRning, J., Lustiger, A., and Marom, G. *Macromolecules* **37**, 3319. (2004).

[108] Sommer, J. U. *The European Physical Journal E: Soft Matter and Biological Physics* **19**, 413 (2006).

[109] Rastogi, S. *Macromolecules* **30**, 7880 (1997).

[110] Schmidt, M., Kusche, R., Issendorff, B. V., and Haberland, H. *Nature* **393**, 238–240 (1998).

[111] Voorhees, P. W. *Journal of Statistical Physics* **38**, 231–252 (1985). 10.1007/BF01017860.

[112] Metatla, N., Palato, S., Commarieu, B., Claverie, J. P., and Soldera, A. *Soft Matter* **8**, 347 (2012).

[113] Sommer, J.-U. and Reiter, G. *Europhys. Lett* **56**, 755 (2001).

[114] Reiter, G., Castelein, G., and Sommer, J.-U. *Phys. Rev. Lett.* **8**, 5918 (2001).

[115] Bar, G., Thomann, Y., and Brandsch, R.and Cantow, H.-J. *Langmuir* **13**, 3807–3812 (1997).

[116] Strobl, G. *The European Physical Journal E: Soft Matter and Biological Physics* **18**, 295–309 (2005). 10.1140/epje/e2005-00032-y.

[117] Zhang, F., Baralia, G. G., Nysten, B., and Jonas, A. M. *Macromolecules* **44**, 7752 (2011).

[118] Loos, J. and Tian, M. *Polymer* **47**, 5574 (2006).

[119] Magonov, S. N., Yerina, N. A., Ungar, G., Reneker, D. H., and Ivanov, D. A. *Macromolecules* **36**, 5637 (2003).

[120] Organ, S. J., Hobbs, J. K., and Miles, M. J. *Macromolecules* **37**, 4562 (2004).

[121] Sommer, J.-U. and Reiter, G. *Thermochim. Acta* **432**, 135 (2005).

[122] Liu, Y.-X. and Chen, E.-Q. *Coordination Chemistry Reviews* **254**, 1011 (2010).

[123] Zhu, D.-S., Liu, Y.-X., Shi, A.-C., and Chen, E.-Q. *Polymer* **47**, 5239–5242 (2006).

[124] de Silva, D. S. M., Zeng, X. B., Ungar, G., and Spells, S. J. *Macromolecules* **35**, 7730 (2002).

[125] Labaig, J. J. PhD thesis, Strasbourg, (1978).

[126] Riegler, H. and Köhler, R. *Nature Physics* **3**, 890–894 (2007).

[127] Fischer, E. W. *Kolloid-Zeitsehrift und Zeitschrift für Polymere,* **231**, 458–503 (1967).

[128] Luo, C. and Sommer, J.-U. *Macromolecules* **44**(6), 1523–1529 (2011).

[129] Fischer, E. W. Z. *Macromolecules* **41**, 2514 (1968).

[130] Yao, Y.-F., Graf, R., Spiess, H. W., and Rastogi, S. *Macromolecules* **41**(7), 2514–2519 (2008).

[131] Yamamoto, T. *The Journal Of Chemical Physics* **129**, 184903 (2008).

[132] Heck, B., Strobl, G., and Cho, T. Y. *Colloid Polym Sci* **282**, 825 (2004).

[133] Basu, N., Osichow, A., Mecking, S., and Reiter, G. *Eur Phys J E* **35** (2012).

[134] Lee, O. and Kamal, M. R. *Polym. Eng. Sci.* **39**, 326 (1999).

[135] Pope, D. P. and Keller, A. *Colloid Polym. Sci.* **256**, 751 (1978).

[136] Rueda, D. R., Ania, F., and Balta Calleja, F. J. *Polymer* **38**, 2027 (1997).

[137] White, H. M. and Bassett, D. C. *Polymer* **38**, 5515 (1997).

[138] Tribout, C., Monasse, B., and Haudin, J. *Colloid Polym. Sci.* **274**, 197 (1996).

[139] Duplay, C., Monasse, B., Haudin, J., and Costa, J. L. *Polym. Int.* **48**, 320 (1999).

[140] Pearce, R. and Vancso, G. J. *Macromolecules* **30**, 5843 (1997).

[141] Godovsky, Y. K. and Magonov, S. N. *Langmuir* **16**, 3549 (2000).

[142] Beekmans, L. G. M. *Morphology Development in Semicrystalline Polymers by in-situ Scanning Force Microscopy.* PhD thesis, University of Twente, (2002).

[143] Leung, O. M. and Goh, M. C. *Science* **255**, 64 (1992).

[144] Hamada, E. and Kaneko, R. *Ultramicroscopy* **184**, 42 (1992).

[145] Brumfield, J., Goss, C., Irene, E., and Murray, R. *Langmuir* **8**, 2810 (1992).

[146] Pickering, J. and Vancso, G. *Appl. Surf. Sci.* **148**, 147 (1999).

[147] Leach, R., Stevens, F., Seiler, C., Langford, S., and Dickinson, J. *Langmuir* **19**, 10225 (2003).

[148] Schmidt, R. H., Haugstad, G., and Gladfelter, W. L. *Langmuir* **19**, 10390 (2003).

[149] Gotsmann, B. and Dürig, U. *Langmuir* **20**, 1495 (2004).

[150] Rüetschi, M., Grütter, P., Fünfschilling, J., and Güntherodt, H.-J. *Science* **265**, 512 (1994).

[151] Kim, J.-H., Yoneya, M., and Yamamoto, J. *Appl. Phys. Lett.* **78**, 3055 (2001).

[152] Jradi, K., Bistac, S., Schmitt, M., Schmatulla, A., and Reiter, G. *Eur. Phys. J. E* **29**, 383 (2009).

[153] Kimura, K., Kobayashi, K., Yamada, H., Horiuchi, T., Ishida, K., and Matsushige, K. *Appl.Phys.Lett.* **82**, 4050 (2003).

[154] Kimura, K., Kobayashi, K., Yamada, H., Horiuchi, T., Ishida, K., and Matsushige, K. *Applied Surface Science* **252**, 5489 (2006).

[155] Kimura, K., Kobayashi, K., Yamada, H., Horiuchi, T., Ishida, K., and Matsushige, K. *Jpn. J. Appl.Phys.* **43**, L1390 (2004).

[156] Gibbs, J. , 55 (1906).

[157] Wunderlich, B. *Crystal nucleation, growth, annealing.* Academic Press, New York, (1976).

[158] Blundell, D., Keller, A., and Kovacs, A. *J. Polm. Sci. Part B* **4**, 481 (1966).

[159] Ziabicki, A. and Alfonso, G. *Colloid Polym.Sci.* **273**, 317–323 (1995).

[160] Caputo, F. E. and Burghardt, W. R. *Macromolecules* **34**, 6684 (2001).

[161] Baert, J., Van Puyvelde, P., and Langouche, F. *Macromolecules* **39**, 9215 (2006).

[162] Kumaraswamy, G., Verma, R. K., and Kornfield, J. A. *Rev. Sci. Instrum.* **70**, 2097 (1999).

[163] Nogales, A., Hsiao, B. S., Somani, R. H., Srinivas, S., Tsou, A. H., Balta-Calleja, F. J., and Ezquerra, T. A. *Polymer* **42**, 5247 (2001).

[164] Macosko, C. W. *Rheology: principles, measurements, and applications.* VCH Publishers, Inc.: New York, (1994).

[165] Mykhaylyk, O. O., Chambon, P., C., I., Fairclough, J. P. A., Terrill, N., and Ryan, A. J. *Macromolecules* **43**, 2389 (2010).

[166] Mykhaylyk, O. O. *Soft Matter* **6**, 4430 (2010).

[167] Mykhaylyk, O. O., Chambon, P., Graham, R. S., Fairclough, J. P. A., Olmsted, P. D., and Ryan, A. J. *Macromolecules* **41**, 1901 (2008).

[168] DHaese, M., Mykhaylyk, O. O., and Van Puyvelde, P. *Macromolecules* **44**, 1783 (2011).

[169] Doi, M. and Edwards, S. F. *The Theory of Polymer Dynamics.* Clarendon Press: Oxford, England, (1986).

[170] Monasse, B. *J. Mater. Sci.* **27**, 6047 (1992).

[171] Lagasse, R. R. and Maxwell, B. *Polym. Eng. Sci.* **16**, 189 (1976).

[172] Vleeshouwers, S. and Meijer, H. E. H. *Rheol. Acta* **35**, 391 (1996).

[173] Bushman, A. C. and McHugh, A. J. *J. Appl. Polym. Sci.* **64**, 2165 (1997).

[174] Floudas, G., Hilliou, L., Lellinger, D., and Alig, I. *Macromolecules* **33**, 6466 (2000).

[175] Janeschitz-Kriegl, H., Ratajski, E., and Stadlbauer, M. *Rheol. Acta* **42**, 355 (2003).

[176] Housmans, J. W., Steenbakkers, R. J. A., Roozemond, P. C., Peters, G. W. M., and Meijer, H. E. H. *Macromolecules* **42**, 5728 (2009).

[177] Bach, A., Rasmussen, H. K., and Hassager, O. *J. Rheol.* **47**, 429 (2003).

[178] Bushman, A. C. and Mchuch, A. J. *J. Polym. Sci. Part B: Polym. Phys.* **34**, 2393 (1996).

[179] Janeschitz-Kriegl, H. and Ratajski, E. *Polymer* **46**, 3856 (2005).

[180] van Meerveld, J., Peters, G. W. M., and Hutter, M. *Rheol. Acta* **44**, 119 (2004).

[181] Tamayo, J. and Garcia, R. *Langmuir* **12**, 4430 (1996).

[182] Garcia, R. and Paulo, A. S. *Phys. Rev. B* **60**, 4961 (1999).

[183] Cong, Y., Liu, H., Wang, D., Zhao, B., Yan, T., and Li, L. *Macromolecules* **44**, 5878 (2011).

[184] Waheed, N., Ko, M. J., and Rutledge, G. C. *Polymer* **46**, 8689 (2005).

[185] Hu, W., Frenkel, D., and Mathot, V. *Macromolecules* **35**, 7172 (2002).

[186] Zhang, J. and Muthukumar, M. *J. Chem. Phys.* **126**, 234904 (2007).

[187] Coppola, S., Balzano, L., Gioffredi, E., Maffettone, P. L., and Grizzuti, N. *Polymer* **45**, 3249 (2004).

[188] Coppola, S., Grizzuti, N., and Maffettone, P. L. *Macromolecules* **34**, 5030 (2001).

[189] Rastogi, S. and Ungar, G. *Macromolecules* **25**, 1445 (1992).

[190] Basset, D. C. *Polymer* **29**, 1539 (1988).

List of Figures

Acknowledgment

Foremost, I would like to express my deep and sincere gratitude to my supervisor Prof. Günter Reiter for the continuous support of my Ph.D study, for his motivation, wide knowledge and logical way of thinking. His guidance and continuous encouragement helped me in all the time of research and writing of this thesis. It was a great opportunity for me to work with him.

Besides my supervisor, I would like to thank the rest of my thesis committee: Prof. Alexander Blumen, Prof. Elizabeth von Hauff, for their encouragement, insightful comments and the time they spent for evaluation of the thesis.

It is a pleasure for me to thank those people in our group who made my stay very easy by their friendly behavior and kind help in particular Mrs. Barbara Heck. I wish to thank all of my fellow lab mates in our group for the helpful discussions, for the time we were working together at lab, and for all the fun we have had in the last three years together. I wish to thank Prof. Gert Strobl, Prof. Achim Kittel, Dr. Warner Stille, Dr. Adam Raegen and Dr. Alexender Schmatula for their postitive and helpful scientific discussion throughout my PhD life.

Also, I want to thank my collaborators Prof. Stefan Mecking and Anna Osichow in University of Konstanz for providing us the polymer I have worked with and for friendly collaboration.

I would like to acknowledge the funding support from The Baden-Württemberg Stiftung.

Last but not the least; I would like to thank my family: my parents and my husband for supporting me in all the way throughout my PhD. life.